Analysis of the Out-of-Control Falling Leaf Motion using a Rotational Axis Coordinate System

Daniel C. Lluch

Thesis submitted to the Faculty of the
Virginia Polytechnic Institute and State University
in partial fulfillment of the requirements for the degree of

Master of Science
in
Aerospace Engineering

Dr. Frederick Lutze - chair
Dr. Mark Anderson
Dr. Wayne Durham

October 1998
Blacksburg, Virginia

Keywords: nonlinear flight dynamics, coordinate system, coordinate transformation

Analysis of the Out-of-Control Falling Leaf Motion using a Rotational Axis Coordinate System

Daniel C. Lluch

(ABSTRACT)

The realm of aircraft flight dynamics analysis reaches from local static stability to global dynamic behavior. It includes aircraft performance issues as well as structural concerns. In the particular aspect of dynamic motions of an aircraft and how we understand them, an alternate coordinate system will be introduced that will lend insight and simplification into the understanding of these dynamic motions. The main contribution of this coordinate system is that one can easily visualize how the instantaneous velocity vector relates to the instantaneous rotation vector, the angular rate vector of the aircraft.

The out-of-control motion known as the Falling Leaf will be considered under the light of this new coordinate system. This motion is not well understood and can lead to loss of the aircraft and crew. Design guidelines will be presented to predict amplitude and frequency of the Falling Leaf.

This work received support from NASA Langley Research Center, contract number NAG-1-1851 #1

Acknowledgments

I would like to thank all those who have helped me through the years in reference to this work as well as throughout my life. First and foremost, I'd like to thank my parents for absolutely always being there and caring as to what was happening in my life. I thank my sisters for feeding me good meals and giving me a place to go during my undergraduate days in Blacksburg. Thanks to all my friends, who have been a huge cornerstone in my life, especially friend and roommate Jin Wook Lim.

I owe where I am today in my academic career to my advisor, Dr Fred Lutze. He gave me an opportunity to prove myself many years ago when he had no obligation too, and I thank him. The remaining members of my committee, Dr Anderson and Dr Durham have made the academic environment extremely pleasant. I could not have asked for a better committee or mentors in this endeavor. Mr John Foster allowed this project to come my way. He made my short stay at NASA a wonderful learning experience. Although not technically my 'boss', I truly hope all my bosses will be like him. Last but certainly not least, thanks to the SimLab crew (including Josh) for always being there and putting up with the guitar playing.

Contents

List of Figures

List of Tables

Nomenclature

$(\hat{\mathbf{i}},\hat{\mathbf{j}},\hat{\mathbf{k}})$ unit vectors in the (x, y, z) direction of the appropriate sub/superscripted coordinate system

$(\lambda, -\eta)$ 2-3 rotation angles defining the transformation from the body-fixed coordinate system to the rotational coordinate system

(μ, γ, χ) 3-2-1 rotation angles defining the transformation from the inertial coordinate system to the wind axis coordinate system

(Φ, Θ, Ψ) 3-2-1 rotation angles defining the transformation from the inertial coordinate system to the rotational coordinate system

(ϕ, θ, ψ) Euler angles, 3-2-1 rotation angles defining the transformation from the inertial coordinate system to the body-fixed coordinate system

(A, B, C) Defined constants in the $\ddot{\Phi}$-equation

(a, b, c, d) Coefficients of characteristic polynomial

$(g_{1_k}, g_{2_k}, g_{3_k})$ Components of gravity represented in the k reference frame

(L, M, N) Body-fixed axis moments

(p, q, r) Body-fixed axis components of the relative angular rate vector between the body-fixed coordinate system and the inertial coordinate system

(p_w, q_w, r_w) Wind axis components of the relative angular rate vector between the wind axis coordinate system and the inertial coordinate system

(u, v, w) Body-fixed axis components of aircraft velocity relative to inertial space

(x'_k, y'_k, z'_k) axis system of appropriate sub/superscript

α Angle of attack, the angle between the x_b-axis and the projection of the aircraft velocity V into the $x_b - z_b$ plane

α_p Rotation angle to rotate from general moments of inertia in some body-fixed axis system to principal moments of inertia in the principal axis system

β Sideslip angle, the angle made by the aircraft velocity V and the projection of the aircraft velocity V into the $x_b - z_b$ plane

β_{ref} Defines frequency of the sine representation of the rolling moment coefficient as $\frac{\pi}{\beta_{ref}}$

δ_{ij} Kronecker delta operator

$\frac{d}{dt}^k(\vec{F})$ Time rate of change of $\vec{F}$ with respect to the k reference frame

ϵ Thrust offset angle measured in the $x_b - z_b$ plane

ϵ_{ij} Alternating tensor operator

Γ Short form of the moment of inertia constant $(I_{xx}I_{zz} - I_{xz}^2)$

$\vec{\omega}_{a/b}^c$ The angular rate of frame a with respect to frame b represented in frame c

$\bar{q}$ Dynamic pressure, $\frac{1}{2}\rho V^2$

ν New variable used in variable transformation

Ω Magnitude of the instantaneous rotation vector, $\vec{\omega}_{b/h}$

ρ Air density

σ Angle between the instantaneous velocity vector and the instantaneous rotation vector

σ_{ref} Value of σ once steady Falling Leaf oscillation has been reached

τ Angle defined by $\alpha - \eta$

A Jacobian matrix

b Wingspan

C Coefficient used in solving for σ_{ref}

C_1 Defined to be equivalent to $\frac{C_{Y\beta}\rho S}{2}$

C_2 Defined to be equivalent to $\frac{-C_{l_{max}}\rho S b}{2}$

c_i Short form of the moments of inertia constants in a body-fixed axis system, $1 \leq c \leq 9$

C_l Rolling moment coefficient

C_Y Body-axis side force coefficient

$C_{l_{max}}$ Amplitude of the sine representation of the rolling moment coefficient

$C_{Y\beta}$ Stability derivative $\frac{\partial C_Y}{\partial \beta}$

D Drag, aerodynamic force along the x_w-axis, defined positive in the negative x_w direction

DOF Degree of freedom

E Total energy

F Evaluated elliptic integral

g Gravity

I_{xx} Moment of Inertia about the x_b-axis

I_{xz} Cross Moment of Inertia

I_{yy} Moment of Inertia about the y_b-axis

I_{zz} Moment of Inertia about the z_b-axis

K Constant of the motion defined by an initial condition for the reduced system of equations of motion

k Constant defining phasing between roll and yaw rates

L Lift, aerodynamic force along the z_w-axis, defined positive in the negative z_w direction

m Aircraft mass

Q Wind axis side force, aerodynamic force along the y_w-axis, defined positive in the negative y_w direction

S Wing planform area

T Thrust, Kinetic Energy

T_{ji} Transformation matrix from i coordinate system to j coordinate system

T_{period} Period of oscillation

T_{x_α} Fundamental transformation matrix about the x-axis through an angle α

V Total aircraft velocity, Potential energy

X Aerodynamic force along the x_b-axis

Y Aerodynamic force along the y_b-axis

Z Aerodynamic force along the z_b-axis

$\hat{\mathbf{n}}$ Row or column vector of a transformation matrix

$\mathbf{I}^k$ Inertia tensor represented in the k reference frame

Chapter 1

Introduction

Issues of aircraft dynamic stability have been under consideration for many years (Ref[10]). Due to high performance needs, aircraft have extended their operating region into the high angle of attack regime. Seeking departure resistant aircraft in this high angle of attack regime has led to establishing roll and yaw departure criteria. Nonlinear coupling between the longitudinal and lateral-directional variables has shown to be a key driver in analyzing global stability (Refs [10], [9]). Stability has also been found to be a function of the dynamic state of the aircraft (Ref [11]).

To contribute to the analysis of aircraft dynamics, focus has been placed on the relationship between the instantaneous rotation vector and the instantaneous velocity vector in the effort to understand how those vectors behave for particular maneuvers (Ref [2], [6]). The work presented here will place all importance on the interaction between the velocity vector and the instantaneous rotation vector to the extent of developing equations of motion that specifically focus on the relationship of these vectors. This representation of the equations of motion requires developing a new coordinate system. A good choice of coordinate system allows one to easily focus on the relationship in question.

In the analysis of vehicle dynamics, one often comes to the realization that a result can be understood in a simpler way if the problem is approached from a different point of view. Consider the motion of a particle shown in Figure 1.1. If the analysis was performed using Cartesian coordinates, namely x-y coordinates, it would show rapidly varying state variables.

$$\dot{x} = f(x, y) \tag{1.1}$$
$$\dot{y} = f(x, y) \tag{1.2}$$

Yet if the same analysis was done using polar coordinates, namely r-θ coordinates, it would show a rapidly varying r and a slowly varying θ.

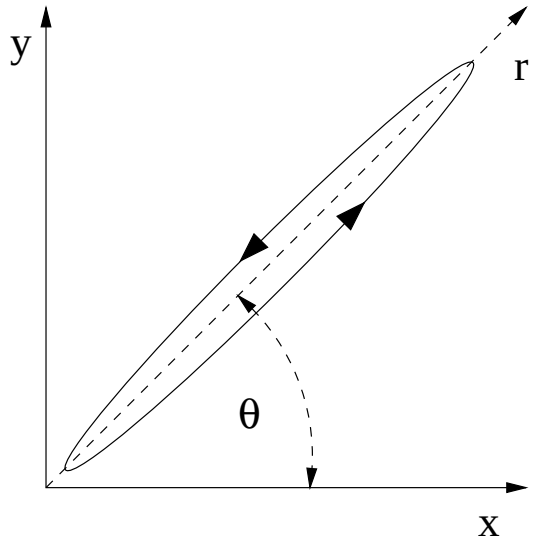

Figure 1.1: Cartesian Polar Comparison

$$\dot{r} = f(r, \theta) \tag{1.3}$$
$$\dot{\theta} = f(r, \theta) \tag{1.4}$$

An intelligent choice of the coordinate system can lend insight into a particular problem, and can lead to assumptions, such as assuming θ to be a constant for this example.

The idea shown above will be applied to a more complex problem. A coordinate system is proposed for the analysis of aircraft dynamics in which some of the variables will be nearly constant. This coordinate system will lend insight into the analysis of dynamic motions of an aircraft. As a direct result of the use of the new coordinate system, key parameters can be identified that establish various characteristics of selected dynamic motions. Stability guidelines will also be developed in terms of the new coordinate system.

1.1 Preliminaries to Deriving Equations of Motion

In order to study the dynamics of an aircraft, the laws that govern the motion must be known. Newton's laws of motion can be applied to a rigid body to derive its equations of motion. One must choose an axis system to represent these laws and the associated aerodynamic forces and moments. As shown above, significant insight can be obtained from an intelligent choice of variables and coordinate system, depending on the particular motion that is to be analyzed. In the sections that follow, the groundwork will be laid in defining the necessary information needed to apply Newton's laws to an aircraft. The mechanics of

defining coordinate systems is shown for those coordinate systems currently in use. It will then be shown how these coordinate systems are used in expressing Newton's laws. For any further information on the content of the sections that follow, see Ref [7].

1.1.1 Coordinate Systems

The first assumption for considering aircraft dynamics is most commonly the flat-earth approximation, which states that the ground-fixed axes are inertial. This assumption also implies the gravity vector is constant in magnitude and direction. When considering stability analysis, this approximation is valid since the aircraft will not be traveling far distances. Most commonly one sees the z-axis point along the direction of gravity, and the x and y axes pointing north and east in the plane of the earth's surface. One can then define the local horizontal axes, (x_h, y_h, z_h) as being parallel to the ground-fixed axes yet fixed at the center of mass of the aircraft and traveling with the aircraft. It is the local horizontal axis system where gravity has its most simplest representation.

It is then necessary to define a coordinate system that is fixed to the aircraft and moves with it in both translation and rotation, referred to as a body-fixed axis system, (x_b, y_b, z_b). The origin of this system is fixed at the center of mass of the aircraft and has the x and z axes in the plane of symmetry of the aircraft with the x-axis pointing out the nose and the z-axis pointing out the bottom. The y-axis then completes the right-hand rule with the axis pointing in the direction of the right wing. There are various interesting choices for the body-fixed axes. In particular, when the (x_b, y_b, z_b) is aligned with the principal moments of inertia, (x_p, y_p, z_p), called the principal axis system. This particular choice of the (x_b, y_b, z_b) significantly reduces the complexity of the inertial terms in the equations of motion yet has the draw back that the moments have to be expressed in the same coordinate system. This representation of the moments may not be directly available.

Another coordinate system of interest is the wind axes system, (x_w, y_w, z_w). The origin is fixed at the center of mass of the aircraft and has the x-axis pointing along the instantaneous velocity vector, the z-axis is in the plane of symmetry pointing out the bottom of the aircraft, and the y-axis then completes the right-hand rule. The instantaneous velocity vector will be the velocity of the aircraft, in both magnitude and direction, relative to inertial space. This particular choice of axes significantly reduces the representation of the aerodynamic forces and moments in the linearized problem, but does not contribute much simplification in the general nonlinear problem. In addition, the terms in the inertia tensor become functions of time.

1.1.2 Transformations

With the defined coordinate systems, information between them can be related by defining transformations between any two of the coordinate systems. Define a rotation about the x-axis to be a 1-rotation, a rotation about the y-axis a 2-rotation, and a rotation about the z-axis a 3 rotation. Euler showed that that one can rotate to any new coordinate system by rotating though, at most, three independent fundamental rotations. For instance, you can get to any new coordinate system via a 1-2-3 rotation, a 3-2-1 rotation, or a 1-3-1 rotation. There are twelve different combinations allowing the transformation from any two coordinate systems. A 1-1-3 rotation is not a valid transformation between any two arbitrary coordinate systems since the first two rotations can be considered one rotation about the x-axis. Fundamental transformation matrices can be defined about each single axis (Ref [7]):

Rotate η about the x-axis:

$$T_{x_\eta} = \begin{bmatrix} 1 & 0 & 0 \\ 0 & \cos\eta & \sin\eta \\ 0 & -\sin\eta & \cos\eta \end{bmatrix} \tag{1.5}$$

Rotate η about the y-axis:

$$T_{y_\eta} = \begin{bmatrix} \cos\eta & 0 & -\sin\eta \\ 0 & 1 & 0 \\ \sin\eta & 0 & \cos\eta \end{bmatrix} \tag{1.6}$$

Rotate η about the z-axis:

$$T_{z_\eta} = \begin{bmatrix} \cos\eta & \sin\eta & 0 \\ -\sin\eta & \cos\eta & 0 \\ 0 & 0 & 1 \end{bmatrix} \tag{1.7}$$

With these fundamental rotation matrices we can now build the transformation matrix between any two of the coordinate systems defined in Sec 1.1.1.

Horizontal and Body-fixed Relationship: Euler Angles

In flight dynamics, the common order for rotation from the local horizontal to the body-fixed coordinate systems is a 3-2-1 rotation. The following set of angles are defined to be the Euler angles, $[\phi, \theta, \psi]$:

1. Rotate through an angle ψ about the z_h-axis to an intermediate coordinate system, (x', y', z').

2. Then rotate through an angle θ about the y'-axis to an intermediate coordinate system, (x'', y'', z'').

3. Finally, rotate through an angle ϕ about the x''-axis to reach the body-fixed axis system, (x_b, y_b, z_b)

Therefore the transformation matrix from the local horizontal system to the body-fixed axis system is,

$$T_{bh} = T_{x_\phi} T_{y_\theta} T_{z_\psi} \tag{1.8}$$

which after evaluation becomes,

$$T_{bh} = \begin{bmatrix} \cos\theta\cos\psi & \cos\theta\sin\psi & -\sin\theta \\ \sin\phi\sin\theta\cos\psi - \cos\phi\sin\psi & \sin\phi\sin\theta\sin\psi + \cos\phi\cos\psi & \sin\phi\cos\theta \\ \cos\phi\sin\theta\cos\psi + \sin\phi\sin\psi & \cos\phi\sin\theta\sin\psi - \sin\phi\cos\psi & \cos\phi\cos\theta \end{bmatrix} \tag{1.9}$$

Horizontal and Wind Relationship

The relationship between the local horizontal coordinate system and the wind axis coordinate system are similar to the Euler angles. The rotations are in the same order yet three new angles are defined, $[\mu, \gamma, \chi]$:

$$T_{wh} = T_{x_\mu} T_{y_\gamma} T_{z_\chi} \tag{1.10}$$

resulting in:

$$T_{wh} = \begin{bmatrix} \cos\gamma\cos\chi & \cos\gamma\sin\chi & -\sin\gamma \\ \sin\mu\sin\gamma\cos\chi - \cos\mu\sin\chi & \sin\mu\sin\gamma\sin\chi + \cos\mu\cos\chi & \sin\mu\cos\gamma \\ \cos\mu\sin\gamma\cos\chi + \sin\mu\sin\chi & \cos\mu\sin\gamma\sin\chi - \sin\mu\cos\chi & \cos\mu\cos\gamma \end{bmatrix} \tag{1.11}$$

Body-fixed and Wind Relationship

The rotation from the body-fixed axes to the wind axes can be fully described by only two fundamental transformations, a 2-3 rotation, because the z_w-axis is also in the plane of symmetry of the aircraft. The angles are $[\beta, -\alpha]$,

1. Rotate through an angle $-\alpha$ about the y_b-axis to an intermediate coordinate system, (x', y', z').

2. Then rotate through an angle β about the z'-axis to reach the wind axes coordinate system, (x_w, y_w, z_w)

Therefore,

$$T_{wb} = T_{z_\beta} T_{y_{-\alpha}} \tag{1.12}$$

Evaluating the above expression gives the transformation matrix from the body-fixed axis system to the wind axis system,

$$T_{wb} = \begin{bmatrix} \cos\alpha\cos\beta & \sin\beta & \sin\alpha\cos\beta \\ -\cos\alpha\sin\beta & \cos\beta & -\sin\alpha\sin\beta \\ -\sin\alpha & 0 & \cos\alpha \end{bmatrix} \tag{1.13}$$

With T_{wb} defined, another relationship can be expressed between the local horizontal and the wind axis systems which relates the eight angles $[\alpha, \beta, \mu, \gamma, \chi, \phi, \theta, \psi]$ of which only five are independent.

$$T_{wh}(\mu, \gamma, \chi) = T_{wb}(\alpha, \beta)\, T_{bh}(\phi, \theta, \psi) \tag{1.14}$$

1.1.3 Properties of Transformation Matrices

The transformation matrix has a few interesting properties. The matrices that are dealt with here are similarity transformations. Let $\hat{\mathbf{n}}$ be any row or column vector of the transformation matrix. The orthogonality condition states,

$$\hat{\mathbf{n}}_i \cdot \hat{\mathbf{n}}_j = 0 \text{ for } i \neq j. \tag{1.15}$$

The normal condition states,

$$\hat{\mathbf{n}}_i \cdot \hat{\mathbf{n}}_j = 1 \text{ for } i = j. \tag{1.16}$$

Both conditions can be combined to form the orthonormal condition, which can be expressed with the Kronecker δ operator,

$$\hat{\mathbf{n}}_i \cdot \hat{\mathbf{n}}_j = \delta_{ij} \text{ where } \delta_{ij} = \begin{cases} 1 & i = j \\ 0 & i \neq j \end{cases} . \tag{1.17}$$

The dextral condition states that a matrix conforms to the right-handed rule. This condition can be expressed with the alternating tensor operator,

$$\hat{\mathbf{n}}_i \times \hat{\mathbf{n}}_j = \epsilon_{ijk} \hat{\mathbf{n}}_k \text{ where } \epsilon_{ijk} = \begin{cases} 1 & ijk = \text{1-2-3 and cyclic perturbations} \\ -1 & ijk = \text{3-2-1 and cyclic perturbations} \\ 0 & \text{otherwise} \end{cases} . \tag{1.18}$$

Because the purpose of the similarity transformation matrix is to only change the representation of given information, it does not scale that information. A vector in space is invariant regardless of what coordinate system it is represented in. Therefore, all the above conditions being satisfied leads to the following:

$$\det T_{yx} = 1 \tag{1.19}$$

(Interesting to note that the determinant is -1 if you are going from a right-handed to left-handed coordinate system or vice-versa and the transformation matrix is not dextral)

Consider having the transformation matrix, T_{yx}, yet having information expressed in the y-coordinate system, (x_y, y_y, z_y). To express the same information in the x-coordinate system, (x_x, y_x, z_x),

$$\hat{\mathbf{n}}^x = T_{xy}\hat{\mathbf{n}}^y = T_{yx}^{-1}\hat{\mathbf{n}}^y = T_{yx}^T\hat{\mathbf{n}}^y \tag{1.20}$$

The orthonormal-dextral transformation matrix has the property that its inverse is its transpose. Information between any two coordinate systems can be easily related once the transformation matrix between the two coordinate systems is defined.

1.1.4 Some useful Relationships

As mentioned in Sec 1.1.1 gravity is most naturally expressed in the local horizontal coordinate system, (x_h, y_h, z_h).

$$\vec{\mathbf{g}}^h = \left\{ \begin{array}{c} 0 \\ 0 \\ g \end{array} \right\} \tag{1.21}$$

Equation 1.9 can be used to express the gravity vector in the body-fixed axis system, (x_b, y_b, z_b).

$$\vec{\mathbf{g}}^b = T_{bh}\vec{\mathbf{g}}^h = g \left\{ \begin{array}{c} -\sin\theta \\ \sin\phi\cos\theta \\ \cos\phi\cos\theta \end{array} \right\} \tag{1.22}$$

Equations 1.9-1.13 can be used to express the gravity vector in the wind axis system, (x_w, y_w, z_w).

$$\begin{aligned} \vec{\mathbf{g}}^w &= T_{wh}\vec{\mathbf{g}}^h = T_{wb}T_{bh}\vec{\mathbf{g}}^h \\ &= g \left\{ \begin{array}{c} -\sin\gamma \\ \sin\mu\cos\gamma \\ \cos\mu\cos\gamma \end{array} \right\} \qquad (1.23) \\ &= g \left\{ \begin{array}{c} (-\cos\alpha\cos\beta\sin\theta + \sin\beta\sin\phi\cos\theta + \sin\alpha\cos\beta\cos\phi\cos\theta) \\ (\cos\alpha\sin\beta\sin\theta + \cos\beta\sin\phi\cos\theta - \sin\alpha\sin\beta\cos\phi\cos\theta) \\ (\sin\alpha\sin\theta + \cos\alpha\cos\phi\cos\theta) \end{array} \right\} \qquad (1.24) \end{aligned}$$

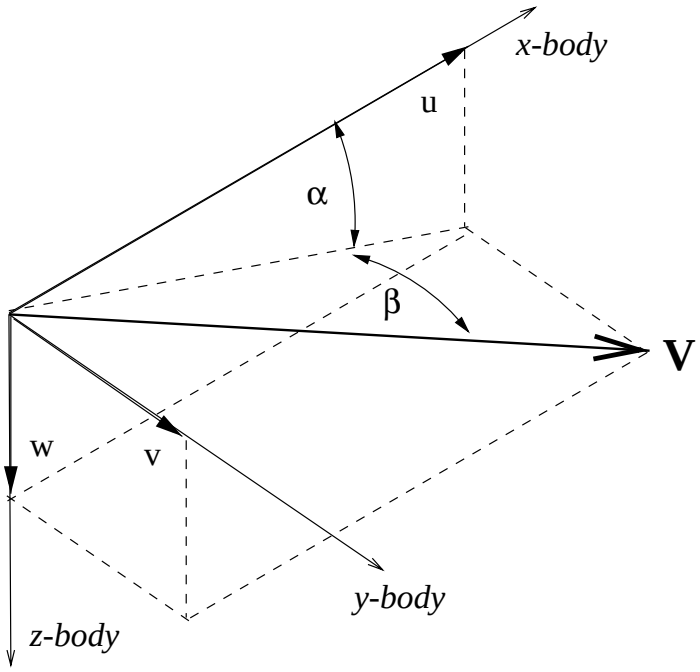

Figure 1.2: Wind Body Comparison

Similarly, the velocity vector is most naturally expressed in the wind axis coordinate system, (x_w, y_w, z_w). By definition,

$$\vec{\mathbf{V}}^w = \left\{ \begin{array}{c} V \\ 0 \\ 0 \end{array} \right\} \tag{1.25}$$

Figure 1.2 shows the how the velocity vector relates to the body-fixed coordinate system, (x_b, y_b, z_b).

$$\vec{\mathbf{V}}^b = \left\{ \begin{array}{c} u \\ v \\ w \end{array} \right\} = T_{bw} \vec{\mathbf{V}}^w \tag{1.26}$$

$$\left\{ \begin{array}{c} u \\ v \\ w \end{array} \right\} = \left\{ \begin{array}{c} V \cos\alpha \cos\beta \\ V \sin\beta \\ V \sin\alpha \cos\beta \end{array} \right\} \tag{1.27}$$

Equation 1.27 gives the relationship between the body-fixed components of the velocity

vector and the wind axis variables. Namely,

$$\tan\alpha = \frac{w}{u} \tag{1.28}$$

$$\sin\beta = \frac{v}{V} \tag{1.29}$$

$$V^2 = u^2 + v^2 + w^2 \tag{1.30}$$

1.1.5 Moments of Inertia

The moments of inertia for a rigid body in a body-fixed coordinate system with an $x-z$ plane of symmetry are defined to be

$$I_{xx} = \int_m (y^2 + z^2)\, dm \tag{1.31}$$

$$I_{yy} = \int_m (x^2 + z^2)\, dm \tag{1.32}$$

$$I_{zz} = \int_m (x^2 + y^2)\, dm \tag{1.33}$$

$$I_{xz} = \int_m xz\, dm \tag{1.34}$$

$$I_{xy} = I_{yz} = 0 \tag{1.35}$$

It is worth noting that one may see the cross moment of inertia defined in literature as the negative of the above thus allowing every element in the inertia tensor be positive. The definition above does conform to the convention seen in aircraft dynamics. The matrix tensor for the inertia terms which contain an $x-z$ plane of symmetry is then

$$\mathbf{I} = \begin{bmatrix} I_{xx} & 0 & -I_{xz} \\ 0 & I_{yy} & 0 \\ -I_{xz} & 0 & I_{zz} \end{bmatrix}^b \tag{1.36}$$

As mentioned in Sec 1.1.1 a great deal of simplification results from choosing the body-fixed coordinate system to line up with the principal directions of the moments of inertia. This transformation can be achieved through a single rotation about the y_b-axis:

$$T_{pb} = \begin{bmatrix} \cos\alpha_p & 0 & -\sin\alpha_p \\ 0 & 1 & 0 \\ \sin\alpha_p & 0 & \cos\alpha_p \end{bmatrix} \tag{1.37}$$

with

$$\alpha_p = \frac{1}{2}\tan^{-1}\left(\frac{2I_{xz}}{I_{xx} - I_{zz}}\right). \tag{1.38}$$

Therefore the principal inertia tensor is given by

$$\mathbf{I} = \begin{bmatrix} I_{xx} & 0 & 0 \\ 0 & I_{yy} & 0 \\ 0 & 0 & I_{zz} \end{bmatrix}^p = T_{pb}\,\mathbf{I}^b\,T_{pb}^T \tag{1.39}$$

T_{pb} can also be used to represent general body-fixed forces and moments in the principal coordinate system, (x_p, y_p, z_p).

$$\vec{\mathbf{F}}^p = T_{pb}\,\vec{\mathbf{F}}^b \tag{1.40}$$

1.1.6 Angular Rates and Kinematics

In deriving the equations of motion for a rigid body, information is usually expressed in non-inertial coordinate systems. It is then necessary to define the angular rate of the chosen coordinate system with respect to the inertial coordinate system. Let $\vec{\boldsymbol{\omega}}_{b/h}$ be the angular rate of change of the body-fixed coordinate system with respect to the local horizontal coordinate system (recall (x_h, y_h, z_h) is considered inertial). As with any other vector, $\vec{\boldsymbol{\omega}}_{b/h}$, can be represented in any coordinate system. Recall from Sec 1.1.2 the Euler rotation angles describe how (x_h, y_h, z_h) relates to (x_b, y_b, z_b). The time rate of change between the body-fixed axes and the local horizontal axes is most naturally expressed in a mixture of coordinate systems and is related to the Euler angle rates as follows,

$$\vec{\boldsymbol{\omega}}_{b/h} = \dot{\phi}\,\hat{\mathbf{i}}_b + \dot{\theta}\,\hat{\mathbf{j}}'' + \dot{\psi}\,\hat{\mathbf{k}}' \tag{1.41}$$

with $\hat{\mathbf{i}}$, $\hat{\mathbf{j}}$, $\hat{\mathbf{k}}$ being unit vectors along the (x, y, z) directions of the appropriate coordinate system. Expressing every term in the body-fixed system,

$$\vec{\boldsymbol{\omega}}_{b/h} = \dot{\phi}\,\hat{\mathbf{i}}_b + \dot{\theta}\,T_{b''}\,\hat{\mathbf{j}}'' + \dot{\psi}\,T_{b'}\,\hat{\mathbf{k}}' \tag{1.42}$$

Defining the body-fixed components and expressing the transformation matrices in terms of there fundamental rotations,

$$\vec{\boldsymbol{\omega}}^b_{b/h} = \begin{Bmatrix} p \\ q \\ r \end{Bmatrix} = \dot{\phi}\begin{Bmatrix} 1 \\ 0 \\ 0 \end{Bmatrix} + \dot{\theta}\,T_{x_\phi}\begin{Bmatrix} 0 \\ 1 \\ 0 \end{Bmatrix} + \dot{\psi}\,T_{x_\phi}\,T_{y_\theta}\begin{Bmatrix} 0 \\ 0 \\ 1 \end{Bmatrix} \tag{1.43}$$

which gives:

$$\left\{ \begin{array}{c} p \\ q \\ r \end{array} \right\} = \left[\begin{array}{ccc} 1 & 0 & -\sin\theta \\ 0 & \cos\phi & \cos\theta\sin\phi \\ 0 & -\sin\phi & \cos\theta\cos\phi \end{array} \right] \left\{ \begin{array}{c} \dot{\phi} \\ \dot{\theta} \\ \dot{\psi} \end{array} \right\} \tag{1.44}$$

The inverse relationship is,

$$\left\{ \begin{array}{c} \dot{\phi} \\ \dot{\theta} \\ \dot{\psi} \end{array} \right\} = \left[\begin{array}{ccc} 1 & \sin\phi\tan\theta & \cos\phi\tan\theta \\ 0 & \cos\phi & -\sin\phi \\ 0 & \sin\phi\sec\theta & \cos\phi\sec\theta \end{array} \right] \left\{ \begin{array}{c} p \\ q \\ r \end{array} \right\} \tag{1.45}$$

(It is important to note that the matrix relating the body axis rates and the time rate of change of the Euler angles is *not* a transformation matrix as defined in Sec 1.1.2.)

Equation 1.45 shows that as the moments (directly) and forces (indirectly) affect the body axis rates, the Euler angles *have* to evolve a certain way. The angular rates completely define how the Euler angles evolve in time. This kinematic relationship is not subject to change or interpretation.

A similar relationship exists for $\vec{\boldsymbol{\omega}}_{w/h}$. Written for convenience,

$$\vec{\boldsymbol{\omega}}^{w}_{w/h} = \left\{ \begin{array}{c} p_w \\ q_w \\ r_w \end{array} \right\} = \left[\begin{array}{ccc} 1 & 0 & -\sin\gamma \\ 0 & \cos\mu & \cos\gamma\sin\mu \\ 0 & -\sin\mu & \cos\gamma\cos\mu \end{array} \right] \left\{ \begin{array}{c} \dot{\mu} \\ \dot{\gamma} \\ \dot{\chi} \end{array} \right\} \tag{1.46}$$

The inverse relationship is,

$$\left\{ \begin{array}{c} \dot{\mu} \\ \dot{\gamma} \\ \dot{\chi} \end{array} \right\} = \left[\begin{array}{ccc} 1 & \sin\mu\tan\gamma & \cos\mu\tan\gamma \\ 0 & \cos\mu & -\sin\mu \\ 0 & \sin\mu\sec\gamma & \cos\mu\sec\gamma \end{array} \right] \left\{ \begin{array}{c} p_w \\ q_w \\ r_w \end{array} \right\} \tag{1.47}$$

It is useful to relate the body axis rates to the wind axis rates.

$$\vec{\boldsymbol{\omega}}_{w/h} = \vec{\boldsymbol{\omega}}_{w/b} + \vec{\boldsymbol{\omega}}_{b/h} \tag{1.48}$$

The new term in Equation 1.48 is most naturally expressed in two coordinate systems,

$$\vec{\boldsymbol{\omega}}_{w/b} = -\dot{\alpha}\,\hat{\mathbf{j}}_b + \dot{\beta}\,\hat{\mathbf{k}}_w \tag{1.49}$$

Equation 1.48 can now be expressed in a variety of ways. In the body-fixed coordinate system,

$$\left\{ \begin{array}{c} p \\ q - \dot{\alpha} \\ r \end{array} \right\} = T_{bw} \left\{ \begin{array}{c} p_w \\ q_w \\ r_w - \dot{\beta} \end{array} \right\} \tag{1.50}$$

Equivalently, solving for the body axis rates and wind axis rates respectively,

$$\begin{Bmatrix} p \\ q \\ r \end{Bmatrix} = T_{bw} \begin{Bmatrix} p_w + \dot{\alpha}\sin\beta \\ q_w + \dot{\alpha}\cos\beta \\ r_w - \dot{\beta} \end{Bmatrix} \tag{1.51}$$

$$\begin{Bmatrix} p_w \\ q_w \\ r_w \end{Bmatrix} = T_{wb} \begin{Bmatrix} p - \dot{\beta}\sin\alpha \\ q - \dot{\alpha} \\ r + \dot{\beta}\cos\alpha \end{Bmatrix} \tag{1.52}$$

1.2 Deriving the Equations of Motion

All the necessary information has now been presented in order to move towards deriving the equations of motion. Because Newton's laws only hold in an inertial reference frame (non-rotating), it is necessary to introduce the time-rate of change of a rotating reference frame. For instance, if $\vec{\mathbf{F}}$ is represented in non-inertial reference frame A, then the time rate of change as seen by the inertial reference frame N (Newtonian) is,

$$\frac{d}{dt}^{N}(\vec{\mathbf{F}}) = \frac{d}{dt}^{A}(\vec{\mathbf{F}}) + \vec{\boldsymbol{\omega}}_{A/N} \times \vec{\mathbf{F}} \tag{1.53}$$

Writing Newton's Law in vector form,

$$\vec{\mathbf{F}} = m\frac{d}{dt}^{N}(\vec{\mathbf{V}}) \tag{1.54}$$

If the velocity in Equation 1.54 is represented in the body-fixed coordinate system,

$$\vec{\mathbf{F}} = m\left(\frac{d}{dt}^{b}(\vec{\mathbf{V}}^b) + \vec{\boldsymbol{\omega}}_{b/h} \times \vec{\mathbf{V}}^b\right) \tag{1.55}$$

Defining the body axis force components, using the body axis velocity components, and incorporating matrix multiplication for the cross-product,

$$\vec{\mathbf{F}}^b = \begin{Bmatrix} F_{x_b} \\ F_{y_b} \\ F_{z_b} \end{Bmatrix} = m\begin{Bmatrix} \dot{u} \\ \dot{v} \\ \dot{w} \end{Bmatrix} + m\begin{bmatrix} 0 & -r & q \\ r & 0 & -p \\ -q & p & 0 \end{bmatrix}\begin{Bmatrix} u \\ v \\ w \end{Bmatrix} \tag{1.56}$$

Evaluating this expression, the body axis force equations become,

$$\begin{Bmatrix} F_{x_b} \\ F_{y_b} \\ F_{z_b} \end{Bmatrix} = m\begin{Bmatrix} \dot{u} + qw - rv \\ \dot{v} + ru - pw \\ \dot{w} + pv - qu \end{Bmatrix} \tag{1.57}$$

Similarly, if the velocity in Equation 1.54 is represented in the wind axis coordinate system,

$$\vec{\mathbf{F}} = m\left(\frac{d}{dt}^{w}(\vec{\mathbf{V}}^{w}) + \vec{\boldsymbol{\omega}}_{w/h} \times \vec{\mathbf{V}}^{w}\right) \tag{1.58}$$

Defining the wind axis force components, using the wind axis velocity components, and incorporating matrix multiplication for the cross-product,

$$\vec{\mathbf{F}}^{w} = \begin{Bmatrix} F_{x_w} \\ F_{y_w} \\ F_{z_w} \end{Bmatrix} = m \begin{Bmatrix} \dot{V} \\ 0 \\ 0 \end{Bmatrix} + m \begin{bmatrix} 0 & -r_w & q_w \\ r_w & 0 & -p_w \\ -q_w & p_w & 0 \end{bmatrix} \begin{Bmatrix} V \\ 0 \\ 0 \end{Bmatrix} \tag{1.59}$$

multiplying through the wind axis force equations become,

$$\begin{Bmatrix} F_{x_w} \\ F_{y_w} \\ F_{z_w} \end{Bmatrix} = m \begin{Bmatrix} \dot{V} \\ V r_w \\ -V q_w \end{Bmatrix} \tag{1.60}$$

Three differential equations are not obvious from Equation 1.60. Equation 1.52 can be used to substitute in for the appropriate wind axis rates and the wind axis force equations take the form,

$$\begin{Bmatrix} F_{x_w} \\ F_{y_w} \\ F_{z_w} \end{Bmatrix} = m \begin{Bmatrix} \dot{V} \\ V(\dot{\beta} - p\sin\alpha + r\cos\alpha) \\ V[\sin\beta(p\cos\alpha + r\sin\alpha) + \cos\beta(\dot{\alpha} - q)] \end{Bmatrix}. \tag{1.61}$$

The two sets of equations given by Equations 1.57 and 1.61 represent Newton's law, $\vec{\mathbf{F}} = m\vec{\mathbf{a}}$, for an aircraft. The identical information is present in both representations, it is the application that dictates which set of equations to use. In the chapters that follow, a particular dynamic motion will call for an introduction of yet another representation of the same information as Equations 1.57 and 1.61. As will be shown, the choice of which axis system to represent the equations of motion can greatly simplify the analysis and lend insight into the problem.

1.2.1 Applied External Forces

The forces that are applied to the aircraft in Equations 1.57 and 1.61 can be broken into three groups:

- Those due to the aerodynamic flow field about the aircraft
- Those due to gravity (i.e. weight of the aircraft)

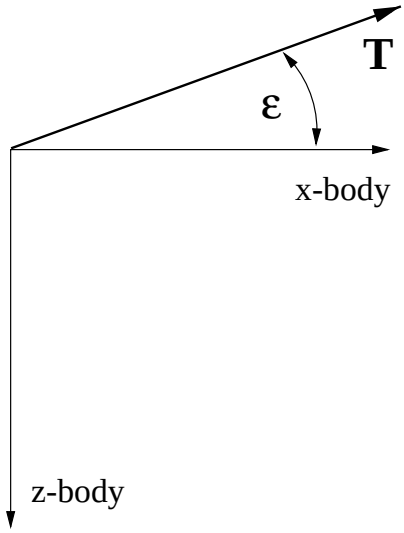

Figure 1.3: Thrust Vector

- Those due to thrust produced by the aircraft

Define the aerodynamics forces as follows,

$$\vec{\mathbf{F}}_A = \left\{ \begin{array}{c} X \\ Y \\ Z \end{array} \right\}^b \qquad \vec{\mathbf{F}}_A = \left\{ \begin{array}{c} -D \\ -Q \\ -L \end{array} \right\}^w \tag{1.62}$$

Notice the equivalence yet also notice that the two vectors are represented in two different coordinate systems. They are related through the T_{wb} transformation matrix, Equation 1.13.

Equations 1.22 and either 1.23 or 1.24 show how gravity is expressed in the body-fixed and wind axis coordinate systems respectively. Multiply the appropriate vector by the mass of the aircraft m, and the result is the component of weight in the desired direction. Therefore,

$$m\vec{\mathbf{g}} = m \left\{ \begin{array}{c} g_{1_b} \\ g_{2_b} \\ g_{3_b} \end{array} \right\}^b \qquad m\vec{\mathbf{g}} = m \left\{ \begin{array}{c} g_{1_w} \\ g_{2_w} \\ g_{3_w} \end{array} \right\}^w , \tag{1.63}$$

where the components of the gravity vector are given by Equations 1.22-1.24.

The direction of thrust will be assumed to be constant in the body-fixed coordinate system. It is further assumed that the thrust vector lies in the plane of symmetry, and the angle made with the x_b-axis is defined to be ϵ as shown in Figure 1.3. Therefore the thrust vector only has components in the x_b-axis and z_b-axis.

$$\vec{\mathbf{T}} = \left\{ \begin{array}{c} T\cos\epsilon \\ 0 \\ -T\sin\epsilon \end{array} \right\}^b \qquad \vec{\mathbf{T}} = \left\{ \begin{array}{c} T_{x_w} \\ T_{y_w} \\ T_{z_w} \end{array} \right\}^w \tag{1.64}$$

where the wind axis components of thrust are,

$$\left\{ \begin{array}{c} T_{x_w} \\ T_{y_w} \\ T_{z_w} \end{array} \right\} = T_{wb} \left\{ \begin{array}{c} T\cos\epsilon \\ 0 \\ -T\sin\epsilon \end{array} \right\} = \left\{ \begin{array}{c} \cos\beta(T\cos\epsilon\cos\alpha - T\sin\epsilon\sin\alpha) \\ \sin\beta(T\cos\epsilon\cos\alpha - T\sin\epsilon\sin\alpha) \\ -T\cos\epsilon\sin\alpha - T\sin\epsilon\cos\alpha \end{array} \right\} \tag{1.65}$$

The applied external forces in Equations 1.57 and 1.61 can now be written as,

$$\left\{ \begin{array}{c} F_{x_b} \\ F_{y_b} \\ F_{z_b} \end{array} \right\} = \left\{ \begin{array}{c} T\cos\epsilon + X + mg_{1_b} \\ Y + mg_{2_b} \\ -T\sin\epsilon + Z + mg_{3_b} \end{array} \right\} \tag{1.66}$$

where the gravity components are given by Equation 1.22, and

$$\left\{ \begin{array}{c} F_{x_w} \\ F_{y_w} \\ F_{z_w} \end{array} \right\} = \left\{ \begin{array}{c} T_{x_w} - D + mg_{1_w} \\ T_{y_w} - Q + mg_{2_w} \\ T_{z_w} - L + mg_{3_w} \end{array} \right\} \tag{1.67}$$

where the thrust components are given by Equation 1.65 and the gravity components are given by either Equation 1.23 or 1.24.

1.2.2 The Moments

Information about the how a rigid body rotates can be derived from using Newton's Law in another form that defines the moments about the point that some vector $\vec{\mathbf{r}}$ is defined from. Namely

$$\vec{\mathbf{M}} \equiv \vec{\mathbf{r}} \times \vec{\mathbf{F}} = \vec{\mathbf{r}} \times m\frac{d}{dt}^N(\vec{\mathbf{V}}) \tag{1.68}$$

To understand the right side of the equation we begin with the angular momentum.

The angular momentum of the particle in Figure 1.4 is defined to be

$$\vec{\mathbf{H}}_D = \vec{\mathbf{r}} \times \vec{\mathbf{V}}m \tag{1.69}$$

For the rigid body shown in Figure 1.5 with center of gravity G, Equation 1.69 can be written in the form

$$\vec{\mathbf{H}}_D = \int \vec{\mathbf{DP}} \times \vec{\mathbf{V}}_P \, dm \tag{1.70}$$

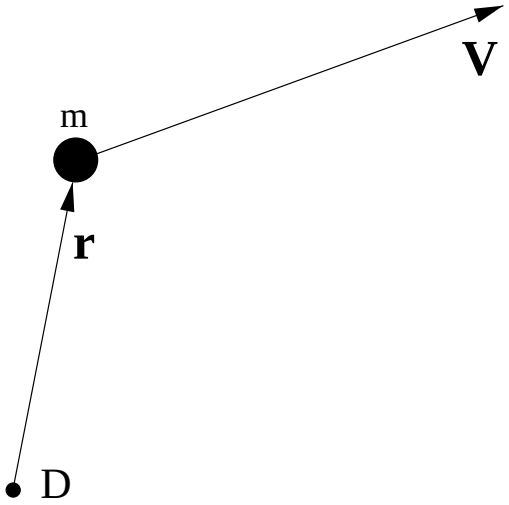

Figure 1.4: Angular Momentum

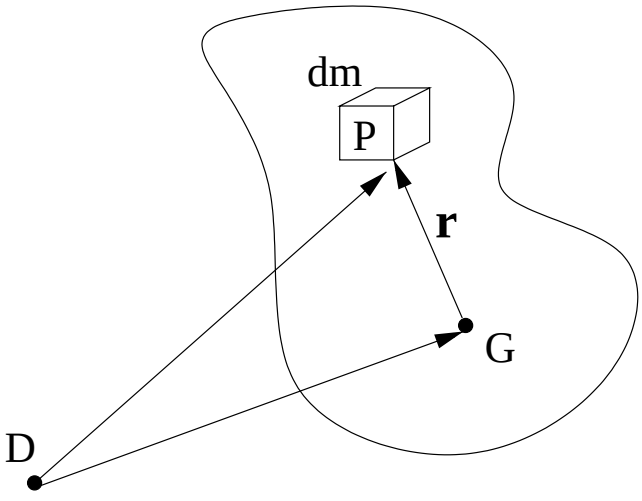

Figure 1.5: Angular Momentum for a Rigid Body

Taking the time rate of change of Equation 1.70,

$$\frac{d}{dt}(\vec{\mathbf{H}}_D) = \int \frac{d}{dt}(\vec{\mathbf{DP}}) \times \vec{\mathbf{V}}_P \, dm + \int \vec{\mathbf{DP}} \times \frac{d}{dt}(\vec{\mathbf{V}}_P) dm \tag{1.71}$$

Suppose D is now set to coincide with G, the center of gravity. The first integral in Equation 1.71 becomes,

$$\begin{aligned}
\int \frac{d}{dt}(\vec{\mathbf{DP}}) \times \vec{\mathbf{V}}_P dm &= \int \frac{d}{dt}\vec{\mathbf{r}} \times \vec{\mathbf{V}}_P dm & (1.72)\\
&= \int (\vec{\boldsymbol{\omega}} \times \vec{\mathbf{r}}) \times (\vec{\mathbf{V}}_G + \vec{\boldsymbol{\omega}} \times \vec{\mathbf{r}}) dm & (1.73)\\
&= \left(\vec{\boldsymbol{\omega}} \times \int \vec{\mathbf{r}} dm\right) \times \vec{\mathbf{V}}_G + \int (\vec{\boldsymbol{\omega}} \times \vec{\mathbf{r}}) \times (\vec{\boldsymbol{\omega}} \times \vec{\mathbf{r}}) dm & (1.74)\\
&= 0 & (1.75)
\end{aligned}$$

The integral in the first term of Equation 1.74 is zero since the integral is being performed about the center of mass. The second integral is zero since it is a vector crossed with itself. Likewise, when D is set to G, the second integral of Equation 1.71 is the right side of Equation 1.68. Therefore,

$$\vec{\mathbf{M}}_G = \frac{d}{dt}^N (\vec{\mathbf{H}}_G) \tag{1.76}$$

Equation 1.70 can also be written in the following manner.

$$\begin{aligned}
\vec{\mathbf{H}}_D &= \int \vec{\mathbf{DP}} \times \vec{\mathbf{V}}_P dm & (1.77)\\
&= \int \left[(\vec{\mathbf{DG}} + \vec{\mathbf{r}}) \times (\vec{\mathbf{V}}_G + \vec{\boldsymbol{\omega}} \times \vec{\mathbf{r}})\right] dm & (1.78)\\
&= \vec{\mathbf{DG}} \times \vec{\mathbf{V}}_G \int dm + \vec{\mathbf{DG}} \times \left(\vec{\boldsymbol{\omega}} \times \int \vec{\mathbf{r}} dm\right) + \int \vec{\mathbf{r}} dm \times \vec{\mathbf{V}}_G + \int \vec{\mathbf{r}} \times (\vec{\boldsymbol{\omega}} \times \vec{\mathbf{r}}) dm & (1.79)\\
&= \vec{\mathbf{DG}} \times m\vec{\mathbf{V}}_G + \mathbf{I}_G \cdot \vec{\boldsymbol{\omega}} & (1.80)
\end{aligned}$$

In the special case when D is set to G the angular momentum can be written as,

$$\vec{\mathbf{H}}_G = \mathbf{I}_G \cdot \vec{\boldsymbol{\omega}} \tag{1.81}$$

Where $\mathbf{I}_G$ represents the moment of inertia tensor.

Keeping in mind that Equation 1.76 is only valid for moments about the center of gravity, the G subscript is dropped. If $\vec{\mathbf{H}}$ is expressed in a body-fixed coordinate system

$$\vec{\mathbf{M}} = \frac{d}{dt}^b (\vec{\mathbf{H}}) + \vec{\boldsymbol{\omega}}_{b/h} \times \vec{\mathbf{H}} \tag{1.82}$$

The inertia tensor, $\mathbf{I}$, in a body-fixed coordinate system is constant. Therefore, using Equation 1.81 the moment equations can be written for a rigid body in the form,

$$\vec{\mathbf{M}} = \mathbf{I}^b \cdot \frac{d}{dt}^b (\vec{\boldsymbol{\omega}}_{b/h}) + \vec{\boldsymbol{\omega}}_{b/h} \times \mathbf{I}^b \cdot \vec{\boldsymbol{\omega}}_{b/h} \tag{1.83}$$

solving for the time rate of change of $\vec{\boldsymbol{\omega}}_{b/h}$,

$$\frac{d}{dt}^b (\vec{\boldsymbol{\omega}}_{b/h}) = (\mathbf{I}^b)^{-1} \left[\vec{\mathbf{M}} - \vec{\boldsymbol{\omega}}_{b/h} \times \mathbf{I}^b \cdot \vec{\boldsymbol{\omega}}_{b/h} \right] \tag{1.84}$$

Introducing the body components of the above vectors, assuming that thrust acts through the center of gravity, using matrix multiplication for the cross product, and defining $\Gamma = I_{xx} I_{zz} - I_{xz}^2$,

$$\begin{aligned}
\begin{Bmatrix} \dot{p} \\ \dot{q} \\ \dot{r} \end{Bmatrix} &= \begin{bmatrix} \frac{I_{zz}}{\Gamma} & 0 & \frac{I_{xz}}{\Gamma} \\ 0 & \frac{1}{I_{yy}} & 0 \\ \frac{I_{xz}}{\Gamma} & 0 & \frac{I_{xx}}{\Gamma} \end{bmatrix} \left[\begin{Bmatrix} L \\ M \\ N \end{Bmatrix} \right. \\
&\quad \left. - \begin{bmatrix} 0 & -r & q \\ r & 0 & -p \\ -q & p & 0 \end{bmatrix} \begin{bmatrix} I_{xx} & 0 & -I_{xz} \\ 0 & I_{yy} & 0 \\ -I_{xz} & 0 & I_{zz} \end{bmatrix} \begin{Bmatrix} p \\ q \\ r \end{Bmatrix} \right] \\
&= \begin{Bmatrix} \frac{I_{zz}}{\Gamma}\{L + (I_{yy} - I_{zz})rq + I_{xz}pq\} \\ \qquad + \frac{I_{xz}}{\Gamma}\{N + (I_{xx} - I_{yy})pq - I_{xz}rq\} \\ \frac{1}{I_{yy}}\{M - I_{xz}(p^2 - r^2) - (I_{zz} - I_{xx})pr\} \\ \frac{I_{xz}}{\Gamma}\{L + (I_{yy} - I_{zz})rq + I_{xz}pq\} \\ \qquad + \frac{I_{xx}}{\Gamma}\{N + (I_{xx} - I_{yy})pq - I_{xz}rq\} \end{Bmatrix}
\end{aligned} \tag{1.85}$$

Similarly if the angular momentum $\vec{\mathbf{H}}$ in Equation 1.76 is expressed in the wind axis coordinate system,

$$\vec{\mathbf{M}} = \frac{d}{dt}^w (\vec{\mathbf{H}}) + \vec{\boldsymbol{\omega}}_{w/h} \times \vec{\mathbf{H}}$$

This representation of the moment equation does not appear frequently since, unlike in the body-fixed axis, the inertia tensor is not constant in the wind axis coordinate system. The moment equations for the wind axis coordinate system can be written in the form,

$$\vec{\mathbf{M}} = \frac{d}{dt}^w (\mathbf{I}^w) \cdot \vec{\boldsymbol{\omega}}_{w/h} + \mathbf{I}^w \cdot \frac{d}{dt}^w (\vec{\boldsymbol{\omega}}_{w/h}) + \vec{\boldsymbol{\omega}}_{w/h} \times \mathbf{I} \cdot \vec{\boldsymbol{\omega}}_{w/h} \tag{1.86}$$

All the terms in the above equation are quite attainable except the time rate of change of the wind axis inertia tensor. Concentrating on this particular term,

$$\mathbf{I}^w = T_{wb}\, \mathbf{I}^b\, T_{wb}^T \tag{1.87}$$

By taking the time rate of change of the above equation, terms involving $\dot{\alpha}$ and $\dot{\beta}$ are introduced. In the general case, the time rate of change of the wind axis inertia matrix can be quite lengthy. The (1,1)-term is printed here,

$$\begin{aligned}\dot{\mathbf{I}}^w(1,1) =& 2\dot{\beta}\sin\beta\cos\beta\big[-I_{xx}\cos^2\alpha + 2I_{xz}\sin\alpha\cos\alpha + I_{yy} - I_{zz}\sin^2\alpha\big] \\ &+ 2\dot{\alpha}\cos^2\beta\big[-I_{xx}\sin\alpha\cos\alpha - I_{xz}\cos(2\alpha) + I_{zz}\sin\alpha\cos\alpha\big]\end{aligned} \tag{1.88}$$

Every term in the time rate of change of the wind axis inertia matrix is similar in complexity to the expression above. Therefore, evaluating Equation 1.86 would be best suited for the computer. The moments applied to the body represented in the wind axis coordinate system can be written as $\vec{\mathbf{M}}^w = T_{wb}\vec{\mathbf{M}}^b$. The advantage of Equation 1.86 is that one would have the time rate of change of the wind axis rates directly available. These equations could be integrated in time and the kinematics could directly be calculated using Equation 1.47. Due to simplicity gained from a constant inertia tensor, the moment equations are usually represented in some body-fixed axis system.

1.3 The Equations of Motion Collected

Force Equations

Using Equations 1.57 and 1.66, the body axis force equations become,

$$\begin{aligned}\dot{u} &= \frac{1}{m}(T\cos\epsilon + X) + rv - qw + g_{1_b} \\ \dot{v} &= \frac{Y}{m} + pw - ru + g_{2_b} \\ \dot{w} &= \frac{1}{m}(-T\sin\epsilon + Z) + qu - pv + g_{3_b}\end{aligned} \tag{1.89}$$

Using Equations 1.61 and 1.67, the wind axis force equations become,

$$\begin{aligned}\dot{V} &= \frac{1}{m}(\cos\beta(T\cos\epsilon\cos\alpha - T\sin\epsilon\sin\alpha) - D) + g_{1_w} \\ \dot{\beta} &= \frac{1}{mV}(\sin\beta(T\cos\epsilon\cos\alpha - T\sin\epsilon\sin\alpha) - Q) \\ &\quad + p\sin\alpha - r\cos\alpha + \frac{g_{2_w}}{V} \\ \dot{\alpha} &= \frac{1}{mV\cos\beta}(-T\cos\epsilon\sin\alpha - T\sin\epsilon\cos\alpha - L) \\ &\quad - \tan\beta(p\cos\alpha + r\sin\alpha) + q + \frac{g_{3_w}}{V\cos\beta}\end{aligned} \tag{1.90}$$

The gravity components are given by Equation 1.22 and either Equation 1.23 or 1.24

$$\left\{ \begin{array}{c} g_{1_b} \\ g_{2_b} \\ g_{3_b} \end{array} \right\} = \left\{ \begin{array}{c} -g\sin\theta \\ g\sin\phi\cos\theta \\ g\cos\phi\cos\theta \end{array} \right\} \tag{1.22}$$

$$\left\{ \begin{array}{c} g_{1_w} \\ g_{2_w} \\ g_{3_w} \end{array} \right\} = \left\{ \begin{array}{c} -g\sin\gamma \\ g\sin\mu\cos\gamma \\ g\cos\mu\cos\gamma \end{array} \right\} \tag{1.23}$$

$$= \left\{ \begin{array}{c} g(-\cos\alpha\cos\beta\sin\theta + \sin\beta\sin\phi\cos\theta + \sin\alpha\cos\beta\cos\phi\cos\theta) \\ g(\cos\alpha\sin\beta\sin\theta + \cos\beta\sin\phi\cos\theta - \sin\alpha\sin\beta\cos\phi\cos\theta) \\ g(\sin\alpha\sin\theta + \cos\alpha\cos\phi\cos\theta) \end{array} \right\} \tag{1.24}$$

Moment Equations

Introducing the convention used in Ref [12] for the constants involving the moments of inertias for a body-fixed coordinate system, Equation 1.85 becomes

$$\begin{array}{rcl} \dot{p} & = & (c_1 r + c_2 p)q + c_3 L + c_4 N \\ \dot{q} & = & c_5 pr - c_6(p^2 - r^2) + c_7 M \\ \dot{r} & = & (c_8 p - c_2 r)q + c_4 L + c_9 N \end{array} \tag{1.91}$$

with

$$\begin{array}{ll} c_1 = \dfrac{(I_{yy} - I_{zz})I_{zz} - I_{xz}^2}{\Gamma} & c_2 = \dfrac{(I_{xx} - I_{yy} + I_{zz})I_{xz}}{\Gamma} \\ c_3 = \dfrac{I_{zz}}{\Gamma} & c_4 = \dfrac{I_{xz}}{\Gamma} \\ c_5 = \dfrac{I_{zz} - I_{xx}}{I_{yy}} & c_6 = \dfrac{I_{xz}}{I_{yy}} \\ c_7 = \dfrac{1}{I_{yy}} & c_8 = \dfrac{(I_{xx} - I_{yy})I_{xx} + I_{xz}^2}{\Gamma} \\ c_9 = \dfrac{I_{xx}}{\Gamma} & \Gamma = I_{xx}I_{zz} - I_{xz}^2 \end{array} \tag{1.92}$$

Kinematic Equations

$$\left\{ \begin{array}{c} \dot{\phi} \\ \dot{\theta} \\ \dot{\psi} \end{array} \right\} = \left[\begin{array}{ccc} 1 & \sin\phi\tan\theta & \cos\phi\tan\theta \\ 0 & \cos\phi & -\sin\phi \\ 0 & \sin\phi\sec\theta & \cos\phi\sec\theta \end{array} \right] \left\{ \begin{array}{c} p \\ q \\ r \end{array} \right\} \tag{1.45}$$

Using Equations 1.47 and 1.52,

$$\begin{Bmatrix} \dot{\mu} \\ \dot{\gamma} \\ \dot{\chi} \end{Bmatrix} = \begin{bmatrix} 1 & \sin\mu\tan\gamma & \cos\mu\tan\gamma \\ 0 & \cos\mu & -\sin\mu \\ 0 & \sin\mu\sec\gamma & \cos\mu\sec\gamma \end{bmatrix} T_{wb} \begin{Bmatrix} p - \dot{\beta}\sin\alpha \\ q - \dot{\alpha} \\ r + \dot{\beta}\cos\alpha \end{Bmatrix}$$

This chapter has derived the equations of motion for an aircraft in two different representations, the body-fixed axis system and the wind axis system. Both representations completely house the identical dynamics and both representations are commonly used throughout the field of aircraft dynamics. Different insight can be gained when using one representation over the the other, and this insight is completely defined by the application in question. The next chapter will introduce yet another and new coordinate system. The equations of motion will be derived with the new coordinate system as the basis for derivation.

Chapter 2

Rotational Reference Frame

As mentioned in Chapter 1, a coordinate system will be introduced to lend insight to the analysis of dynamic motions of an aircraft. The system proposed is not a good choice for the complete flight envelope of an aircraft for reasons that will become obvious, yet it is proposed for the analytical applications that may lend understanding into the drivers and causes of particular motions.

The rotational coordinate system, (x_r, y_r, z_r), has it's origin fixed at the center of mass of the aircraft. It has the x-axis pointing along the same line as the instantaneous rotation vector, $\vec{\boldsymbol{\omega}}_{b/h}$, but its positive direction always being in the front hemisphere of the body-fixed coordinate system (see Ref [6]). The z-axis is in the plane of symmetry of the aircraft pointing out the bottom of the aircraft, and the y-axis then completes the right-hand rule.

2.1 Coordinate System Relationships

With the introduction of the rotational coordinate system, relationships can be derived between it and the coordinate systems defined in Sec 1.1.1. Figure 2.1 shows how the the body-fixed coordinate system relates to the rotational and wind coordinate systems.

Body-fixed and Rotational Relationship

The rotation from the body-fixed to the rotational axes coordinate system is analogous to the body-fixed/wind relationship shown in Section 1.1.2. The relationship can be fully described by only two fundamental transformations, a 2-3 rotation. The angles are $[\lambda, -\eta]$;

1. Rotate through an angle $-\eta$ about the y_b-axis to an intermediate coordinate system, (x', y', z').

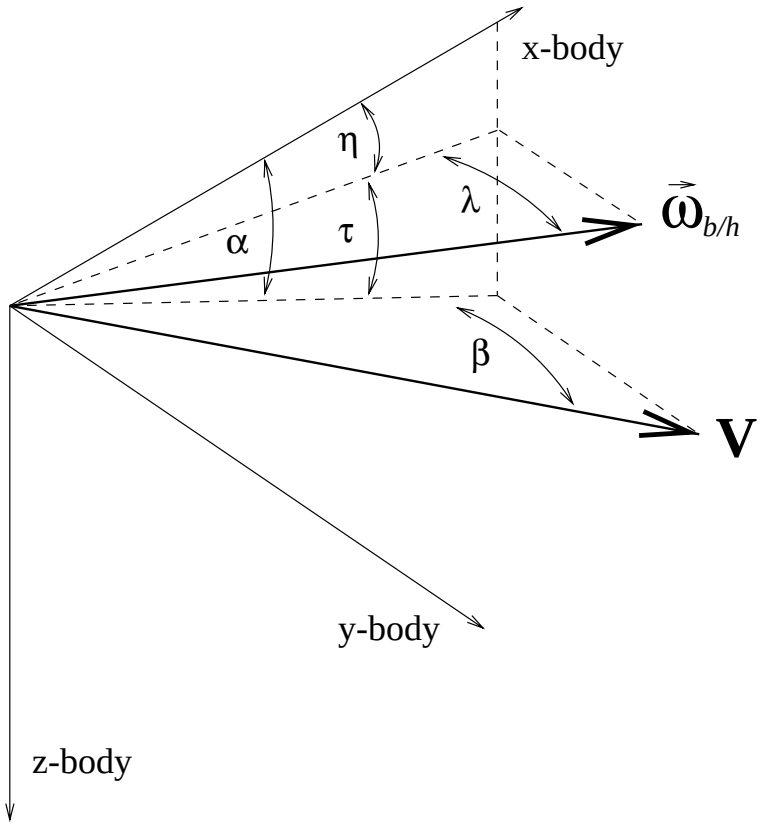

Figure 2.1: Rotational Coordinate System

2. Then rotate through an angle λ about the z'-axis to reach the rotational axes coordinate system, (x_r, y_r, z_r)

Therefore,

$$T_{rb} = T_{z_\lambda} T_{y_{-\eta}} \tag{2.1}$$

Evaluating the above expression gives the transformation from the body-fixed axis system to the rotational axis system.

$$T_{rb} = \begin{bmatrix} \cos\eta\cos\lambda & \sin\lambda & \sin\eta\cos\lambda \\ -\cos\eta\sin\lambda & \cos\lambda & -\sin\eta\sin\lambda \\ -\sin\eta & 0 & \cos\eta \end{bmatrix} \tag{2.2}$$

Wind Axes and Rotational Relationship

As mentioned in Sec 1.1.2, two coordinate systems can be related by any three independent fundamental rotations. The rotation from the wind axes to the rotational coordinate system can be obtained by a 3-2-3 rotation. These rotations can be easily visualized in Figure 2.1 and are given by the angles $[\lambda, \tau, -\beta]$,

1. Rotate through an angle $-\beta$ about the z_w-axis to an intermediate coordinate system, (x', y', z').
2. Then rotate through an angle τ about the y'-axis to an intermediate coordinate system, (x'', y'', z'').
3. Finally, rotate through an angle λ about the z''-axis to reach the rotational axis system, (x_r, y_r, z_r)

Therefore,

$$T_{rw} = T_{z_\lambda} T_{y_\tau} T_{z_{-\beta}} \tag{2.3}$$

Evaluating the above expression gives the transformation matrix from the wind axis system to the rotational axis system,

$$T_{rw} = \begin{bmatrix} \cos\lambda\cos\tau\cos\beta + \sin\lambda\sin\beta & -\cos\lambda\cos\tau\sin\beta + \sin\lambda\cos\beta & -\cos\lambda\sin\tau \\ -\sin\lambda\cos\tau\cos\beta + \cos\lambda\sin\beta & \sin\lambda\cos\tau\sin\beta + \cos\lambda\cos\beta & \sin\lambda\sin\tau \\ \sin\tau\cos\beta & -\sin\tau\sin\beta & \cos\tau \end{bmatrix} \tag{2.4}$$

Horizontal and Rotational Relationship

The relationship between the local horizontal and the rotational coordinate systems will also follow the convention used in Sec 1.1.2. The three new angles will be defined as the corresponding capital Greek letter of the Euler angles, $[\Phi, \Theta, \Psi]$;

$$T_{rh} = T_{x_\Phi} T_{y_\Theta} T_{z_\Psi} \tag{2.5}$$

Evaluating the above expression gives the transformation matrix from the local horizontal axis system to the rotational axis system.

$$T_{rh} = \begin{bmatrix} \cos\Theta\cos\Psi & \cos\Theta\sin\Psi & -\sin\Theta \\ \sin\Phi\sin\Theta\cos\Psi - \cos\Phi\sin\Psi & \sin\Phi\sin\Theta\sin\Psi + \cos\Phi\cos\Psi & \sin\Phi\cos\Theta \\ \cos\Phi\sin\Theta\cos\Psi + \sin\Phi\sin\Psi & \cos\Phi\sin\Theta\sin\Psi - \sin\Phi\cos\Psi & \cos\Phi\cos\Theta \end{bmatrix} \tag{2.6}$$

Another representation for the transformation between local horizontal axes and rotational axes exists that relates the eight angles $[\eta, \lambda, \Phi, \Theta, \Psi, \phi, \theta, \psi]$ of which only five are independent. Namely,

$$T_{rh}(\Phi, \Theta, \Psi) = T_{rb}(\eta, \lambda)\, T_{bh}(\phi, \theta, \psi) \tag{2.7}$$

This relationship will be used later for a reduced system. Equating terms from the matrices on either side of Equation 2.7 will give the the three independent spherical relationships between five independent angles and the remaining three dependent angles (also see Ref [6]).

2.2 Relating Information Among the Systems

The body axis rotation vector, $\vec{\boldsymbol{\omega}}_{b/h}$, is most naturally expressed in the rotational coordinate system, (x_r, y_r, z_r). By definition,

$$\vec{\boldsymbol{\omega}}^r_{b/h} = \begin{Bmatrix} \Omega \\ 0 \\ 0 \end{Bmatrix} \tag{2.8}$$

The inverse of the matrix in Equation 2.2 can be used to relate the body axis rates and Ω,

$$\begin{Bmatrix} p \\ q \\ r \end{Bmatrix} = T_{br} \begin{Bmatrix} \Omega \\ 0 \\ 0 \end{Bmatrix} = \begin{Bmatrix} \Omega\cos\eta\cos\lambda \\ \Omega\sin\lambda \\ \Omega\sin\eta\cos\lambda \end{Bmatrix} \tag{2.9}$$

Equation 2.9 gives the relationship between the body-fixed components of the rotation vector and the rotational axis variables. Namely,

$$\tan\eta = \frac{r}{p} \tag{2.10}$$

$$\sin\lambda = \frac{q}{\Omega} \tag{2.11}$$

$$\Omega^2 = p^2 + q^2 + r^2 \tag{2.12}$$

also from Figure 2.1,

$$\alpha = \eta + \tau \tag{2.13}$$

It is also useful to have the body axis gravity components in terms these new variables. In addition to the relationship in Equation 1.22,

$$\vec{\mathbf{g}}^b = T_{br}T_{rh}\vec{\mathbf{g}}^h = \left\{ \begin{array}{c} g(-\sin\Theta\cos\eta\cos\lambda - \sin\Phi\cos\Theta\cos\eta\sin\lambda - \cos\Phi\cos\Theta\sin\eta) \\ g(\sin\Phi\cos\Theta\cos\lambda - \sin\Theta\sin\lambda) \\ g(-\sin\Theta\sin\eta\cos\lambda - \sin\Phi\cos\Theta\sin\eta\sin\lambda + \cos\Phi\cos\Theta\cos\eta) \end{array} \right\} \tag{2.14}$$

2.3 Rotational Kinematics

It is beneficial to step back and examine what is being done. The rotational coordinate system is a coordinate system that is aligned along on the angular rate vector of *another* coordinate system, namely $\vec{\boldsymbol{\omega}}_{b/h}$. The rotational coordinate system has it's *own* angular rate vector that expresses how it rotates with respect to inertial space, namely $\vec{\boldsymbol{\omega}}_{r/h}$. These two angular rate vectors are *different*, and differ by the relative angular rate between the two systems.

The kinematics are derived in the same way as in Sec 1.1.6.

$$\vec{\boldsymbol{\omega}}^r_{r/h} = \left\{ \begin{array}{c} p_r \\ q_r \\ r_r \end{array} \right\} = \left[\begin{array}{ccc} 1 & 0 & -\sin\Theta \\ 0 & \cos\Phi & \cos\Theta\sin\Phi \\ 0 & -\sin\Phi & \cos\Theta\cos\Phi \end{array} \right] \left\{ \begin{array}{c} \dot{\Phi} \\ \dot{\Theta} \\ \dot{\Psi} \end{array} \right\} \tag{2.15}$$

The inverse relationship gives,

$$\left\{ \begin{array}{c} \dot{\Phi} \\ \dot{\Theta} \\ \dot{\Psi} \end{array} \right\} = \left[\begin{array}{ccc} 1 & \sin\Phi\tan\Theta & \cos\Phi\tan\Theta \\ 0 & \cos\Phi & -\sin\Phi \\ 0 & \sin\Phi\sec\Theta & \cos\Phi\sec\Theta \end{array} \right] \left\{ \begin{array}{c} p_r \\ q_r \\ r_r \end{array} \right\} \tag{2.16}$$

It is useful to relate the rotational axis rates to the body-fixed axis rates.

$$\vec{\boldsymbol{\omega}}_{r/h} = \vec{\boldsymbol{\omega}}_{r/b} + \vec{\boldsymbol{\omega}}_{b/h} \tag{2.17}$$

The new term in Equation 2.17 is most naturally expressed in two coordinate systems,

$$\vec{\boldsymbol{\omega}}_{r/b} = -\dot{\eta}\,\hat{\mathbf{j}}_b + \dot{\lambda}\,\hat{\mathbf{k}}_r \tag{2.18}$$

Equation 2.17 can now be expressed in a variety of ways. In the rotational coordinate system,

$$\left\{ \begin{array}{c} p_r - \Omega \\ q_r \\ r_r - \dot{\lambda} \end{array} \right\} = T_{rb} \left\{ \begin{array}{c} 0 \\ -\dot{\eta} \\ 0 \end{array} \right\} \tag{2.19}$$

Equivalently, solving for the rotational axis rates,

$$\left\{ \begin{array}{c} p_r \\ q_r \\ r_r \end{array} \right\} = \left\{ \begin{array}{c} \Omega - \dot{\eta}\sin\lambda \\ -\dot{\eta}\cos\lambda \\ \dot{\lambda} \end{array} \right\} \tag{2.20}$$

2.4 Rotational Force and Moment Equations

A rigorous derivation will follow showing the steps to achieve a new set of force and moment equations. Taking the time rate of change of Equation 2.12, using Equation 2.9 to substitute for the body axis rates, and dividing both sides by two,

$$\dot{\Omega} = \dot{p}\cos\eta\cos\lambda + \dot{q}\sin\lambda + \dot{r}\sin\eta\cos\lambda \tag{2.21}$$

Taking the time rate of change of Equations 2.10 and 2.11 respectively,

$$\begin{aligned} \dot{\eta}\sec^2\eta &= \frac{\dot{r}}{p} - \dot{p}\frac{r}{p^2} \\ &= \frac{1}{p}(\dot{r} - \dot{p}\tan\eta) \\ \dot{\eta} &= \frac{\cos\eta}{\Omega\cos\lambda} \end{aligned} \tag{2.22}$$

$$\begin{aligned} \dot{\lambda}\cos\lambda &= \frac{\dot{q}}{\Omega} - \dot{\Omega}\frac{q}{\Omega^2} \\ &= \frac{1}{\Omega}(\dot{q} - \dot{\Omega}\sin\lambda) \\ \dot{\lambda} &= \frac{1}{\Omega\cos\lambda}(\dot{q} - \dot{\Omega}\sin\lambda) \end{aligned} \tag{2.23}$$

The next step is to replace all the time rate of change variables on the right side of Equations 2.21-2.23. Equation 2.9 is used to substitute for the (p, q, r)'s on the right side of Equation 1.91,

$$\left\{ \begin{array}{c} \dot{p} \\ \dot{q} \\ \dot{r} \end{array} \right\} = \left\{ \begin{array}{c} \Omega^2\sin\lambda\cos\lambda(c_1\sin\eta + c_2\cos\eta) + c_3 L + c_4 N \\ \Omega^2\cos^2\lambda(\frac{c_5}{2}\sin 2\eta - c_6\cos 2\eta) + c_7 M \\ \Omega^2\sin\lambda\cos\lambda(c_8\cos\eta + c_2\sin\eta) + c_4 L + c_9 N \end{array} \right\} \tag{2.24}$$

equivalently,

$$\left\{ \begin{array}{c} \dot{p} \\ \dot{q} \\ \dot{r} \end{array} \right\} = \left\{ \begin{array}{c} \frac{\Omega^2}{2} \sin 2\lambda (c_1 \sin\eta + c_2 \cos\eta) + c_3 L + c_4 N \\ \Omega^2 \cos^2\lambda (\frac{c_5}{2} \sin 2\eta - c_6 \cos 2\eta) + c_7 M \\ \frac{\Omega^2}{2} \sin 2\lambda (c_8 \cos\eta + c_2 \sin\eta) + c_4 L + c_9 N \end{array} \right\} \tag{2.25}$$

Substituting for the time rates of change, Equations 2.21-2.23 become the moment equations represented in the new coordinate system,

$$\begin{aligned}
\dot{\Omega} &= \Omega^2 \sin\lambda \cos^2\lambda \left[\frac{c_1 + c_5 + c_8}{2} \sin 2\eta + (c_2 - c_6) \cos 2\eta \right] \\
&\quad + c_7 M \sin\lambda + (c_3 L + c_4 N) \cos\eta \cos\lambda + (c_4 L + c_9 N) \sin\eta \cos\lambda \qquad (2.26) \\
\dot{\eta} &= \Omega \sin\lambda \big(c_8 \cos^2\eta - 2 c_2 \sin\eta \cos\eta - c_1 \sin^2\eta \big) \\
&\quad + \frac{1}{\Omega \cos\lambda} \Big[(c_4 L + c_9 N) \cos\eta - (c_3 L + c_4 N) \sin\eta \Big] \qquad (2.27) \\
\dot{\lambda} &= \Omega \cos^3\lambda \left(\frac{c_5}{2} \sin 2\eta - c_6 \cos 2\eta \right) + \frac{c_7 M \cos\lambda}{\Omega} \\
&\quad - \Omega \sin^2\lambda \cos\lambda \left[\frac{c_1 + c_8}{2} \sin 2\lambda + c_2 \cos 2\lambda \right] \\
&\quad - \frac{\cos\eta \sin\lambda}{\Omega} \Big(c_3 L + c_4 N \Big) - \frac{\sin\eta \sin\lambda}{\Omega} \Big(c_4 L + c_9 N \Big) \qquad (2.28)
\end{aligned}$$

Equations 2.26-2.28 are a different representation of the body-fixed moment equations given by Equation 1.91. It is important to note that the aerodynamic moments L, M, N and the constants involving the inertia terms c_i are all still the associated values for the body-fixed axis system. Equations 2.26-2.28 are still body-fixed moment equations that describe how $\vec{\boldsymbol{\omega}}_{b/h}$ changes in time.

The wind axis force equations, Equation 1.90, are modified as follows. Using Equation 2.9 and Equation 2.13,

$$\begin{aligned}
p \sin\alpha - r \cos\alpha &= \Omega \cos\lambda \big(\cos\eta \sin(\eta + \tau) - \sin\eta \cos(\eta + \tau) \big) \\
&= \Omega \cos\lambda \big(\cos\eta (\sin\eta \cos\tau + \cos\eta \sin\tau) - \sin\eta (\cos\eta \cos\tau - \sin\eta \sin\tau) \big) \\
&= \Omega \cos\lambda \big(\sin\tau (\sin^2\eta + \cos^2\eta) \big) \\
&= \Omega \cos\lambda \sin\tau \qquad (2.29) \\
p \cos\alpha + r \sin\alpha &= \Omega \cos\lambda \big(\cos\eta \cos(\eta + \tau) + \sin\eta \sin(\eta + \tau) \big) \\
&= \Omega \cos\lambda \big(\cos\eta (\cos\eta \cos\tau - \sin\eta \sin\tau) + \sin\eta (\sin\eta \cos\tau + \cos\eta \sin\tau) \big) \\
&= \Omega \cos\lambda \big(\cos\tau (\sin^2\eta + \cos^2\eta) \big) \\
&= \Omega \cos\lambda \cos\tau \qquad (2.30)
\end{aligned}$$

Taking the time rate of change of Equation 2.13,

$$\dot{\tau} = \dot{\alpha} - \dot{\eta} \tag{2.31}$$

The force equations in the new coordinate system can then be written as,

$$\dot{V} = \frac{1}{m}\Big(\cos\beta(T\cos\epsilon\cos(\eta+\tau) - T\sin\epsilon\sin(\eta+\tau)) - D\Big) + g_{1_w} \tag{2.32}$$

$$\dot{\beta} = \frac{1}{mV}\Big(\sin\beta(T\cos\epsilon\cos(\eta+\tau) - T\sin\epsilon\sin(\eta+\tau)) - Q\Big) + \Omega\cos\lambda\sin\tau + \frac{g_{2_w}}{V} \tag{2.33}$$

$$\dot{\tau} = \frac{1}{mV\cos\beta}\Big(-T\cos\epsilon\sin(\eta+\tau) - T\sin\epsilon\cos(\eta+\tau) - L\Big)$$
$$-\Omega\cos\lambda\cos\tau\tan\beta + \Omega\sin\lambda + \frac{g_{3_w}}{V\cos\beta} - \dot{\eta} \tag{2.34}$$

where the $\dot{\eta}$ in Equation 2.34 is given by Equation 2.27.

Using Equations 1.45 and 2.9, the kinematics are then written as

$$\begin{Bmatrix} \dot{\phi} \\ \dot{\theta} \\ \dot{\psi} \end{Bmatrix} = \begin{bmatrix} 1 & \sin\phi\tan\theta & \cos\phi\tan\theta \\ 0 & \cos\phi & -\sin\phi \\ 0 & \sin\phi\sec\theta & \cos\phi\sec\theta \end{bmatrix} \begin{Bmatrix} \Omega\cos\eta\cos\lambda \\ \Omega\sin\lambda \\ \Omega\sin\eta\cos\lambda \end{Bmatrix} \tag{2.35}$$

The kinematics can also be represented with two other sets of angles, namely (μ, γ, χ) or (Φ, Θ, Ψ). This representation of the kinematics is valid yet, in the general case, will introduce time rates of change $(\dot{\alpha}, \dot{\beta})$ and $(\dot{\eta}, \dot{\lambda})$ respectively on the right hand side of the kinematic equations. Bringing these time rates of change on the right hand side is not desirable for analytical purposes yet it is not an issue if running simulations using computers.

2.4.1 Concerns

Upon inspection of the equations of motion proposed, there are various problems that arise. Many of the problems are analogous to those encountered in the wind axis coordinate system. For example, if total velocity, V, or the x_b-component of velocity, u, were ever zero α and β become undefined. These conditions are only likely for a helicopter or a tilt rotor aircraft. For the system in question,

- Equations 2.27 and 2.28 become undefined when Ω is zero
- λ is undefined when Ω is zero, Equation 2.11
- If the rotation vector is comprised of pure pitch rate, with roll and yaw rates zero, then λ is 90 degrees and Equations 2.27 and 2.28 are undefined as well
- Motion consisting of pure yaw rate can not be described as η is undefined

As stated at the beginning of the chapter, *dynamic motions* are of interest. Therefore, Ω being zero is not an issue although care must be taken as Ω can go through zero, and generally does. Motion with pure a longitudinal angular rate is not an issue since a subset of the above equations can be used to analyze that particular motion. Knowing that λ is 90 degrees and η is zero, and both angles are fixed, two degrees of freedom are removed, thus allowing the removal of the equations that cause difficulty. A similar procedure can be performed for the analysis of a flat spin. An example follows that shows how a subset of dynamic motions can be extracted from the equations of motion proposed above.

2.4.2 Special Case: $\vec{\Omega}$ fixed along $\vec{\mathbf{V}}$

Consider the case where the rotation vector lines up with the velocity vector at all times. This condition can easily be visualized by considering todays basic rotary balance wind tunnel testing techniques. From Figure 2.1, it can be seen that

$$\tau = 0 \quad (\eta = \alpha) \tag{2.36}$$
$$\lambda = \beta \tag{2.37}$$

And taking the time rate of change,

$$\dot{\tau} = 0 \quad (\dot{\eta} = \dot{\alpha}) \tag{2.38}$$
$$\dot{\lambda} = \dot{\beta} \tag{2.39}$$

These conditions remove two degrees of freedom, complete dynamics can be described by a 4DOF model. Namely,

$$\dot{V} = \frac{1}{m}\Big(\cos\beta(T\cos\epsilon\cos\eta - T\sin\epsilon\sin\eta) - D\Big) + g_{1_w} \tag{2.40}$$
$$\dot{\beta} = \frac{1}{mV}\Big(\sin\beta(T\cos\epsilon\cos\eta - T\sin\epsilon\sin\eta) - Q\Big) + \frac{g_{2_w}}{V} \tag{2.41}$$
$$\begin{aligned}\dot{\Omega} &= \Omega^2\sin\beta\cos^2\beta\left[\frac{c_1 + c_5 + c_8}{2}\sin 2\eta + (c_2 - c_6)\cos 2\eta\right] \\ &\quad + c_7 M\sin\beta + (c_3 L + c_4 N)\cos\eta\cos\beta + (c_4 L + c_9 N)\sin\eta\cos\beta\end{aligned} \tag{2.42}$$
$$\begin{aligned}\dot{\eta} &= \Omega\sin\beta\big(c_8\cos^2\eta - 2c_2\sin\eta\cos\eta - c_1\sin^2\eta\big) \\ &\quad + \frac{1}{\Omega\cos\beta}\Big[(c_4 L + c_9 N)\cos\eta - (c_3 L + c_4 N)\sin\eta\Big]\end{aligned} \tag{2.43}$$

Two algebraic relations come from $\dot{\tau} = 0$ (or $\dot{\eta} = \dot{\alpha}$) and $\dot{\lambda} = \dot{\beta}$. The following expressions can be used to solve for the forces and moments necessary for the rotation vector to line up

with the velocity vector. Those expressions are given by,

$$\begin{aligned}\Omega\sin\beta\big(c_8\cos^2\eta - 2c_2\sin\eta\cos\eta - c_1\sin^2\eta\big) + \frac{1}{\Omega\cos\beta}\Big[(c_4L + c_9N)\cos\eta - (c_3L + c_4N)\sin\eta\Big] \\ = \frac{1}{mV\cos\beta}(-T\cos\epsilon\sin\eta - T\sin\epsilon\cos\eta - L) - \Omega\sin\beta + q + \frac{g_{3_w}}{V\cos\beta}\end{aligned} \tag{2.44}$$

and

$$\begin{aligned}\Omega\cos^3\beta\left(\frac{c_5}{2}\sin 2\eta - c_6\cos 2\eta\right) + \frac{c_7M\cos\beta}{\Omega} - \Omega\sin^2\beta\cos\beta\left[\frac{c_1 + c_8}{2}\sin 2\beta + c_2\cos 2\beta\right] \\ - \frac{\cos\eta\sin\beta}{\Omega}\Big(c_3L + c_4N\Big) - \frac{\sin\eta\sin\beta}{\Omega}\Big(c_4L + c_9N\Big) \\ = \frac{1}{mV}(\sin\beta(T\cos\epsilon\cos\eta - T\sin\epsilon\sin\eta) - Q) + \frac{g_{2_w}}{V}\end{aligned} \tag{2.45}$$

with the gravity components taking the form,

$$\begin{Bmatrix} g_{1_w} \\ g_{2_w} \\ g_{3_w} \end{Bmatrix} = \begin{Bmatrix} g(-\cos\eta\cos\beta\sin\theta + \sin\beta\sin\phi\cos\theta + \sin\eta\cos\beta\cos\phi\cos\theta) \\ g(\cos\eta\sin\beta\sin\theta + \cos\beta\sin\phi\cos\theta - \sin\eta\sin\beta\cos\phi\cos\theta) \\ g(\sin\eta\sin\theta + \cos\eta\cos\phi\cos\theta) \end{Bmatrix} \tag{2.46}$$

Finally the kinematics can take the form,

$$\begin{Bmatrix} \dot\phi \\ \dot\theta \\ \dot\psi \end{Bmatrix} = \begin{bmatrix} 1 & \sin\phi\tan\theta & \cos\phi\tan\theta \\ 0 & \cos\phi & -\sin\phi \\ 0 & \sin\phi\sec\theta & \cos\phi\sec\theta \end{bmatrix} \begin{Bmatrix} \Omega\cos\eta\cos\beta \\ \Omega\sin\beta \\ \Omega\sin\eta\cos\beta \end{Bmatrix} \tag{2.47}$$

The two algebraic expressions are not very pleasing to the eye, yet they do include the necessary conditions for the proposed motion. Further assumptions can greatly simplify the results just presented. For instance, assuming thrust acts along the x_b-axis making ϵ zero, and assuming principle moments of inertia are two assumptions that would greatly reduce the complexity of the problem.

The next chapter will introduce a new motion that will require applying assumptions and constraints to the rotational equations of motion, Equations 2.26-2.28 and 2.32-2.34, similar to those above. Analysis will then be conducted on the reduced set of equations and will lend insight into the motion by concentrating on how the instantaneous rotation vector interacts with the instaneous velocity vector.

Chapter 3

The Falling Leaf

In recent years, the aircraft flight envelope has developed beyond what would have been imaginable in the time directly following the Wright brothers. Linear behaving aircraft has now become a subset, although still a very important one, to the global nonlinear characteristics exhibited in flight. Analysis techniques have been formulated to capture global dynamics and behavior of not only aircraft Ref [4, 8], but spacecraft Ref [1], and a variety of other vehicles .

Recently, analysis of a particular motion known as the "Falling Leaf" has been undertaken in Ref [3]. This motion is a prime candidate for the equations of motion proposed in Chapter 2 as will become evident in this chapter. Application of the methods proposed earlier will be applied and analysis will be undertaken with a new set of variables in order to lend insight to the dynamic motion known as the "Falling Leaf"

3.1 The Motion Defined

The Falling Leaf is characterized by a large coupled longitudinal/lateral-directional out-of-control oscillation. Angles of attack and sideslip can easily reach values of 70 degrees. Roll and yaw rates are in-phase while pitch rate is nearly zero. The motion is sustained for as long as 60 seconds, and recovery has not been guaranteed. Pilot input does not significantly affect the motion (once it has started). Understanding of this motion is incomplete, and design criteria is non-existent until recent guidelines introduced in Ref [3]. This motion is highly disorienting and it may by difficult for the pilot to identify that the aircraft has even entered into the motion. Tactical effectiveness is compromised and loss of aircraft has been attributed to this motion.

The identical assumptions from Ref [3] will be applied to the rotational equations of motion, Equations 2.26-2.28 and 2.32-2.34, and a dynamicly identical model will be developed.

Analysis of the reduced set of equations will shed light on some issues that were unanswered in the previous work.

3.2 Model Development

The identical assumptions from Ref [3] will be applied to the rotational equations of motion. Table 3.1 lists the assumptions made by Ref [3] and translates them to the new set of variables.

Therefore, Equations 2.26-2.28 and Equations 2.32-2.34 take the form

$$\dot{\Omega} = \frac{L}{I_{xx}} \cos\eta + \frac{N}{I_{zz}} \sin\eta \tag{3.1}$$

$$0 = \frac{N}{I_{zz}} \cos\eta - \frac{L}{I_{xx}} \sin\eta \tag{3.2}$$

$$0 = \frac{\Omega}{2} c_5 \sin 2\eta + \frac{c_7 M}{\Omega} \tag{3.3}$$

$$\dot{V} = \big(Y + mg_{2_b}\big) \frac{\sin\beta}{m} \tag{3.4}$$

$$\dot{\beta} = \Omega \sin\tau + \big(Y + mg_{2_b}\big) \frac{\cos\beta}{mV} \tag{3.5}$$

$$\dot{\tau} = -\Omega \cos\tau \tan\beta \tag{3.6}$$

The differential equations of interest are then

$$\dot{V} = \big(Y + mg_{2_b}\big) \frac{\sin\beta}{m} \tag{3.7}$$

$$\dot{\beta} = \Omega \sin\tau + \big(Y + mg_{2_b}\big) \frac{\cos\beta}{mV} \tag{3.8}$$

$$\dot{\tau} = -\Omega \cos\tau \tan\beta \tag{3.9}$$

$$\dot{\Omega} = \frac{L}{I_{xx} \cos\eta} \tag{3.10}$$

with the following algebraic relations that must hold,

$$\frac{N}{I_{zz}} \cos\eta = \frac{L}{I_{xx}} \sin\eta \tag{3.11}$$

$$\frac{M}{I_{yy}} = \frac{\Omega^2}{2} c_5 \sin 2\eta \tag{3.12}$$

The gravity term will be addressed in the next section along with the kinematics of the reduced model.

Table 3.1: Assumptions for Reduced Model

Old System $\mathbf{x}^T = (V, \beta, \alpha, p, q, r)$	*New System* $\mathbf{x}^T = (V, \beta, \tau, \Omega, \eta, \lambda)$
zero net force in the x_b and z_b directions. From Equation 1.66 $$\left\{ \begin{array}{c} F_{x_b} \\ F_{y_b} \\ F_{z_b} \end{array} \right\} = \left\{ \begin{array}{c} 0 \\ Y + mg_{2_b} \\ 0 \end{array} \right\}$$	translating to wind axis system and applying these wind axis forces to the rotational system $$\left\{ \begin{array}{c} F_{x_w} \\ F_{y_w} \\ F_{z_w} \end{array} \right\} = T_{wb} \left\{ \begin{array}{c} F_{x_b} \\ F_{y_b} \\ F_{z_b} \end{array} \right\} = \left\{ \begin{array}{c} (Y + mg_{2_b}) \sin\beta \\ (Y + mg_{2_b}) \cos\beta \\ 0 \end{array} \right\}$$
Pitch rate fixed at zero $$\dot{q} = q = 0$$	Equivalently the instantaneous rotation vector is constrained within the plane of symmetry $$\dot{\lambda} = \lambda = 0$$
In phase roll and yaw rates, $$r = kp$$	Fixes angle of rotation vector with respect to body axis $$\eta = \tan^{-1}(k)$$
Thrust acts along x_b-axis, $\epsilon = 0$ Principle moments of inertia, $I_{xz} = 0$	SAME

Equations 3.7-3.10 constitute the force and moment equations for a 4 degree of freedom model identical to that of Ref [3]. The only difference will come from how the kinematics are dealt with and how the forces and moments are represented.

3.2.1 Constants of the Motion

Three constants of the motion exist given the assumptions made in Table 3.1. These constants will be derived and explained. Finally, the constants will allow the problem to be reduced further, yet have the same dynamics of the higher order model. In addition to reduction of the model, these constants will lend insight and understanding in to the conditions and drivers of the Falling Leaf.

Force Constant

Equations 3.7-3.9 will be referred to as the force equations. The force equations can then be combined in the following manner. Rewriting Equation 3.8,

$$\dot{\beta} = -\dot{\tau}\frac{\sin\tau}{\cos\tau\tan\beta} + \dot{V}\frac{\cos\beta}{V\sin\beta} \tag{3.13}$$

multiplying both sides by $\tan\beta$ and moving all terms to the left hand side

$$\dot{\beta}\tan\beta + \dot{\tau}\tan\tau - \frac{\dot{V}}{V} = 0 \tag{3.14}$$

This equation can be integrated and results in a constant of the motion.

$$-\ln\cos\beta - \ln\cos\tau - \ln V = \ln\frac{1}{K} \tag{3.15}$$

$$\ln(V\cos\beta\cos\tau) = \ln K \tag{3.16}$$

taking the exponential of each side

$$V\cos\beta\cos\tau = K \tag{3.17}$$

To get a physical understanding of what this constant of the motion means, it is useful to introduce a new variable. Figure 3.1 shows that σ is the angle between the instantaneous rotation vector and the instantaneous velocity vector. The relationship between σ and the state variables is as follows,

$$\cos\sigma = \cos\beta\cos\tau \tag{3.18}$$

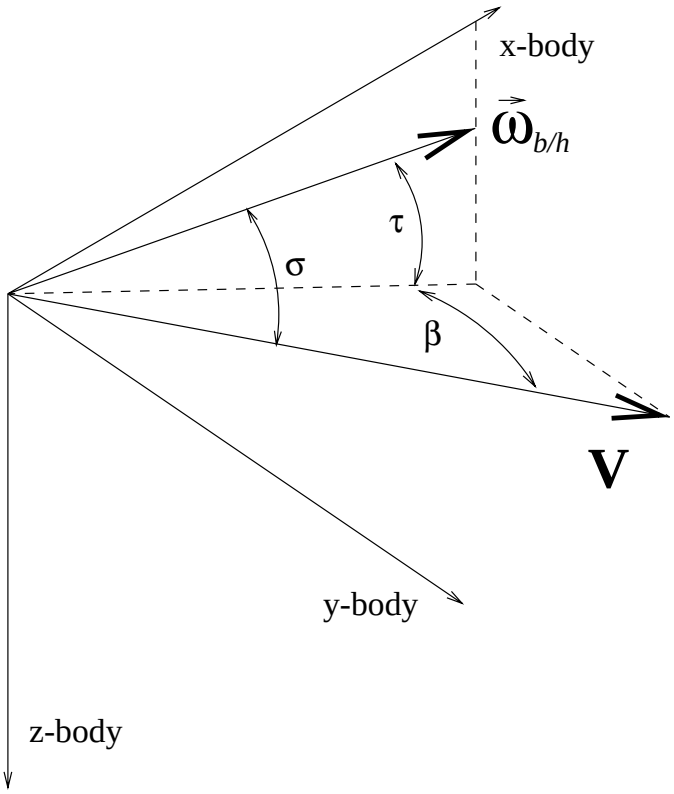

Figure 3.1: Define σ

The above relationship is only valid when the rotation vector is constrained within the plane of symmetry of the aircraft. That is when λ in Figure 2.1 is zero, or equivalently, body axis pitch rate q is zero.

Using the new variable σ, Equation 3.17 can be written as,

$$V \cos \sigma = K \tag{3.19}$$

which states that the component of velocity along the instantaneous rotation vector is a constant. The affect of this constant on the motion of the proposed model will be analyzed. The existence of this constant can be directly linked to the first assumption in Table 3.1, which states there is zero net force in the x_b and z_b directions.

Kinematic Constant

As stated in Sec 1.1.6, the kinematics are not subject to change or interpretation. Given angular rates the kinematic angles *must* evolve in a certain way. Yet again, a intelligent coordinate system choice to relate to inertial space can greatly simplify the problem and lend understanding to the mechanics of the motion. Another two constants are readily identifiable by using the kinematics derived in Sec 2.3. The assumptions made in Table 3.1 fix the rotational reference frame with respect to the body-fixed reference frame. Particularly for this case, $\lambda = 0$ and $\eta = \tan^{-1} k$. With these angles being constant, Equation 2.20 reduces to

$$\left\{ \begin{array}{c} p_r \\ q_r \\ r_r \end{array} \right\} = \left\{ \begin{array}{c} \Omega \\ 0 \\ 0 \end{array} \right\} \tag{3.20}$$

Therefore, Equation 2.16 simply becomes,

$$\left\{ \begin{array}{c} \dot{\Phi} \\ \dot{\Theta} \\ \dot{\Psi} \end{array} \right\} = \left\{ \begin{array}{c} \Omega \\ 0 \\ 0 \end{array} \right\} \tag{3.21}$$

This result is quite interesting. It states that the pitch angle and heading angle of the rotational coordinate system are constant. In inertial space, the rotational coordinate system solely has a roll angle that changes in time. It is also important to note that this result will apply for *any* instance that the instantaneous rotation vector is fixed in direction (magnitude may vary) with respect to the body-fixed axis system. Namely, when $\vec{\boldsymbol{\omega}}_{r/b}$ in Equation 2.17 is zero.

The next step is to relate the kinematic angles $[\Phi, \Theta, \Psi]$ with the conventional Euler angles $[\phi, \theta, \psi]$. This relation can be shown in general by using Equation 2.7. For the reduced model

given by Table 3.1, the two sets of angles are related as follows with Θ and Ψ being two constants of the motion.

$$\tan\Phi = \frac{\sin\phi\cos\theta}{\sin\eta\sin\theta + \cos\eta\cos\phi\cos\theta} \tag{3.22}$$

$$\sin\Theta = \cos\eta\sin\theta - \sin\eta\cos\phi\cos\theta \tag{3.23}$$

$$\tan\Psi = \frac{\cos\eta\cos\theta\sin\psi + \sin\eta(\cos\phi\sin\theta\sin\psi - \sin\phi\cos\psi)}{\cos\eta\cos\theta\cos\psi + \sin\eta(\cos\phi\sin\theta\cos\psi + \sin\phi\sin\psi)} \tag{3.24}$$

These angles come into play when describing the representation of gravity in the force equations using Equation 2.14. The effect of the above constants will be analyzed. For now these constants will allow the dynamics of the reduced model to be completely expressed as shown in the following section.

3.2.2 Reduced Model: Equations Collected

Force Equations

$$\dot{\beta} = \Omega\sin\tau + \big(Y + mg\sin\Phi\cos\Theta\big)\frac{\cos^2\beta\cos\tau}{Km} \tag{3.25}$$

$$\dot{\tau} = -\Omega\cos\tau\tan\beta \tag{3.9}$$

Moment Equations

$$\dot{\Omega} = \frac{L}{I_{xx}\cos\eta} \tag{3.26}$$

Kinematics

$$\dot{\Phi} = \Omega \tag{3.27}$$

Similar to the Euler angles, the heading angle Ψ of the rotational coordinate system does not appear on the right hand side of the equations, thus that constant of the motion is not of interest. The other constants of the motion are given by initial condition and η is given by the relationship in Table 3.1.

3.2.3 The Forces and Moments

The equations of motion shown above still incorporate general forces and moments. Body axis side force Y and rolling moment L are the only forces and moments that appear. The representation of forces and moments will be addressed in general and then applied to the particular problem posed above.

As a subset of the work presented here, aerodynamic forces and moments were considered at high angles of attack and sideslip. Data was gathered from Ref [13] and the F-18C aerodynamic database to construct a representative curve for each of the force and moment coefficients. An in depth review of the work will not be presented but the final product is shown in Appendix A. Static wind tunnel testing has included angle of attack test points up to 90°. The sideslip region has not been as extreme, commonly being ±15° or ±20° in most aerodynamic databases with often some of the forces and moments, such as the lift coefficient, not having a functional dependence on sideslip because of the assumption that the aircraft will not experience large sideslip excursions. Ref [13] contains data for sideslip sweeps of ±90 which served as a basis for construction of the curves in Appendix A in the large sideslip regions. The data gathered showed the trends of the force and moment coefficients that occurs throughout the large operating region consisting of $0 < \alpha < 90°$ and $\beta \pm 90°$. For example, $C_{n\beta}$ loses stability at high angles of attack, and local $C_{l\beta}$ (not secant derivative) becomes positive at large values of sideslip possibly resulting in positive rolling moment (secant derivative also loses stability) at extreme values of sideslip.

It is convenient to represent the aerodynamics as simply as possible yet capture the general behavior across the operating region. The body axis side force and rolling moment are linear in the model used by Ref [3]. Keeping in mind the results from Appendix A, it is a good first approximation on a global scale to have body-axis side force as linear in β. A linear rolling moment in β is acceptable in the small sideslip region yet if trying to model on a global scale it is a poor choice. To a first approximation the rolling moment L is chosen to be the negative of a sine function in β. This representation allows for $C_{l\beta}$ to change sign as β increases as well as have a positive rolling moment at large sideslip conditions.

Therefore the body-axis side force and the rolling moment coefficients are written respectively as,

$$C_Y = C_{Y\beta}\beta \tag{3.28}$$

$$C_l = -C_{l_{max}} \sin\left(\frac{\pi}{\beta_{ref}}\beta\right) \tag{3.29}$$

Where $C_{Y\beta}$ is the conventional stability derivative indicating the slope of the C_Y vs β curve, $C_{l_{max}}$ is the maximum value of C_l as indicated by Figure 3.2, and $\beta_{ref} = \beta|_{C_l=0|_{\beta\neq 0}}$, which is the value of β (non-zero) where rolling moment is zero, also indicated in Figure 3.2.

Conventional dimensionalization for the force and moment coefficients is used, with $\bar{q}$ being

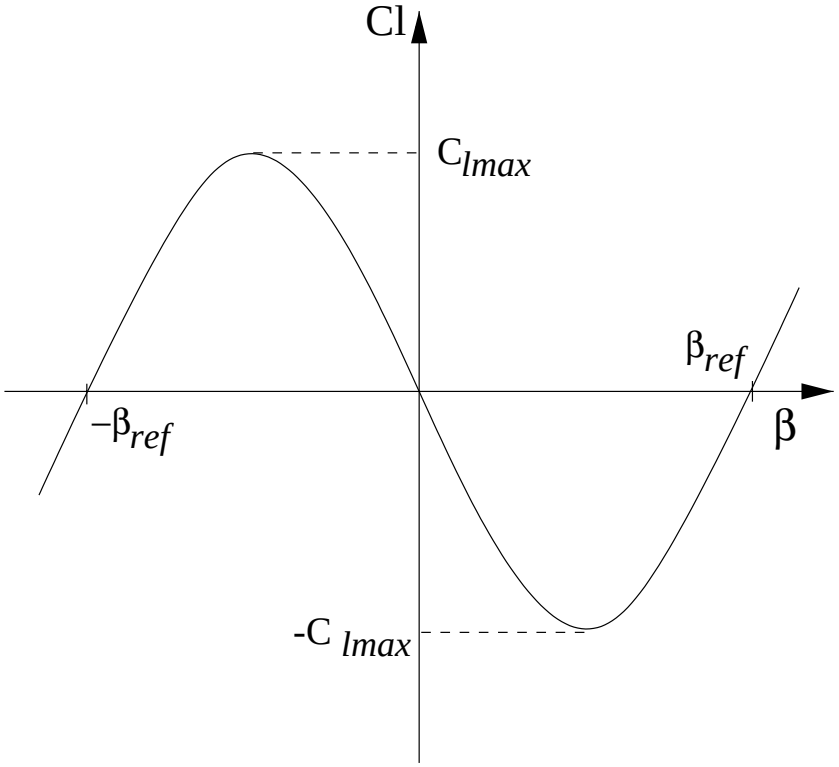

Figure 3.2: C_l vs β

the dynamic pressure, $\frac{1}{2}\rho V^2$,

$$Y = C_Y\, \bar{q} S \tag{3.30}$$

$$L = C_l\, \bar{q} S b \tag{3.31}$$

Using the coefficients defined above and Equation 3.17 to substitute for aircraft velocity V, the side force and rolling moment can be written as,

$$Y = C_1 \frac{K^2 \beta}{\cos^2\beta \cos^2\tau} \tag{3.32}$$

$$L = C_2 \frac{K^2 \sin\left(\frac{\pi}{\beta_{ref}}\beta\right)}{\cos^2\beta \cos^2\tau} \tag{3.33}$$

with,

$$C_1 = \frac{C_{Y\beta}\rho S}{2} \tag{3.34}$$

$$C_2 = \frac{-C_{l_{max}}\rho S b}{2} \tag{3.35}$$

Using this representation for the side force and rolling moment, Equations 3.25 and 3.26 can be written as,

$$\dot{\beta} = \Omega \sin\tau + \frac{C_1 K \beta}{m\cos\tau} + \frac{g \sin\Phi \cos\Theta \cos^2\beta \cos\tau}{K} \tag{3.25$'$}$$

$$\dot{\Omega} = \frac{C_2 K^2}{I_{xx}\cos\eta} \frac{\sin\left(\frac{\pi}{\beta_{ref}}\beta\right)}{\cos^2\beta\cos^2\tau} \tag{3.26$'$}$$

3.3 Model Validation and Simulation

The assumptions made in Table 3.1 are consistent with real observed motions exhibited by aircraft as shown in Ref [3]. Onset of the motion has been attributed to unobserved sideslip buildup that is commonly seen in low speed, high bank angle turns. Representative initial conditions will be used and translated into the new set of variables. The constants of the motion associated with the reduced system will be calculated. The reduced system will then be simulated and the results presented. Real flight data can be seen in Ref [3], and is reprinted with permission in Figure 3.3.

Typical values of a fighter-type aircraft for the parameters that appear in the equations of motion are shown in Table 3.2. Representative initial conditions will be drawn from Fig 3.3 and are summarized as follows,

$$\{V, \alpha, \theta, \beta, p, r, \phi\}_0 = \{245 \text{ ft/s}, 25^\circ, 0, 35^\circ, -15^\circ/\text{s}, -5^\circ/\text{s}, 60^\circ\} \tag{3.36}$$

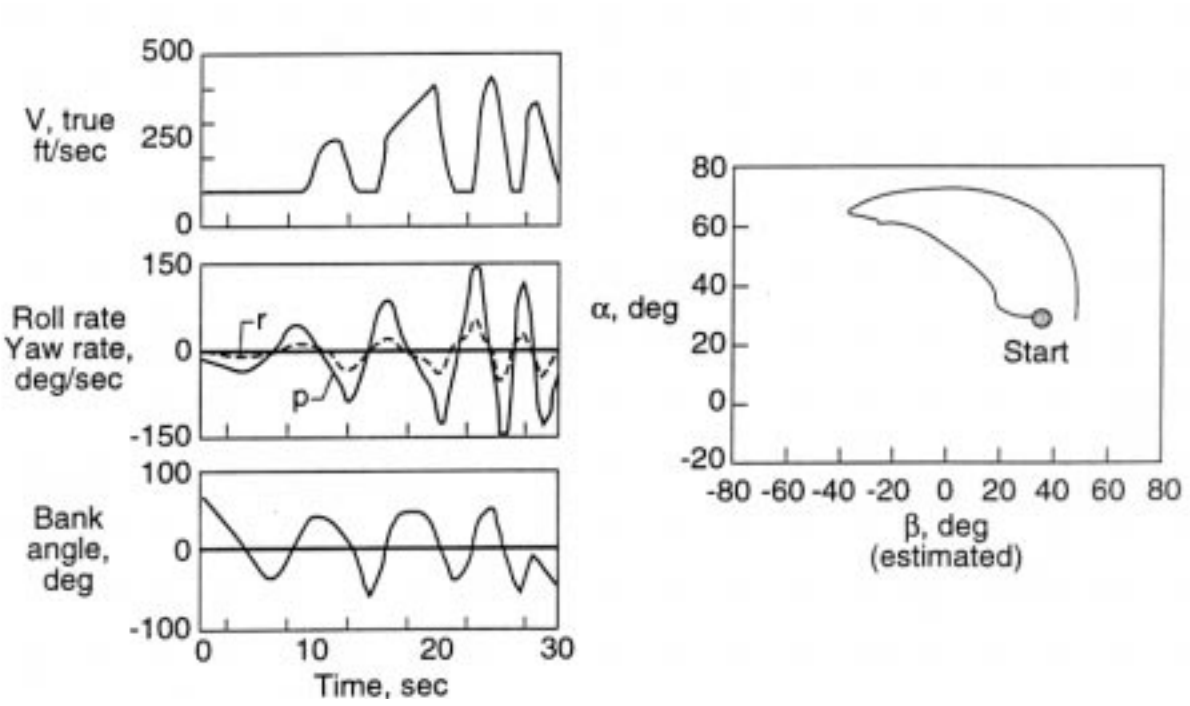

Figure 3.3: Real Falling Leaf Data, F-18C
reprinted from Ref [3]

Table 3.2: Model Parameters

$S = 400$ ft^2	$b = 37$ ft
$\rho = .001648$ slugs/ft^3	$I_{xx} = 24290$ slugs ft^2
$m = 1120$ slugs	$C_{Y\beta} = -.95$
$C_{l_{max}} = .06$	$\beta_{ref} = 60^\circ$
$k = .36$	$\eta = \tan^{-1}(k)$

The velocity time history shows the probe losing effectiveness at high angles of attack. Initial velocity was then taken to be a low speed condition consistent with the first reading of the probe. These initial conditions can be translated to the new set of variables in the following manner. Using Equation 2.13,

$$\tau_0 = \alpha_0 - \eta = 5^\circ \tag{3.37}$$

Using Equation 2.12,

$$\Omega_0 = sign(p_0)\sqrt{p_0^2 + r_0^2} = -16^\circ/\text{s} \tag{3.38}$$

Using Equation 3.22,

$$\Phi_0 = \tan^{-1}\left(\frac{\sin\phi_0\cos\theta_0}{\sin\eta\sin\theta_0 + \cos\eta\cos\phi_0\cos\theta_0}\right) = 62^\circ \tag{3.39}$$

Using Equation 3.17, one of the constants of the motion is

$$K = V_0\cos\beta_0\cos\tau_0 = 200 \text{ ft/s} \tag{3.40}$$

Using Equation 3.23, another constant of the motion is

$$\Theta = \sin^{-1}\left(\cos\eta\sin\theta_0 - \sin\eta\cos\phi_0\cos\theta_0\right) = -10^\circ \tag{3.41}$$

Therefore the initial condition for the new set of variables is

$$\{\beta, \tau, \Omega, \Phi\} = \{35^\circ, 5^\circ, -16^\circ/s, 62^\circ\} \tag{3.42}$$

With the constants of the motion being $K = 200$ ft/s and $\Theta = -10^\circ$.

The system consisting of Equations 3.9, 3.27, 3.25′, and 3.26′ can now be simulated. The results for these initial conditions are shown in Figures 3.4 and 3.5. In comparison to the real flight data in Figure 3.3, variables match up reasonably well. The best being the body-axis rates, reaching peaks of approximately 150°/s and 50°/s for p and r, respectively. Steady state velocity for the actual data was approximately 400 ft/s compared to 350 ft/s for the simulated data. The angle of attack and sideslip angle were estimated for the real data and were not available for the full duration of the motion. Yet that data matches very well in magnitude and shape of the 'umbrella' curve of $\alpha vs \beta$ that has now become a standard graph in the analysis of the Falling Leaf. The model proposed captures very well the curling over of beta that can be seen in the estimated α vs β plot. The curling feature can be directly related to the fact that the rolling moment was represented as a sine curve as opposed to linear for this particular case. The frequency of the motion is a close match as well, with a period of approximately 6.1 seconds.

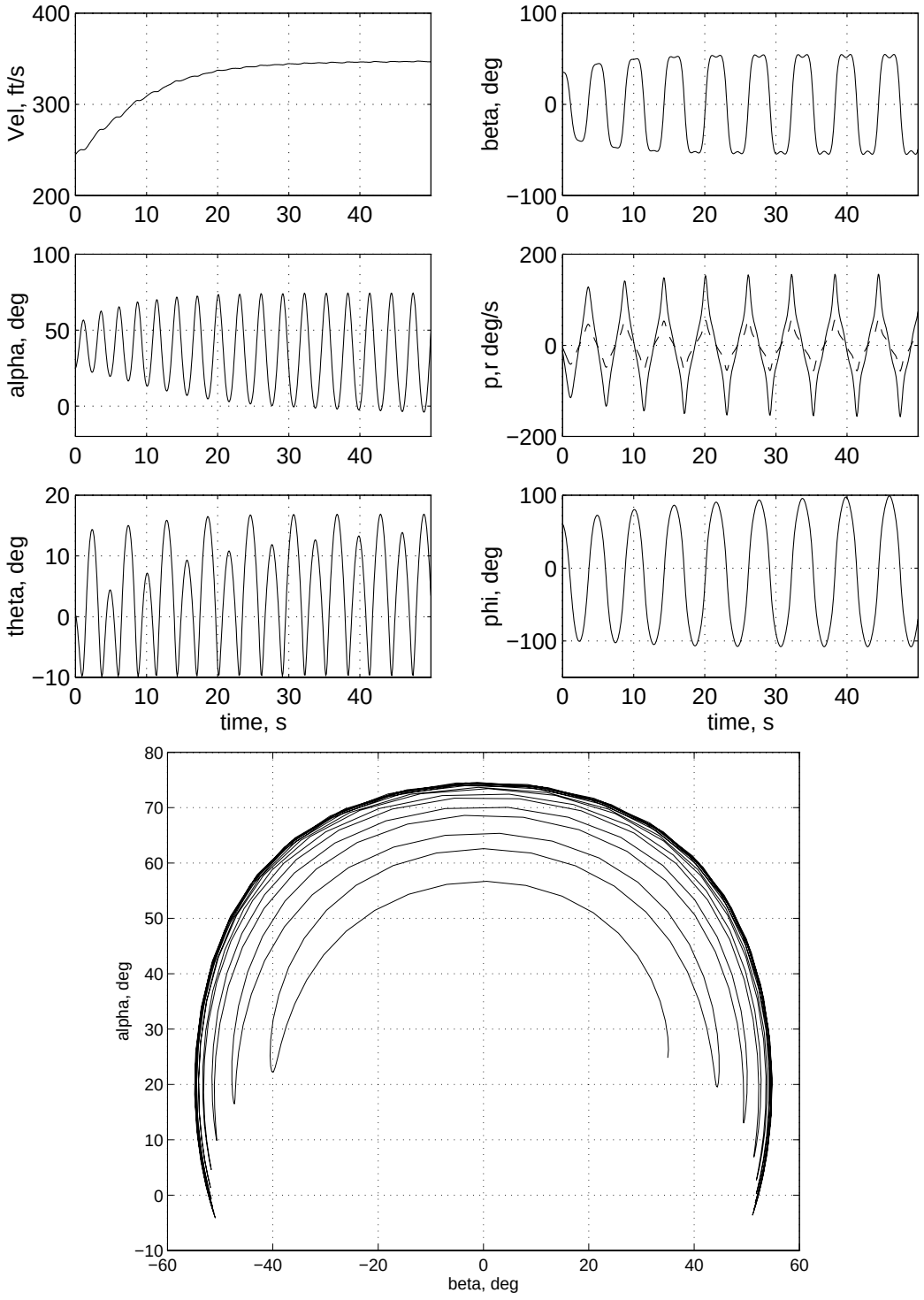

Figure 3.4: Simulation of Falling Leaf represented in $\{V, \alpha, \theta, \beta, p, r, \phi\}$

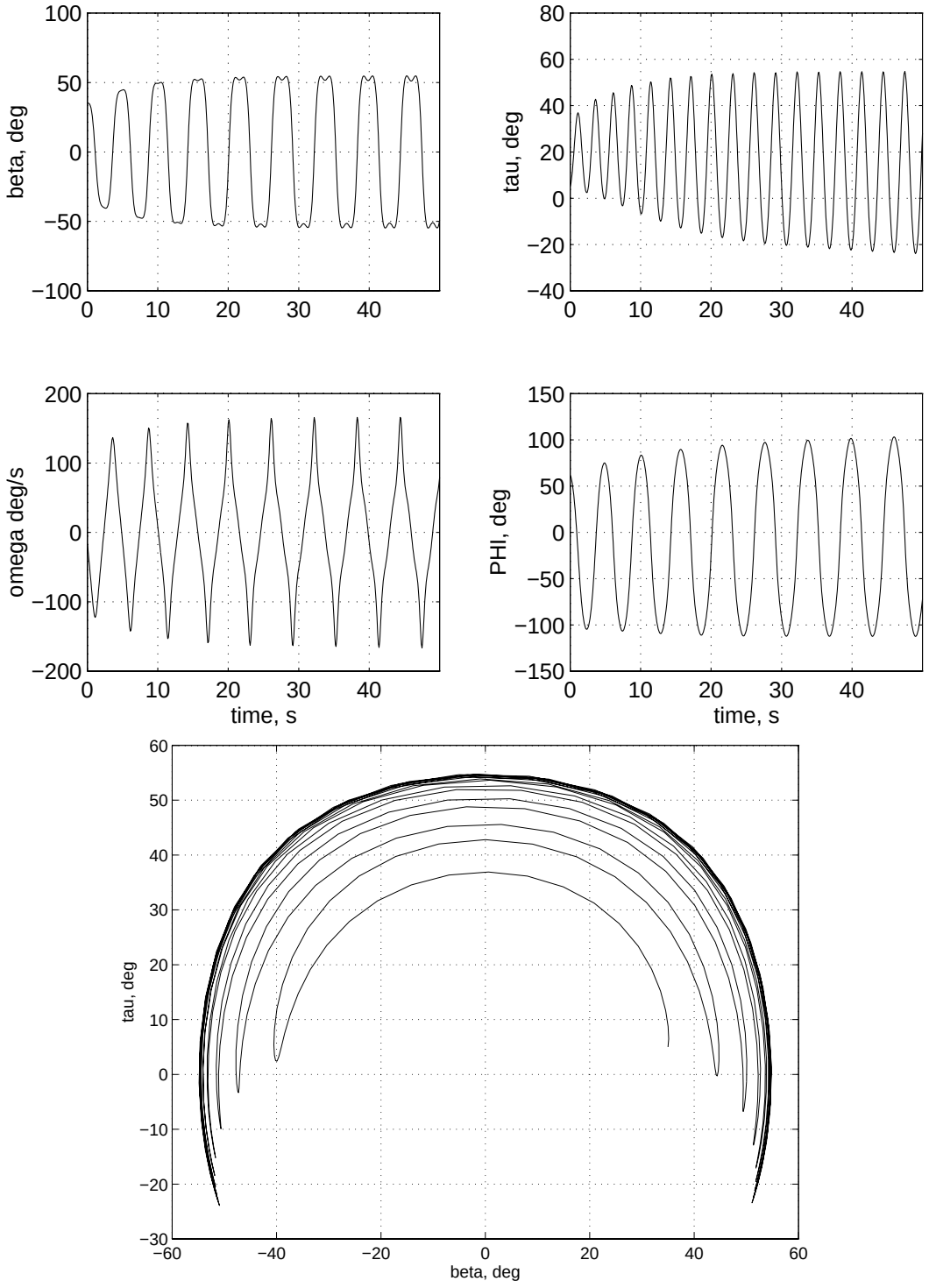

Figure 3.5: Simulation of Falling Leaf represented in $\{\beta, \tau, \Omega, \Phi\}$

Concentrating on the α vs β and the τ vs β plots, it can be seen that the shapes are identical. Furthermore, from Equation 2.13, α and τ differ by the constant η. In order to understand the full importance of the use of τ in place of α, focus is placed on the velocity trace. As can be seen velocity seems to be approaching a steady-state value. Equation 3.19 then states that σ is approaching a constant value, defined to be σ_{ref}. Recall from Figure 3.1, σ is the angle between the instantaneous velocity vector and the instantaneous rotation vector. The right hand side of Equation 3.18 is then approaching $\cos\sigma_{ref}$. Equation 3.18 also shows that at $\beta = 0$, $\tau = \sigma_{ref}$ and at $\tau = 0$, $\beta = \sigma_{ref}$. This result is quite important and will be addressed in the next chapter.

3.4 Summary

Due to the model structure, a near steady state limit cycle is converged upon with any initial disturbance in the lateral-directional variables. An understanding of the drivers and parameters that affect amplitude and frequency is needed. As shown in the previous section, the proposed model compares quite well with the known motion. Furthermore, the initial simplification and insight that the new rotational coordinate system has provided is noteworthy and will receive an in-depth analysis in the next chapter.

The assumptions under which the proposed model, Equations 3.9, 3.27, 3.25′, and 3.26′, is valid will be reviewed.

1. Zero net force in the x_b and z_b directions. From Equation 1.66, this assumption states that the sum of the forces due to thrust, aerodynamics, and gravity offset each other at *all* times. This assumption directly lends to the existence of the constant of the motion K as shown in Section 3.2.1.

2. Pitch rate is fixed at zero. Equivalently from Figure 2.1, λ is zero. This assumption is the removal of a degree-of-freedom, constraining the instantaneous rotation vector to be in the plane of symmetry of the aircraft and allows Equation 3.18 to be valid at all times. An algebraic expression exists that *must* be satisfied in order for this degree-of-freedom to be removed, namely Equation 2.28 reduces to,

$$c_7 M = \Omega^2 \left(c_6 \cos 2\eta - \frac{c_5}{2} \sin 2\eta \right) \tag{3.43}$$

   The pitching moment must satisfy Equation 3.43 if the pitch rate q is fixed at zero.

3. The ratio of the body-axis roll and yaw rates is a constant. This assumption is a removal of another degree-of-freedom, fixing the angle η in Figure 2.1 to be the constant $\tan^{-1}(k)$. Another algebraic equation *must* be satisfied in order for this degree-of-freedom to be removed, namely Equation 2.27 reduces to,

$$L\left(c_3 \sin\eta - c_4 \cos\eta\right) = N\left(c_9 \cos\eta - c_4 \sin\eta\right) \tag{3.44}$$

Although only the in-phase case will be considered, when k is positive, this assumption also does allow for a strictly out-of-phase condition to be set, when k is negative. With this assumption and assumption #2, the rotational coordinate system is now fixed with respect to the body-fixed coordinate system. With these two coordinate systems fixed with respect to each other the kinematic constants of the motion exist as shown in Section 3.2.1.

4. Principal moments of inertia, $I_{xz} = 0$. This assumption is quite common in the analysis of aircraft dynamics. Inherent in this assumption is that the moments are known about the principle axes. This representation of the moments is not usually the case, yet the assumption is valid when the rates experienced are small and I_{xz} is small relative to the other terms in the inertia tensor. For the particular motion of the Falling Leaf, rates can reach substantial values. The $\dot{q}$ equation of Equation 1.91 was considered at rates typical of the Falling Leaf. It was found that inclusion of a typical I_{xz} value can change the sign necessary on the pitching moment M to keep $\dot{q} = 0$ (see assumption #2). This fact must be kept in mind in validating the second assumption on this list. Using the expression shown in assumption #2, it can be easily shown that for typical values $c_5 = -.06869$ and $c_6 = -.02471$, the critical value is $\eta = 17.8°$. (The critical value for η is the angle necessary to rotate the inertia tensor to principle axis, see Sec 1.1.5). This value is directly in the range for η given by assumption #3. It would not be possible to keep $\dot{q} = 0$ without the inclusion of the I_{xz} term. For the present work this assumption is made from the observation of the very fact that the pitch rate q is very close to zero throughout the motion of the Falling Leaf.

5. The ϵ angle in defining the direction of thrust is zero. This assumption has no bearing on the results presented since assumption #1 removes thrust from the problem. Inherent in the definition of how thrust is oriented with respect to the body-fixed axis system was that it was constrained in the plane of symmetry of the aircraft, see Section 1.2.1. Relaxing this constraint would allow for a control to enter into the picture through the F_{y_b}-term in Equation 1.66, which in turn can possibly lead to recovery techniques by using the thrust as a control. This possibility is more attractive for thrust vectored aircraft its analysis is beyond the scope of this work.

6. The representation of the forces and moments are derived in Section 3.2.3. The only forces and moments that appear are body-axis side force and rolling moment. It is shown to be good approximation to have side force represented as linear and the rolling moment represented as the sine function shown in Figure 3.2.

Chapter 4

Analysis of the Falling Leaf

This chapter will perform an in depth analysis of the Falling Leaf motion in order to obtain an understanding of the drivers that control the characteristics of the motion. The characteristics of interest are amplitude, frequency, and the shape of the motion. The model that was developed in Chapter 3 will be used for the analysis. Recall that the state vector is now comprised of 4 variables, namely $\{\beta, \tau, \Omega, \Phi\}$. The equations are reprinted here for ease of reference.

$$\dot{\beta} = \Omega \sin\tau + \big(Y + mg \sin\Phi \cos\Theta\big) \frac{\cos^2\beta \cos\tau}{Km} \tag{4.1}$$

$$\dot{\tau} = -\Omega \cos\tau \tan\beta \tag{4.2}$$

$$\dot{\Omega} = \frac{L}{I_{xx} \cos\eta} \tag{4.3}$$

$$\dot{\Phi} = \Omega \tag{4.4}$$

The body-axis side force and the rolling moment in the above equations are represented as follows,

$$Y = C_1 \frac{K^2 \beta}{\cos^2\beta \cos^2\tau} \qquad C_1 = \frac{C_{Y\beta} \rho S}{2} \tag{4.5}$$

$$L = C_2 \frac{K^2 \sin\left(\frac{\pi}{\beta_{ref}}\beta\right)}{\cos^2\beta \cos^2\tau} \qquad C_2 = \frac{-C_{l_{max}} \rho S b}{2} \tag{4.6}$$

Refer to Chapter 3 for any further information on the constants that appear above.

The state variables $\{\beta, \tau, \Omega, \Phi\}$ along with two constants of the motion, K and Θ, completely describe the dynamics that will be analyzed. Velocity will be determined from the state

variables and the constant of the motion K using Equation 3.17. The simulation from Section 3.3 is reprinted in Figure 4.1.

4.1 Predicting the Amplitude

As stated briefly at the conclusion of Chapter 3, as the velocity approaches near steady-state, the angle σ approaches a constant value σ_{ref}. This σ_{ref} characterizes a major part of the motion. From Equation 3.18, when $\beta = 0$ the maximum value of τ is σ_{ref}, once the motion has settled into a near limit cycle. This point also defines maximum angle of attack. Therefore we can write

$$\cos\beta\cos\tau = \cos\sigma_{ref} \tag{4.7}$$

For the remainder of this section the assumption is that $\dot{V}$ goes to zero and the motion has reached a steady state limit cycle. Although the velocity never reaches a constant value, always getting slightly larger, Figure 4.1 shows that the this assumption is valid. It is this assumption that will allow the prediction of σ_{ref}.

Setting $\dot{V}$ to zero, Equation 3.7 requires that

$$Y + mg\cos\Theta\sin\Phi = 0 \tag{4.8}$$

Since in general $\beta \neq 0$, Equations 4.5 and 4.7 are used to rewrite Equation 4.8 as,

$$\frac{\sin\Phi}{\beta} = -\frac{C_1K^2}{mg\cos\Theta\cos^2\sigma_{ref}} \tag{4.9}$$

The right hand side of Equation 4.9 is constant, and furthermore the same equation enforces that $\Phi = 0$ when $\beta = 0$. The value of Φ is not known for any $\beta \neq 0$ as of yet. The only point that is known in the oscillation is at $\beta = \Phi = 0, \tau = \sigma_{ref}$. Therefore σ_{ref} cannot be determined from Equation 4.9 directly. Taking the time rate of change of Equation 4.9,

$$\frac{\dot{\Phi}\cos\Phi}{\beta} - \frac{\dot{\beta}\sin\Phi}{\beta^2} = 0 \tag{4.10}$$

Using Equations 4.1, 4.4, and 4.8 this expression becomes,

$$\frac{\Omega\cos\Phi}{\beta} - \frac{\Omega\sin\tau\sin\Phi}{\beta^2} = 0 \tag{4.11}$$

Factoring out a $\frac{\Omega}{\beta}$ and using Equation 4.9 this expression can be written as

$$\cos\Phi + \sin\tau\left(\frac{C_1K^2}{mg\cos\Theta\cos^2\sigma_{ref}}\right) = 0 \tag{4.12}$$

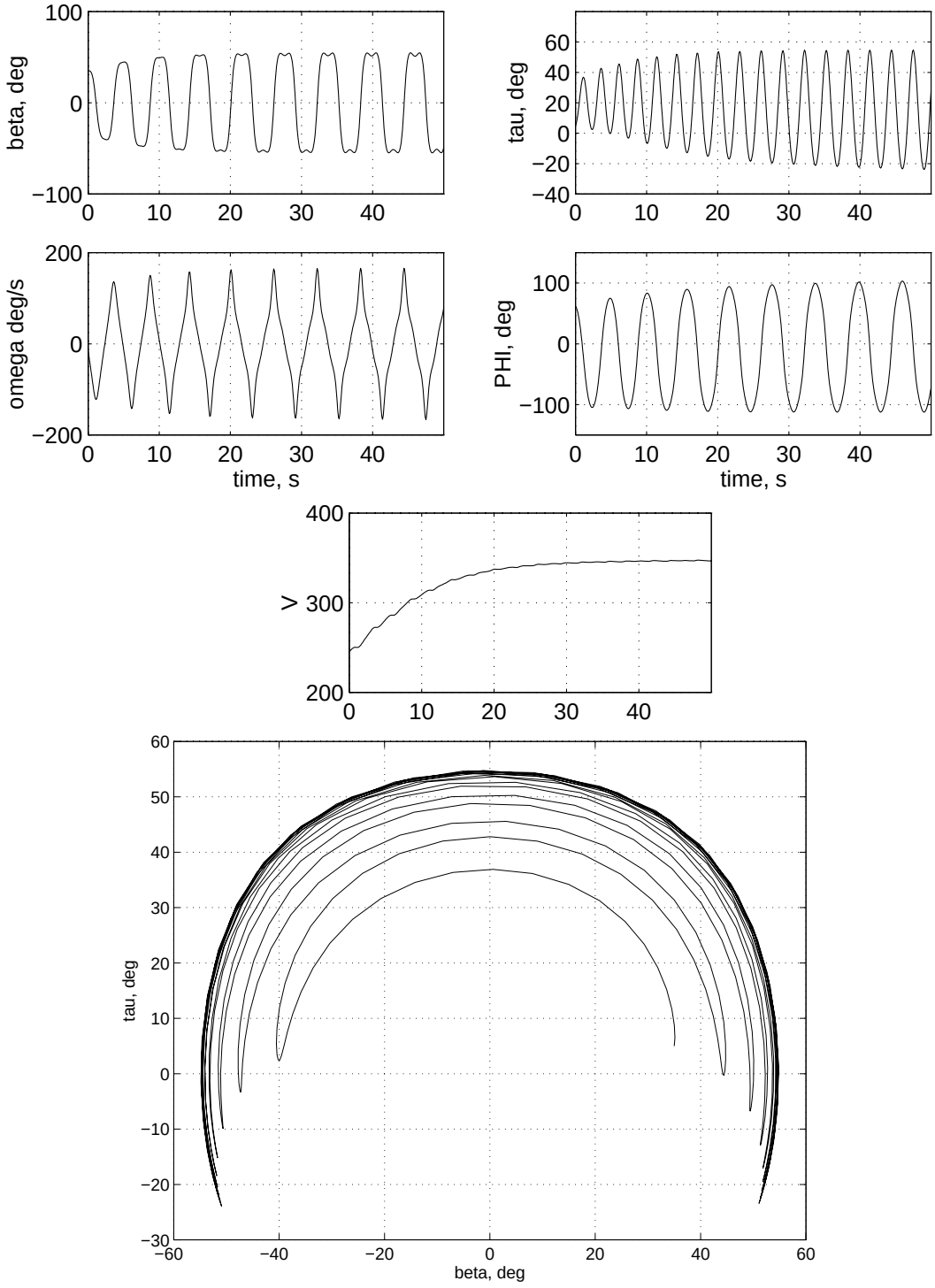

Figure 4.1: Falling Leaf Simulation

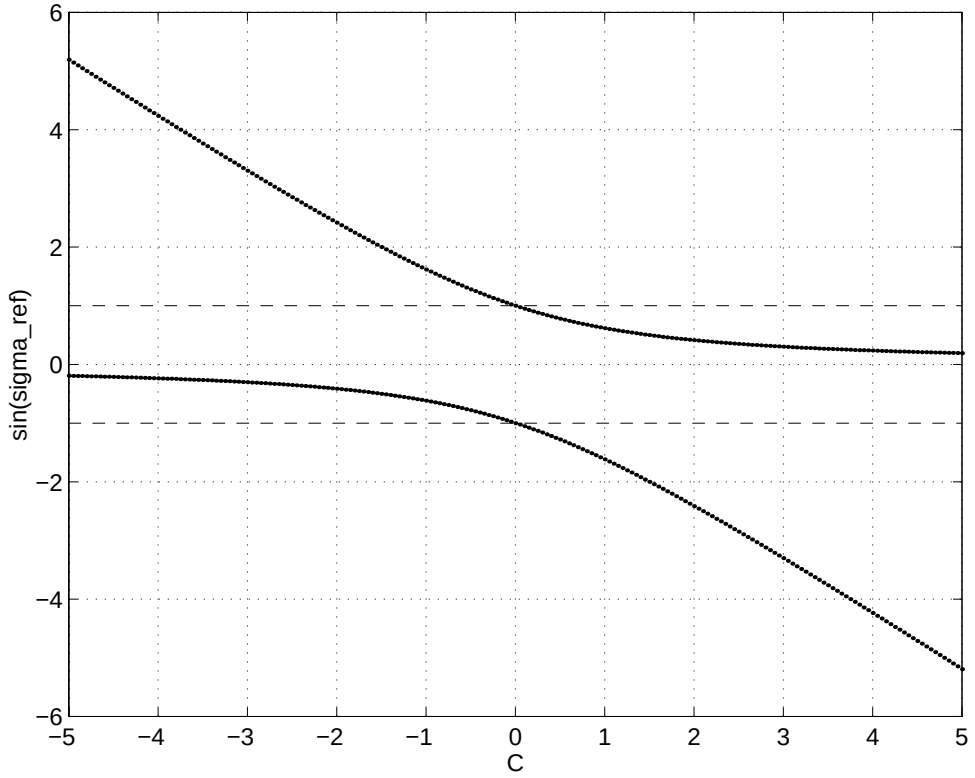

Figure 4.2: $\sin\sigma_{ref}$ vs C

Applying the information about the one point that is known in the oscillation with Equation 4.12, namely $\beta = 0$ and $\Phi = 0$ when $\tau = \sigma_{ref}$. Equation 4.12 can be rewritten to express σ_{ref} in terms of a new constant C

$$\frac{\cos^2\sigma_{ref}}{\sin\sigma_{ref}} = -\frac{C_1 K^2}{mg\cos\Theta} = C \tag{4.13}$$

Rewriting the above expression as a quadratic in $\sin\sigma_{ref}$,

$$\sin^2\sigma_{ref} + C\sin\sigma_{ref} - 1 = 0 \tag{4.14}$$

The solutions to Equation 4.14 are shown in Figure 4.2. Only one acceptable real root (magnitude ≤ 1) exists for any given C other than $C = 0$. The constant C will be deconstructed to analyze the effect of the various parameters on the amplitude σ_{ref}.

$$C = -\frac{C_{Y\beta}\rho S K^2}{2mg\cos\Theta} \tag{4.15}$$

Because the stability derivative $C_{Y\beta}$ is always negative and every other term in C is positive, only the positive values of C are of interest. For convenience, the corresponding root of

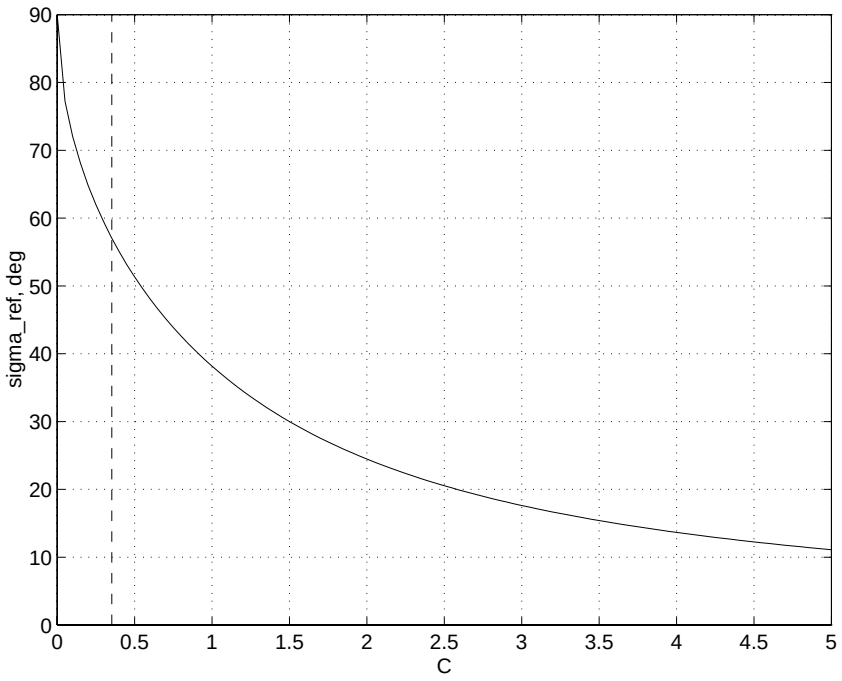

Figure 4.3: σ_{ref} vs C

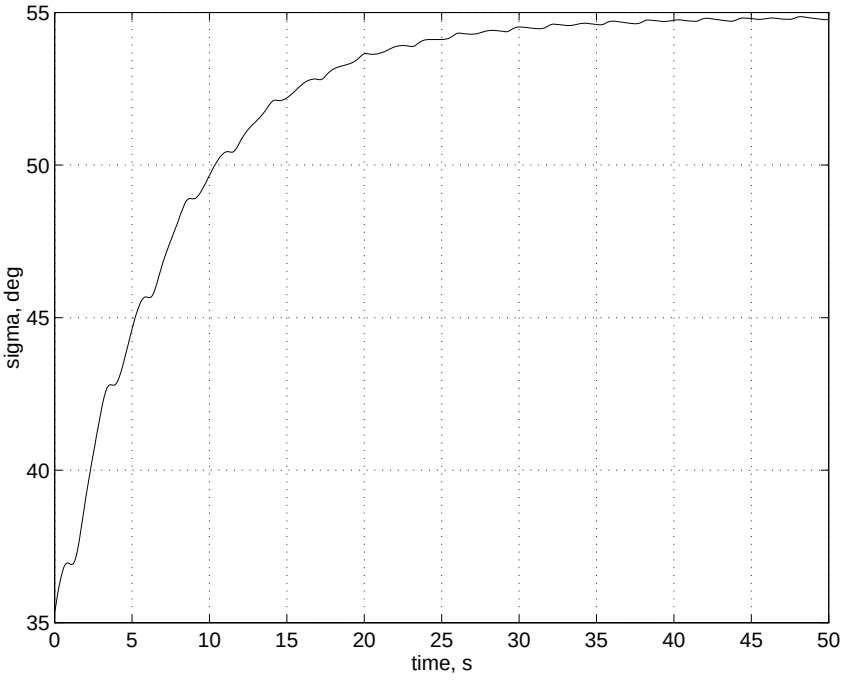

Figure 4.4: σ vs t for simulation run

interest of Equation 4.14 is

$$\sin \sigma_{ref} = \frac{-C + \sqrt{C^2 + 4}}{2} \tag{4.16}$$

Figure 4.3 shows the possible values of σ_{ref} as a function of C. The vertical dotted line on the plot is the value of C for the simulation run shown in Figure 4.1. Figure 4.4 shows the time history of σ for the simulation in Figure 4.1. The estimated σ_{ref} using the method derived above gives a value of 57°, while the actual σ_{ref} appears to be approaching approximately 55°.

The estimation of σ_{ref} is very good. The above estimation will always be greater than the actual σ_{ref}, and furthermore the error decreases as the values of σ_{ref} decreases. The error with the estimation comes from the assumption that $\dot{V} = 0$. The velocity approaches a near constant value, yet it is continually increasing slightly. Yet the assumption is still valid from inspection of the velocity time history in Figure 4.1.

4.2 Predicting the Frequency

The previous section states that the limit cycle motion will be constrained by σ_{ref}. Namely, the steady-state oscillation *must* follow Equation 4.7. Solving for τ,

$$\tau = \cos^{-1}(\cos \sigma_{ref} \sec \beta) \tag{4.17}$$

Figure 4.5 shows the shape of the Falling Leaf at three different σ_{ref}'s. The largest σ_{ref} corresponds to the estimated value of the validation run calculated in the previous section. It is known that the Falling Leaf is a symmetric oscillation about $\beta = 0$. Figure 4.5 then represents the 'track' that the motion must be in when it reaches a steady-state oscillation. It will oscillate about $\beta = 0$, but what is not known yet is the value of τ_{min}. It will be shown that the frequency of the oscillation is directly tied into determining the value of τ_{min}, along with the values of Φ_{max} and Ω_{max}.

It is now assumed that the near limit cycle has been reached. The second term in Equation 4.1 is therefore assumed to be zero at all times because velocity is assumed to have reached a constant value. Equation 4.7 is valid and allows the order of the system to be reduced by one. Either β or τ can be removed from the problem. Here, τ will be eliminated. Rewriting Equation 4.7,

$$\cos \tau = \frac{\cos \sigma_{ref}}{\cos \beta} \tag{4.18}$$

Using this expression to substitute for τ in the reduced form of Equation 4.1,

$$\dot{\beta} = \Omega \left(1 - \frac{\cos^2 \sigma_{ref}}{\cos^2 \beta}\right)^{1/2} \tag{4.19}$$

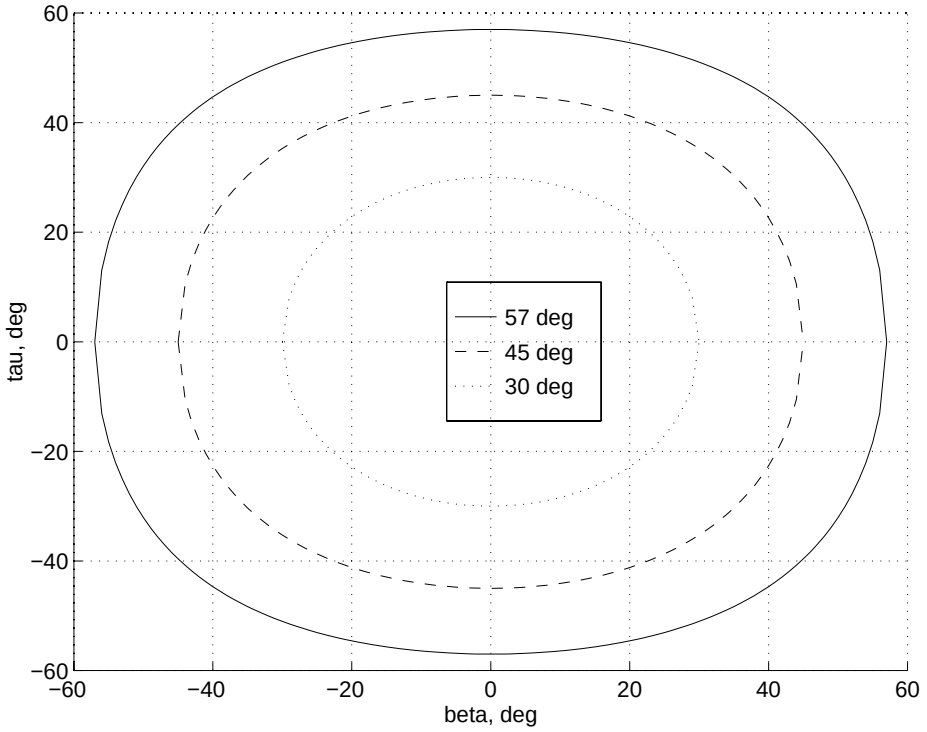

Figure 4.5: Falling Leaf Shape for various σ_{ref}

Using Equation 4.4 and separating variables,

$$\dot{\Phi} = \frac{\dot{\beta}}{\left(1 - \frac{\cos^2\sigma_{ref}}{\cos^2\beta}\right)^{1/2}} \tag{4.20}$$

Multiplying both sides by dt, factoring out a $\frac{1}{\cos^2\beta}$ from the square root term in the denominator, and using trigonometric identities,

$$d\Phi = \frac{\cos\beta d\beta}{\left(\sin^2\sigma_{ref} - \sin^2\beta\right)^{1/2}} \tag{4.21}$$

Apply the following transformation introducing an alternate variable ν,

$$\sin\beta = \sin\sigma_{ref}\sin\nu \tag{4.22}$$

It follows that,

$$d\beta = \frac{\sin\sigma_{ref}\cos\nu}{\cos\beta}d\nu \tag{4.23}$$

Using this transformation Equation 4.21 can be written as,

$$\begin{aligned} d\Phi &= \frac{\cos\beta\left(\frac{\sin\sigma_{ref}\cos\nu}{\cos\beta}d\nu\right)}{\left(\sin^2\sigma_{ref}-\sin^2\sigma_{ref}\sin^2\nu\right)^{1/2}} \\ &= d\nu \end{aligned} \tag{4.24}$$

Integrating both sides,

$$\Phi = \nu - constant \tag{4.25}$$

Substituting into Equation 4.22,

$$\sin\beta = \sin\sigma_{ref}\sin\left(\Phi + constant\right) \tag{4.26}$$

Equation 4.9 states that $\Phi = 0$ when $\beta = 0$, therefore the constant of the integral must be 0.

$$\sin\beta = \sin\sigma_{ref}\sin\Phi \tag{4.27}$$

Once the assumption that $\dot{V} = 0$ is made, Equation 4.27 is completely valid. That is, once one assumes velocity has reached a constant value, σ_{ref} is then defined and β and Φ are related as stated in Equation 4.27.

Equation 4.27 also allows the order of the system to be further reduced by one. Everywhere that β appears will be replaced by the variable Φ as dictated by Equation 4.27. The rolling moment in Equation 4.3 is the only equation left in which β appears. Furthermore, taking the time rate of change of Equation 4.4,

$$\ddot{\Phi} = \dot{\Omega} \tag{4.28}$$

and substituting Equation 4.3,

$$\ddot{\Phi} = \frac{L}{I_{xx}\cos\eta} \tag{4.29}$$

The complete dynamics of the Falling Leaf motion *once it has reached a constant velocity* can be written as,

$$\ddot{\Phi} = A\sin\left(B\sin^{-1}(C\sin\Phi)\right) \tag{4.30}$$

with

$$A = \frac{C_2K^2}{I_{xx}\cos\eta\cos^2\sigma_{ref}} \tag{4.31}$$

$$B = \frac{\pi}{\beta_{ref}} \tag{4.32}$$

$$C = \sin\sigma_{ref} \tag{4.33}$$

Refer to Chapter 3 for any further information on the above constants.

The form of Equation 4.30 is quite important. Because it does not contain $\dot{\Phi}$, an energy potential exists for the system. Energy is therefore a constant once the motion has reached the limit cycle.

4.2.1 Applying Energy Methods

Energy methods are now introduced into the analysis. Defining $\dot{\Phi}dt = d\Phi$ Equation 4.30 can be written as,

$$\ddot{\Phi}\dot{\Phi}dt = A\sin\left(B\sin^{-1}(C\sin\Phi)\right)d\Phi \tag{4.34}$$

Now integrating each side and rearranging

$$\frac{\dot{\Phi}^2}{2} - \int A\sin\left(B\sin^{-1}(C\sin\Phi)\right)d\Phi = E \tag{4.35}$$

$$T \quad + \quad V \quad = E \tag{4.36}$$

Equation 4.35 states that the sum of the "kinetic energy" T and the "potential energy" V is constant and is equal to the "total energy" E. The above terms are in quotes because they are a scaled version of their respective names. As can be seen, the integral that defines the potential energy is not trivial. To evaluate this integral two theorems will be used (see Ref [5]),

- Within the common range of convergence, two or more power series can be added, subtracted, and multiplied term-by-term. The resultant series is at least convergent within the common range of convergence.
- If a power series is convergent, then the integral of the series term-by-term is convergent.

Now the following infinite series are reprinted from Ref [5],

$$\sin x = x - \frac{x^3}{3!} + \frac{x^5}{5!} - \frac{x^7}{7!} + \cdots \quad (|x| < \infty) \tag{4.37}$$

$$\sin^{-1}x = x + \frac{1}{2\cdot 3}x^3 + \frac{1\cdot 3}{2\cdot 4\cdot 5}x^5 + \frac{1\cdot 3\cdot 5}{2\cdot 4\cdot 6\cdot 7}x^7 + \cdots \quad (|x| < 1) \tag{4.38}$$

These series can now be combined and integrated as stated by the potential term in Equation 4.35. The resulting energy potential has the form

$$V = \sum_{i=1}^{\infty} a_i\, x^{2i} \tag{4.39}$$

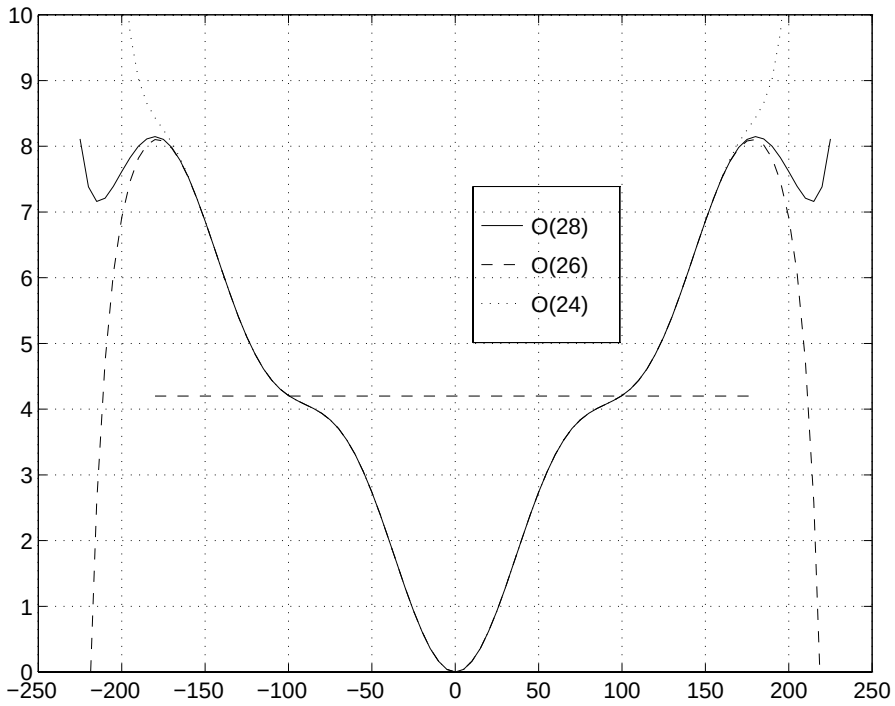

Figure 4.6: Potential Energy Curve

with the first few coefficients,

$$a_1 = \frac{ABC}{2} \tag{4.40}$$

$$a_2 = -\frac{ABC}{24}\left[C^2(B^2-1)+1\right] \tag{4.41}$$

$$a_3 = \frac{ABC}{720}\left[C^4(B^4-10B^2+9)+C^2(10B^2-10)+1\right] \tag{4.42}$$

$$a_4 = -\frac{ABC}{40320}\left[C^6(B^6-35B^4+259B^2-225) + C^4(35B^4-350B^2+315)+C^2(91B^2-91)+1\right] \tag{4.43}$$

$$\vdots$$

Figure 4.6 shows Equation 4.39 plotted to various lengths of the series. The values for the constants A, B, C are from the validation simulation in Chapter 3. As expected the most accurate is the curve corresponding to $O(28)$, which is the curve that keeps the first 13 terms, up to the Φ^{26}-term, of the series given by Equation 4.39. Each decrease in the order of the final term is characterized by the loss of a turn in the potential curve near the extreme values of $\pm 180^\circ\Phi$. It is important to realize that the potential described by Equation 4.35 is the integral of a periodic function, therefore the potential must be a periodic function as well.

Table 4.1: Initial Conditions

state →	β	τ	Ω	Φ
↓ line type\ref→	35°	5°	$-16^\circ/s$	62°
-	*ref*	*ref*	*ref*	*ref*
- -	60	15	-50	90
-·	0	30	0	0
···	-40	50	50	-90

Effectively, the full potential can be plotted by cutting the range from -180° to $+180^\circ$ and repeating it to the right and left of itself.

As validation, the horizontal dashed line in Figure 4.6 represents the total energy level for the validation run shown in Figure 4.1. This value was achieved by calculating the kinetic energy at the $\Phi = 0$ point. Equation 4.27 states $\beta = 0$ when $\Phi = 0$. This result coincides with $\tau_{max} = \sigma_{ref}$ and $\Omega = \Omega_{max}$. Picking off the value of Ω_{max}, kinetic energy can be calculated as shown by Equation 4.35. Furthermore, potential energy at $\Phi = 0$ is zero by Equation 4.39, therefore the kinetic energy is the total energy of the system by Equation 4.35. Once the energy level is known, every point in the oscillation is known as well. Validating Φ_{max} can be done by inspection of where the total energy line intersects the potential curve. From Figure 4.6, the maximum is approximately 100° which matches very well with Figure 4.1.

The problem now is how to determine the final energy level for arbitrary initial conditions. Unfortunately, that has not been determined. Somehow the initial condition must define final energy level, yet that connection has not been made. By running simulations it can be shown that the largest impact in final energy level is initial τ. Figure 4.7 shows the energy levels reached when starting from various initial conditions that are summarized in Table 4.1. Some of the changes in initial condition are quite substantial and physically may not be feasible, yet the purpose is to analyze how large changes affect the output. For each plot in Figure 4.7, only one state is changed, which corresponds to a column in Table 4.1. For example, the top-left plot of Figure 4.7 represents the final energy level for various simulations starting at the initial condition except for β, which is given by the first column of Table 4.1. As can be seen the largest contributer to a change in final energy is τ. It was found that the farther τ_0 is from σ_{ref} the higher the final energy level. The higher the final energy level means higher values of Φ_{max} and Ω_{max}. As energy level is increased, sideslip β tends to increase towards σ_{ref} and if the energy level reaches a critical value, where $\beta_{max} = \sigma_{ref}$, β then decreases even though Φ is still growing larger, all the while satisfying Equation 4.27. Recall Figure 4.5 which shows the final trace of $\tau vs \beta$. It is the final energy level that defines τ_{min} on this curve. Furthermore there exists an energy level in which an oscillation will not occur. Namely, any energy level that is above the highest point in the potential curve will not exhibit oscillatory behavior. The motion associated with this energy

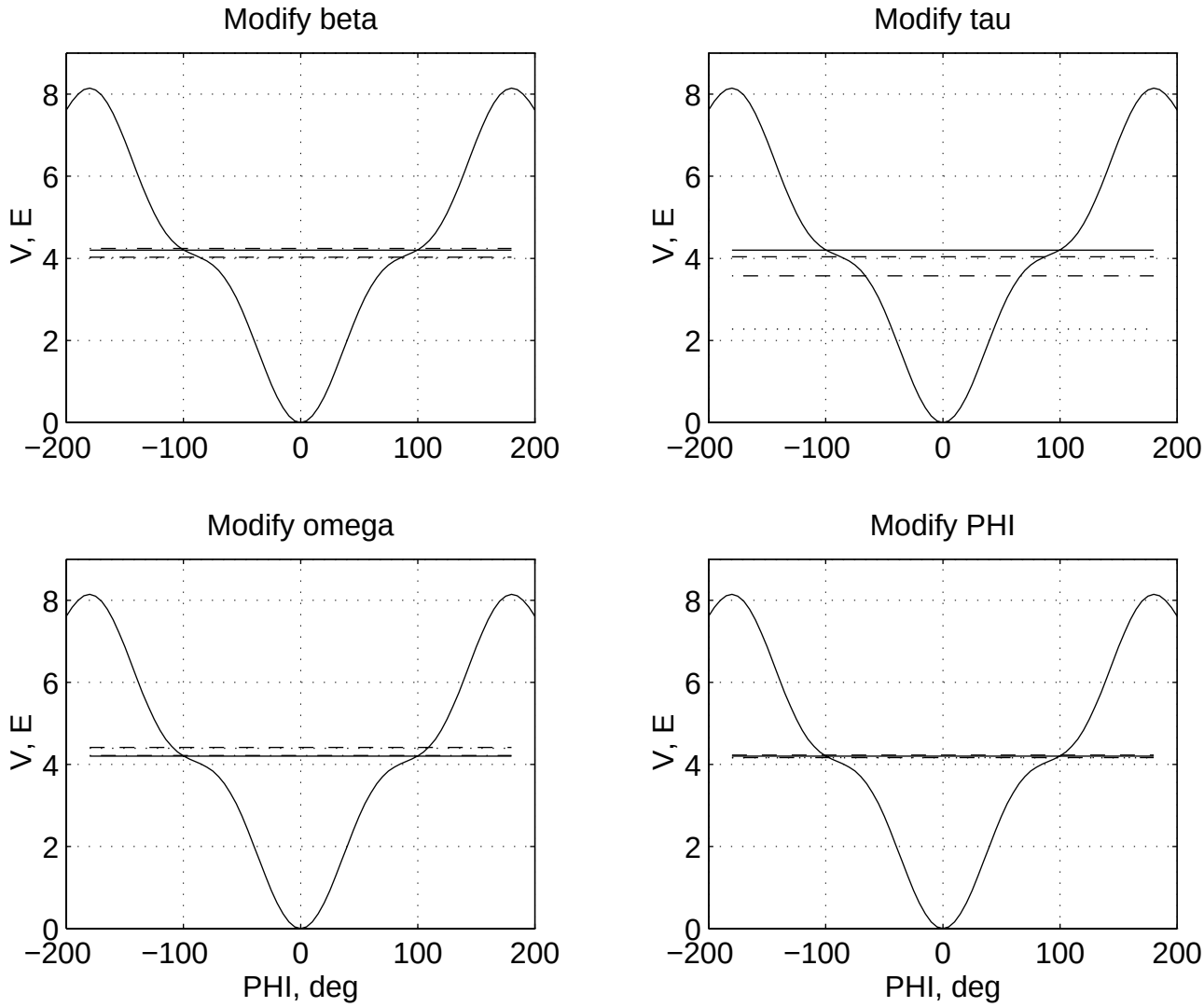

Figure 4.7: Sensitivity of final energy level to initial conditions
Legend given by Table 4.1

level will follow the appropriate track, similar to those shown in Figure 4.5, always in a clockwise or counter-clockwise direction. This result is similar to a pendulum that initially is given enough energy to swing over the top. Assuming no energy loss, the pendulum will continue to swing over the top in which ever direction it was started.

The final energy level defines the frequency of the oscillation as well as τ_{min}, Ω_{max}, and Φ_{max}. Because the final energy level has not been linked with initial condition, a *very* rough approximation will be given. As shown from Figure 4.7, the initial condition of τ is the most important initial condition in defining final energy level. This characteristic is only valid when τ is far from σ_{ref}. As τ approaches σ_{ref} the initial values of the remaining states become larger players in the definition of the final energy level, when in the limit $\tau = \sigma_{ref}$ the final energy level is completely defined by the lateral-directional states. Entrance into the Falling Leaf is usually far from the maximum angle of attack that is seen in the oscillation, this means that τ_0 is far from σ_{ref}. With this situation in mind, the following approximation is proposed. Assume that τ_0 completely defines the final energy level in the following manner. Assume that τ_0 is a value in the near limit cycle and use Equation 4.7 to calculate β. Equation 4.27 can be used to then calculate a value of Φ at this point. Assume that the potential energy at this value of Φ is the total energy of the system. For the simulation run corresponding to Figure 4.1, the approximated total energy level is $E = 4.04$ corresponding to $\Phi = 87^\circ$ as compared to 100° for the simulation. Figure 4.8 shows the actual final energy level along with the approximated value.

For the case shown in Figure 4.8, a small change in total energy causes a large change in Φ_{max} due to the shallowness of the potential at these particular values of Φ. This area is the worst place to make the assumption that has been made. Yet it is continued to illustrate the information contained in the energy constant. Equation 4.35 can now be rearranged in the following manner,

$$T = E - V \tag{4.44}$$

$$\frac{d\Phi}{dt} = \sqrt{2(E - V)} \tag{4.45}$$

The following integral can be formed,

$$\int_0^{\Phi_{max}} \frac{d\Phi}{\sqrt{2(E - V)}} = \int_0^{\frac{T_{period}}{4}} dt \tag{4.46}$$

The potential energy V is given by Equation 4.39. T_{period} is the period of the oscillation. This integral can be evaluated numerically and for this example yields $T_{period} = 5.6$ sec. The period calculated by running the simulation and extracting Ω_{max} is approximately 6.7 sec. The actual period by obtained inspecting one of the oscillating states is approximately 6.1 sec. These results are not a very good match, but it does give an idea of the frequency. There are two main reasons for the inaccuracies;

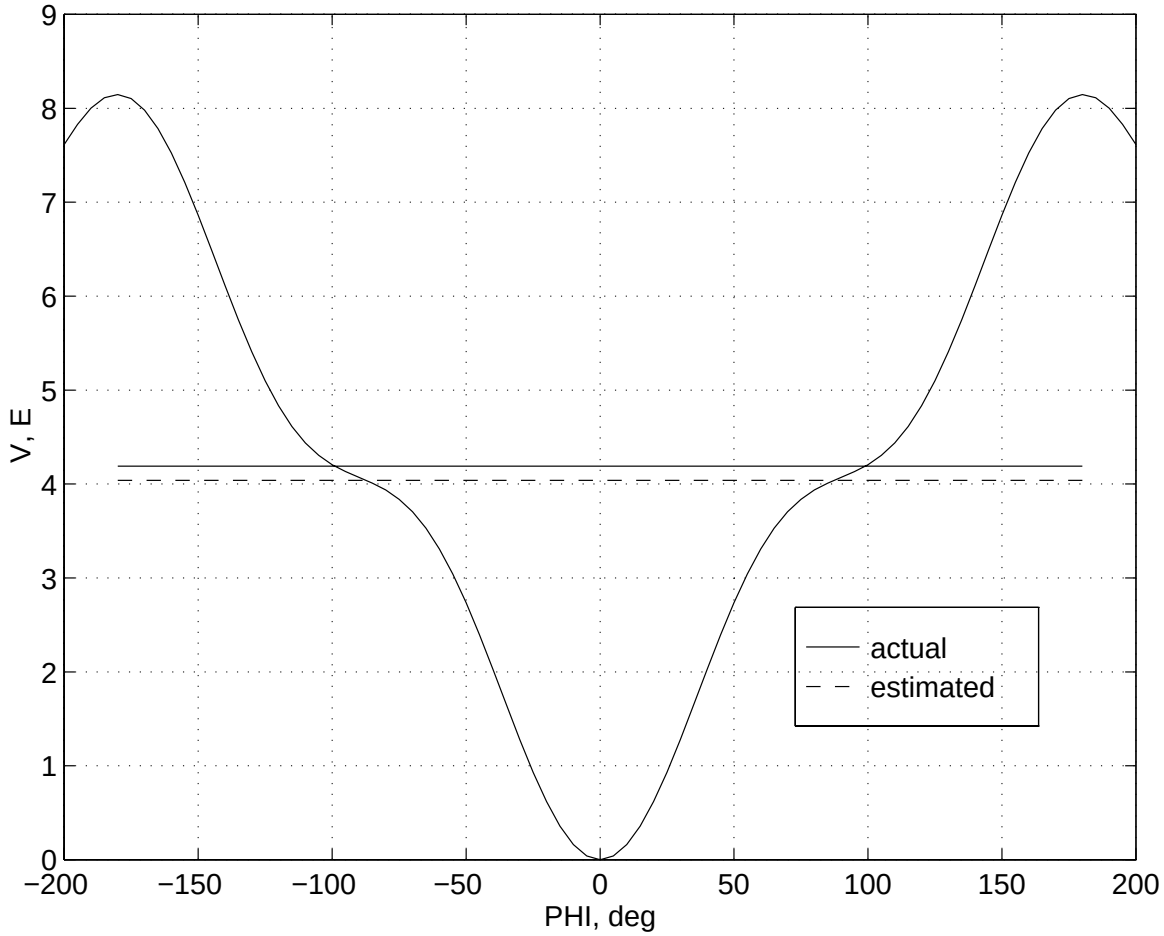

Figure 4.8: Approximation of final energy level

1. Energy is not constant, although it is close to being a constant,
2. The fact that at the point of interest a small change in total energy is a large change in Φ_{max}.

4.3 Linear Analysis

Additional information can be obtained by performing a linear analysis on Equations 4.1-4.6. The initial step in the analysis is to calculate the Jacobian matrix, conventionally the A-matrix. This step is achieved by taking the partial derivative of every differential equation with respect to each state while also incorporating the functional relations defined in Equations 4.5 and 4.6.

$$\begin{aligned}
\frac{\partial \dot{\beta}}{\partial \beta} &= -\frac{2\cos\beta\cos\tau\sin\beta}{Km}\left(Y + mg\sin\Phi\cos\Theta\right) \\
&\quad + \frac{C_1 K}{m\cos\tau}\left(1 + 2\beta\tan\beta\right) && (4.47)\\
\frac{\partial \dot{\beta}}{\partial \tau} &= \Omega\cos\tau - \frac{\cos^2\beta\sin\tau}{Km}\left(Y + mg\sin\Phi\cos\Theta\right) \\
&\quad + \frac{2C_1 K\beta\sin\tau}{m\cos^2\tau} && (4.48)\\
\frac{\partial \dot{\beta}}{\partial \Omega} &= \sin\tau && (4.49)\\
\frac{\partial \dot{\beta}}{\partial \Phi} &= \frac{\cos^2\beta\sin\tau}{Km} mg\cos\Theta\cos\Phi && (4.50)
\end{aligned}$$

$$\begin{aligned}
\frac{\partial \dot{\tau}}{\partial \beta} &= -\frac{\Omega\cos\tau}{\cos^2\beta} && (4.51)\\
\frac{\partial \dot{\tau}}{\partial \tau} &= \Omega\sin\tau\tan\beta && (4.52)\\
\frac{\partial \dot{\tau}}{\partial \Omega} &= -\cos\tau\tan\beta && (4.53)\\
\frac{\partial \dot{\tau}}{\partial \Phi} &= 0 && (4.54)
\end{aligned}$$

$$\frac{\partial \dot{\Omega}}{\partial \beta} = \frac{C_2 K^2}{I_{xx} \cos\eta \cos^2\beta \cos^2\tau} \left[\frac{\pi}{\beta_{ref}} \cos\left(\frac{\pi}{\beta_{ref}}\beta\right) + 2\tan\beta \sin\left(\frac{\pi}{\beta_{ref}}\beta\right) \right] \tag{4.55}$$

$$\frac{\partial \dot{\Omega}}{\partial \tau} = \frac{2C_2 K^2 \tan\tau \sin\left(\frac{\pi}{\beta_{ref}}\beta\right)}{I_{xx} \cos\eta \cos^2\beta \cos^2\tau} \tag{4.56}$$

$$\frac{\partial \dot{\Omega}}{\partial \Omega} = 0 \tag{4.57}$$

$$\frac{\partial \dot{\Omega}}{\partial \Phi} = 0 \tag{4.58}$$

$$\frac{\partial \dot{\Phi}}{\partial \beta} = 0 \tag{4.59}$$

$$\frac{\partial \dot{\Phi}}{\partial \tau} = 0 \tag{4.60}$$

$$\frac{\partial \dot{\Phi}}{\partial \Omega} = 1 \tag{4.61}$$

$$\frac{\partial \dot{\Phi}}{\partial \Phi} = 0 \tag{4.62}$$

By inspection of the equations of motion, any non-zero lateral-directional state will not allow equilibrium solutions. Therefore the reference flight condition will be chosen to be $\{\beta, \tau, \Omega, \Phi\} = \{0, \tau_0, 0, 0\}$. This reference flight condition allows the Jacobian to be written as follows,

$$A = \begin{bmatrix} \frac{C_1 K}{m \cos\tau_0} & 0 & \sin\tau_0 & \frac{g\cos\Theta\cos\tau_0}{K} \\ 0 & 0 & 0 & 0 \\ \frac{C_2 K^2 \frac{\pi}{\beta_{ref}}}{I_{xx}\cos\eta\cos^2\tau_0} & 0 & 0 & 0 \\ 0 & 0 & 1 & 0 \end{bmatrix} \tag{4.63}$$

By inspection, there exists a zero eigenvalue associated with the longitudinal state τ. This result is not a concern since the longitudinal dynamics decouple from the lateral-directional dynamics. Writing the characteristic polynomial for the lateral-directional states,

$$a\lambda^3 + b\lambda^2 + c\lambda + d = 0 \tag{4.64}$$

with

$$a = 1 \tag{4.65}$$

$$b = -A_{11} = -\frac{C_1 K}{m \cos \tau_0} \tag{4.66}$$

$$c = -A_{31} A_{13} = -\frac{C_2 K^2 \sin \tau_0 \frac{\pi}{\beta_{ref}}}{I_{xx} \cos \eta \cos^2 \tau_0} \tag{4.67}$$

$$d = -A_{31} A_{14} = -\frac{C_2 K g \cos \Theta \frac{\pi}{\beta_{ref}}}{I_{xx} \cos \eta \cos \tau_0} \tag{4.68}$$

Routh's criteria for stability can be applied and it states that the real part of all roots will be negative for a third order polynomial if,

$$a, b, c, d > 0 \tag{4.69}$$

$$bc - ad > 0 \tag{4.70}$$

Keeping in mind that the constants C_1 and C_2 are both negative by definition, the first condition is met for all $\tau_0 > 0$. The second condition reduces to the following,

$$\frac{C_2 K \frac{\pi}{\beta_{ref}}}{I_{xx} \cos \eta \cos \tau_0} \left(\frac{C_1 K^2 \sin \tau_0}{m \cos^2 tau_0} + g \cos \Theta \right) > 0 \tag{4.71}$$

The first term is always negative, requiring that the term in the parenthesis must be negative as well. Rewriting the second term,

$$\frac{\sin \tau_0}{\cos^2 \tau_0} < -\frac{mg \cos \Theta}{C_1 K^2} \tag{4.72}$$

This formula bears a striking resemblance to Equation 4.13 and is in fact the reciprocal. Following the same procedure as solving for σ_{ref}, it is shown that for linear stability τ_0 must be greater than σ_{ref}. This result is quite interesting. To show its validity, Figure 4.9 shows the same initial condition as Figure 4.1 except τ_0 is now 65° as opposed to 5°As can be seen, all the state time histories show a stable oscillatory behavior. The system will converge on a static equilibrium solution with zero for all lateral-directional states and approximately $\tau = 65°$.

The physical interpretation of the stable solution is a very high angle of attack equilibrium, for the case shown $\alpha = \tau + \eta \approx 85°$ (using Equation 2.13). Velocity also reaches a steady value.

4.4 Design Drivers

The results that were found in this chapter will be reviewed and the effect and lessons learned will be summarized. Drivers of the amplitude and frequency will be examined and

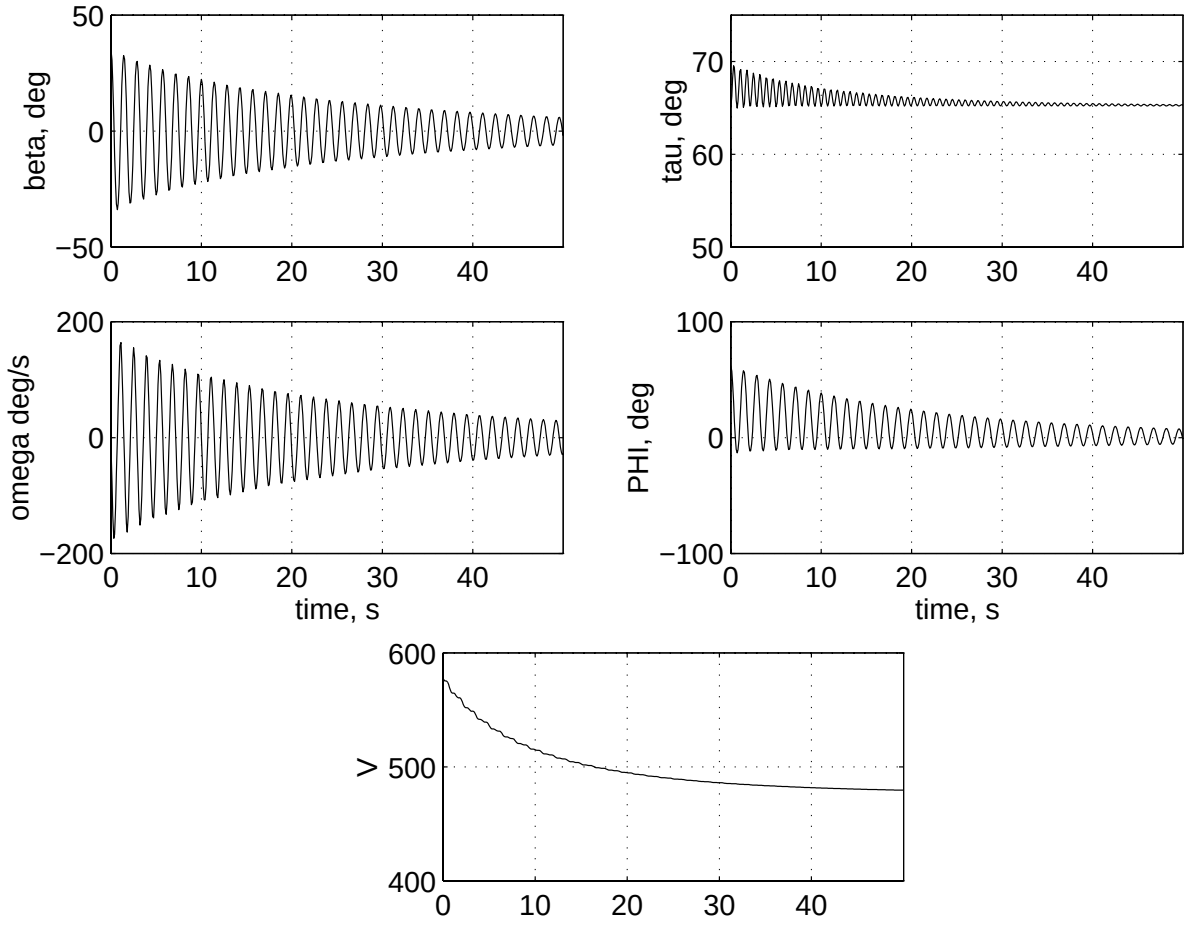

Figure 4.9: Stable initial condition, $\{\beta, \tau, \Omega, \Phi\} = \{35°, 65°, -16°/s, 62°\}$

generalizations will be drawn as to what is beneficial and what is detrimental in reference to the Falling Leaf.

The variable σ_{ref} is first on the inspection list. It is beneficial to have σ_{ref} as small as possible for two reasons. A small σ_{ref} will make maximum angle of attack small, as well as increase the region of stability where the oscillatory solution does not exist. The driving factor for the value of σ_{ref} is the constant C. Figure 4.3 showed how σ_{ref} varies with C. Reprinting C from Equation 4.13 in it's deconstructed form,

$$C = -\frac{C_{Y\beta}\rho S K^2}{2mg\cos\Theta} \tag{4.73}$$

Anti-Falling Leaf conditions include having a high value of $C_{Y\beta}$, being low in altitude, and keeping mass to a minimum. The value of K should be as high as possible. The physical interpretation of K from Sec 3.2.1 and Equation 3.19 will be reviewed. K represents the component of velocity in the direction of the body-axis angular rate vector. The extreme condition is that all of the velocity is along the direction of the instantaneous rotation vector. The angle Θ is a constant of the motion and represents the pitch angle of the rotational coordinate system with respect to inertial space. This angle being as large as possible would be most beneficial. Unobserved sideslip buildup and downward acceleration are prime conditions for the initiation of this motion and furthermore are detrimental in how they effect the Falling Leaf motion if the motion is entered. It has been thought that the Falling Leaf was somehow linked with altitude. Pilots would find themselves out of the motion at low altitude. It is proposed that this effect is the from the change in density, which translates to a decrease in σ_{ref}. Recall that the model was shown to be stable in the linear analysis for $\tau > \sigma_{ref}$. The necessary change in density may be calculated such that the Falling Leaf destroys its existence by the drop in altitude. A 10,000 ft change in altitude from 15,000 ft to 5,000 ft translated to a decrease in σ_{ref} of 7° for the simulation shown in this chapter. A guideline may be developed that states how much altitude loss is desired for Falling Leaf recovery, and if that altitude is not available loss of aircraft is possible. Notice that the rolling moment has not contributed in the definition of σ_{ref}.

Establishing σ_{ref} will fix the maximum angle of attack and establish the 'track' that the motion must lie in shown by Figure 4.5. Initial conditions were found to be a large driver in the final energy level that defines frequency, Φ_{max}, and τ_{min}. Rolling moment has a large effect here as well. To analyze how the rolling moment affects the frequency of the Falling Leaf, the following is proposed. Figure 4.10 shows three different representations of the rolling moment. The rolling moment is defined as the sine function reprinted here,

$$C_l = -C_{l_{max}} \sin\left(\frac{\pi}{\beta_{ref}}\beta\right) \tag{4.74}$$

The three different representations are shown in Table 4.2 Each representation of the rolling moment will be used in the simulation using the exact initial condition that is used in

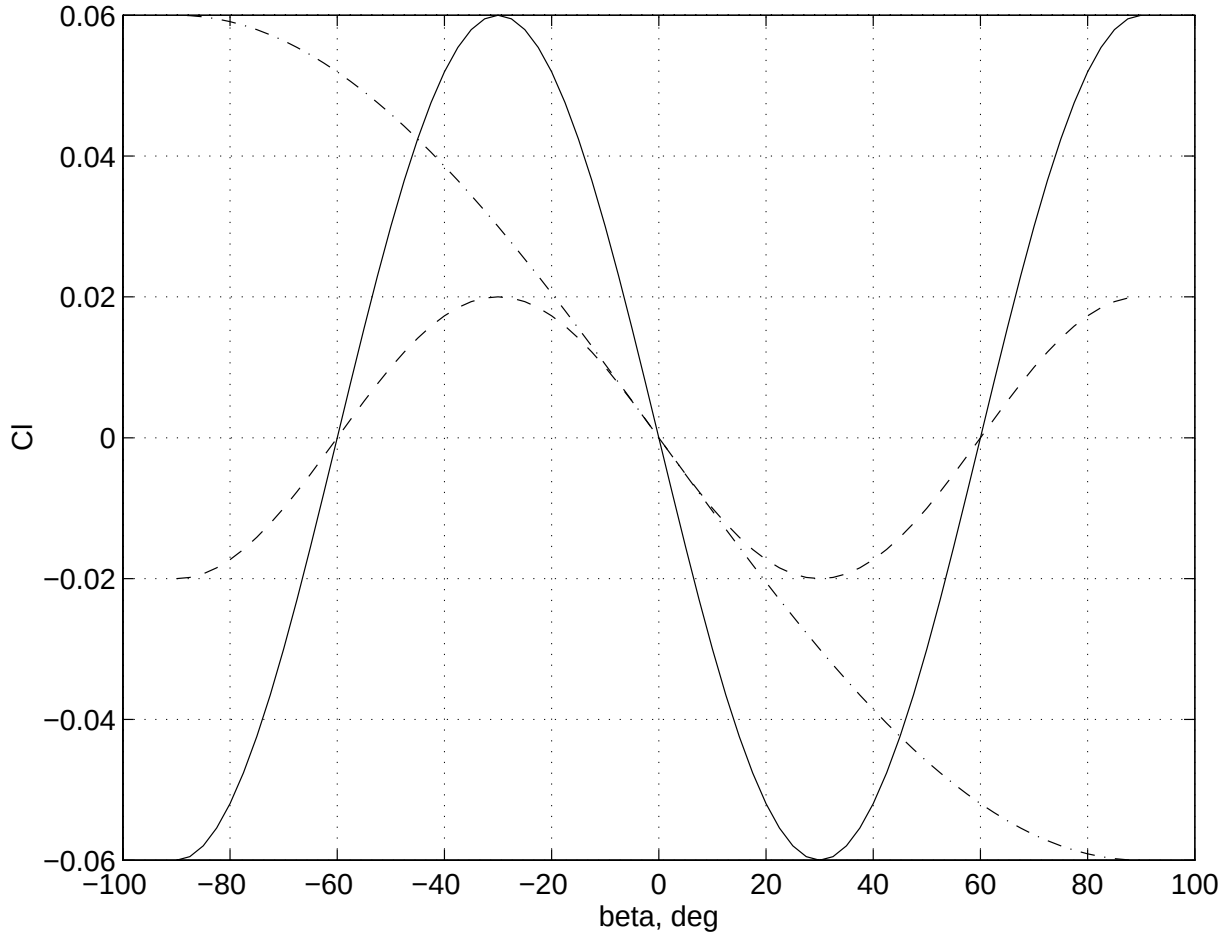

Figure 4.10: Various rolling moment curves
Legend given by Table 4.2

Table 4.2: Rolling Moment Parameters

line type	$C_{l_{max}}$	β_{ref}
-(ref)	.06	60°
–	.02	60°
-·	.06	180°

Figure 4.1. The final energy level will be calculated in the same manner as in the last section, by extracting Ω_{max} from the time history once the motion has reached a near steady oscillation. The time histories for each variable are shown for every run.

Figure 4.11 corresponds to the dashed rolling moment in Figure 4.10. This rolling moment has a $C_{l_{max}} = .02$ with the value of β_{ref} remaining the same as in the reference case. It is noted that $\tau_{max} = \sigma_{ref}$ as it must be given Equation 4.7. The frequency change is obvious from the time histories, with a period of approximately 10 sec. The interesting result is that the magnitude of the oscillation is the same. This fact is most easily verified by inspection of the appropriate energy curve in Figure 4.13. The horizontal total energy lines cross their respective potential curves at the same angle $\Phi \approx 100^\circ$. the angular distance that needs to be traveled is the same for both cases yet the adjusted rolling moment allows a longer time in which to cover the same distance. The change in period then manifests itself in the decrease of Ω_{max}.

The second modified rolling moment returns to $C_{l_{max}} = .06$ and now has a $\beta_{ref} = 180^\circ$ as shown in Figure 4.10. Although this representation is inconsistent with the results shown in Appendix A, it is the most similar to a linear rolling moment that is used routinely. This case was chosen because of the effect on the potential energy curve. For this case, Equation 4.30 reduces to,

$$\ddot{\Phi} = AC \sin \Phi \tag{4.75}$$

This simplification is quite significant. The above equation is identical in form to the equation of motion for a pendulum. The dynamics of a pendulum is a well known and studied problem. The analytical solution is shown here for completeness and is as follows. Integrating the equation of motion,

$$\frac{\dot{\Phi}^2}{2} = -AC \cos \Phi + constant \tag{4.76}$$

It is known that when Φ is maximum that $\dot{\Phi} = 0$. Therefore,

$$constant = AC \cos \Phi_{max} \tag{4.77}$$

substituting in the constant,

$$\frac{\dot{\Phi}^2}{2} = AC(\cos \Phi_{max} - \cos \Phi) \tag{4.78}$$

It is necessary to have the constant on the outside of the parenthesis to be positive. Realizing that A is defined negative, a new constant is defined such that $P = -AC$. Continuing,

$$\frac{\dot{\Phi}^2}{2} = P(\cos \Phi - \cos \Phi_{max}) \tag{4.79}$$

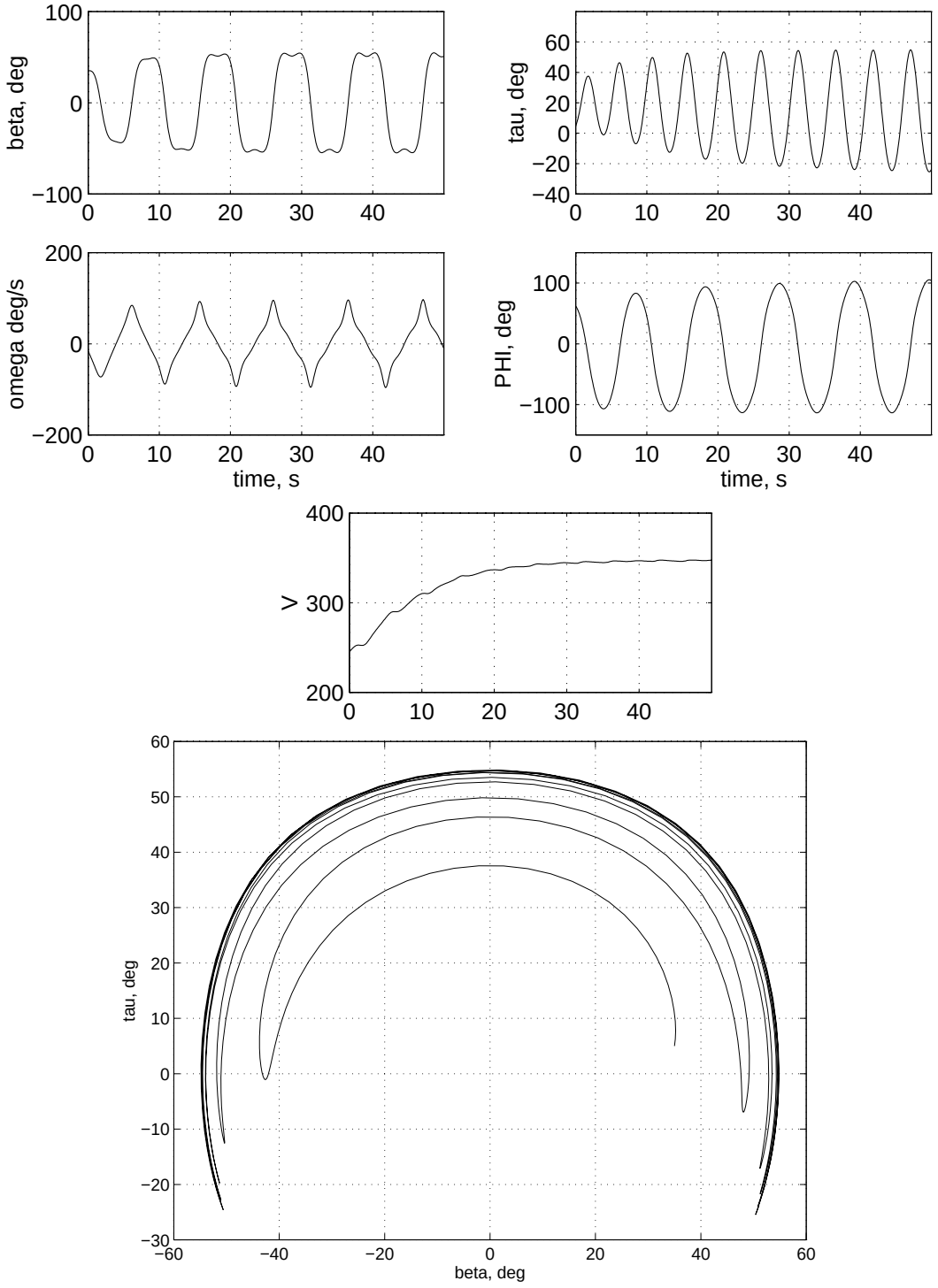

Figure 4.11: Simulation with '–' rolling moment

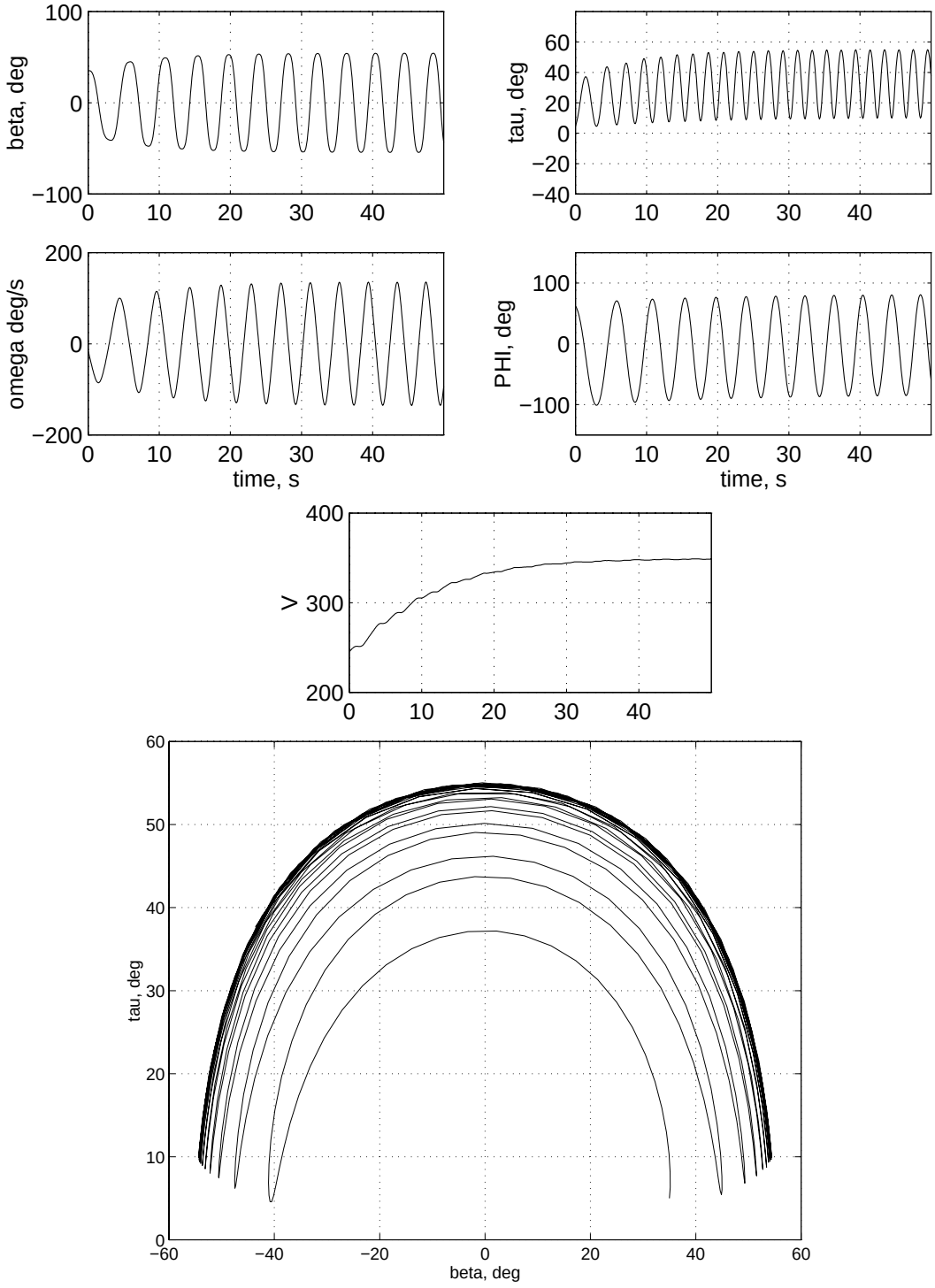

Figure 4.12: Simulation with '-·' rolling moment

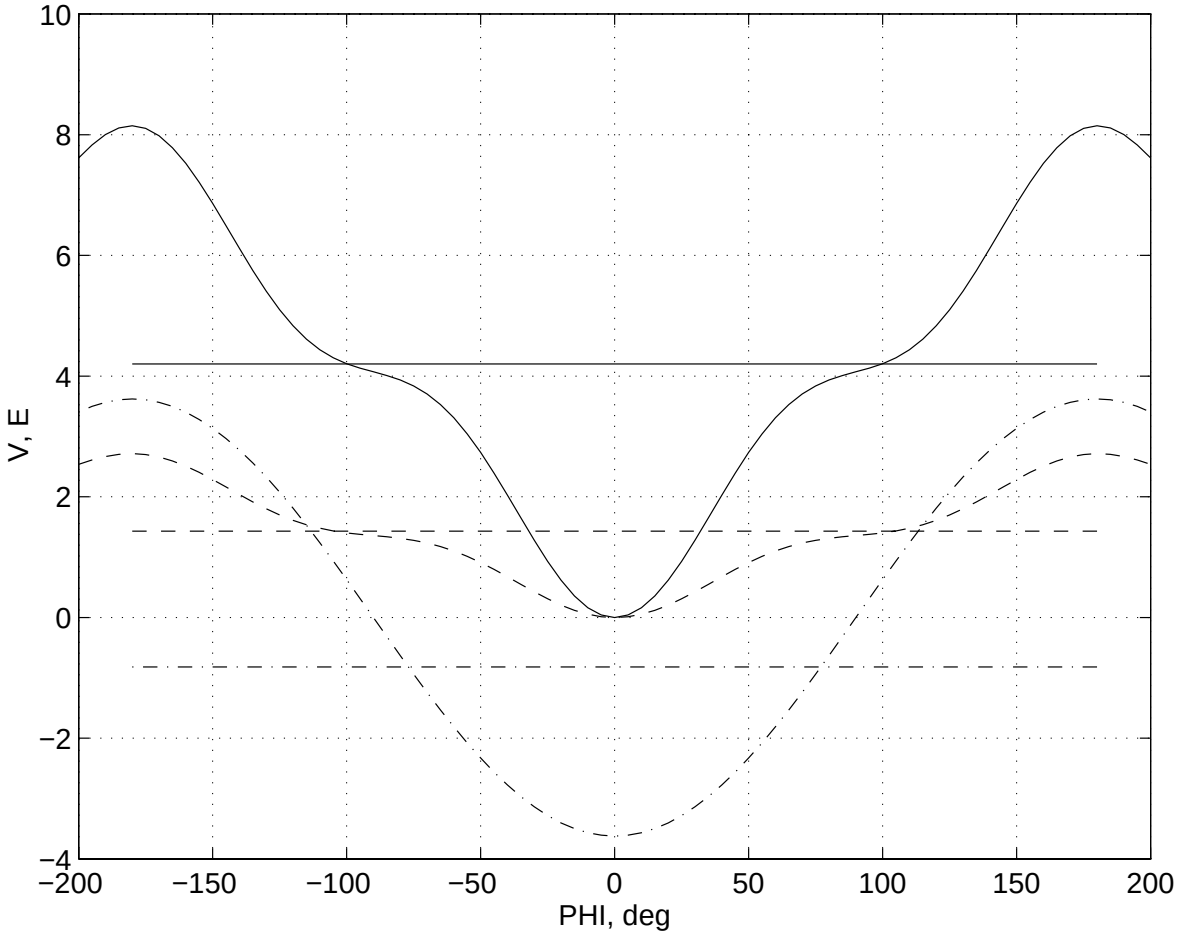

Figure 4.13: Energy curves for various rolling moments
Legend given by Table 4.2

Using half angle relations,

$$\frac{\dot{\Phi}^2}{2} = 2P\left(sin^2\frac{\Phi_{max}}{2} - \sin^2\frac{\Phi}{2}\right) \tag{4.80}$$

Separating variables,

$$\frac{d\left(\frac{\phi}{2}\right)}{\sqrt{\sin^2\frac{\Phi_{max}}{2} - \sin^2\frac{\Phi}{2}}} = \sqrt{P}dt \tag{4.81}$$

Introducing the following transformation and the new variable ν,

$$\sin\frac{\Phi}{2} = \sin\frac{\Phi_{max}}{2}\sin\nu \tag{4.82}$$

It follows that

$$d\left(\frac{\Phi}{2}\right) = \frac{\sin\frac{\Phi_{max}}{2}\cos\nu}{\cos\frac{\Phi}{2}}d\nu \tag{4.83}$$

Substituting in this transformation,

$$\frac{d\nu}{\sqrt{1 - \sin^2\frac{\Phi_{max}}{2}\sin^2\nu}} = \sqrt{P}dt \tag{4.84}$$

To take the integral of both sides, the limits on ν need to be expressed. From the transformation, $\nu = \frac{\pi}{2}$ when $\Phi = \Phi_{max}$. Likewise, $\nu = 0$ when $\Phi = 0$.

$$\int_0^{\frac{\pi}{2}} \frac{d\nu}{\sqrt{1 - c^2\sin^2\nu}} = \int_0^{\frac{T_{period}}{4}} \sqrt{P}dt \tag{4.85}$$

where $c = \sin\frac{\Phi_{max}}{2}$.

The integral on the left hand side constitutes an elliptic integral of the first kind. The solution to such an integral can be written as

$$F = \frac{\pi}{2}\left(1 + \frac{c^2}{4} + \frac{9c^4}{64} + \frac{25c^2}{256} + \frac{1225c^8}{16384} + \cdots + \left(\frac{(2i)!}{2^{2i}(i!)^2}\right)^2 c^{2i}\right) \tag{4.86}$$

The period can then be solved for as follows,

$$T_{period} = \frac{4F}{\sqrt{P}} \tag{4.87}$$

The above expression states that the frequency is dependent on amplitude. Either value needs to be known before the other can be calculated. For the particular rolling moment under analysis, the final amplitude is known through simulation. With that amplitude being approximately $\Phi = 80°$, the period is calculated to be 3.75 sec. Again this value is in the range of the correct period, but errors do arise for the same reasons mentioned earlier in this section.

Rolling moment plays a large part in the final quasi-steady Falling Leaf oscillation. Recall the rolling moment coefficient is given by Equation 3.2. The rolling moment acts as a spring through the parameter $C_{l_{max}}$, controlling the frequency of the motion, while changing β_{ref} affects both frequency and amplitude of the motion.

4.5 Concluding Remarks

In closing, remarks will be made stating possible directions for further research into the analysis of the Falling Leaf and other dynamic motions. The coordinate system proposed has definite advantages in understanding selected dynamic motions by allowing the establishment of relationships between the rotation vector and the velocity vector. Spins are also a good candidate for analysis using this system. Analysis of rotary balance wind tunnel data is another good candidate for this system. Rotary balance testing can have both the rotation vector and the velocity vector fixed in inertial space. Defining the relationships between inertial space and the respective rotational and wind axis coordinate systems via the body-fixed coordinate system would be interesting. Defining these relationships would introduce (η, λ) and (α, β) respectively.

The analysis of the Falling Leaf included the assumption that the value of k in Table 3.1 was positive. Analyzing the possibility of $k < 0$ would lead to different dynamic motions that may be interesting.

In reference to the particular case of the Falling Leaf, the relaxation of the constraint that η is a constant is another issue that would be of interest. The removal of that constraint would allow the rotation vector to move within the plane of symmetry of the aircraft. A first glance at this issue is presented here. Assume one has reached the Falling Leaf motion, and has at one's disposal time histories of angle of attack and sideslip corresponding to the motion. The rolling and yawing moment coefficients are assumed to be represented by the appropriate function in Appendix A. Figure 4.14 shows two traces of yawing moment coefficient as a function of sideslip angle through the motion. The solid line corresponds to the yawing moment that is seen as a function of α and β given the function in Appendix A. The dotted line is what the yawing moment must be so that η is constant given the rolling moment is defined by the function in Appendix A. It is proposed that the Falling Leaf can have an oscillating η. The constraint of having $\eta = constant$ sets a very rigorous condition on the relationship between rolling moment and yawing moment. Figure 4.14 shows how

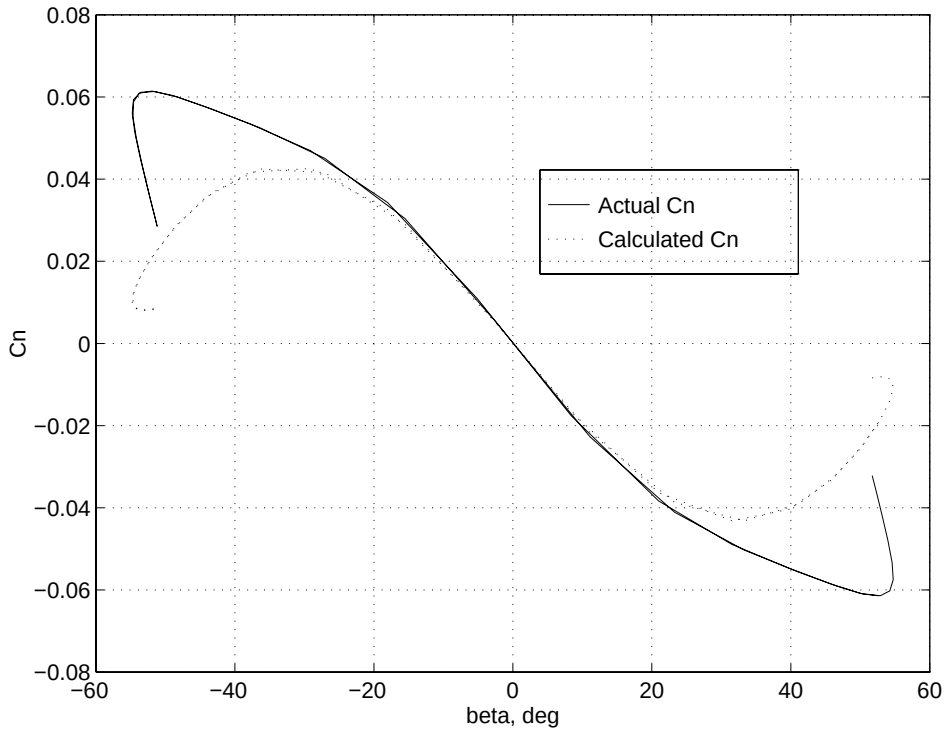

Figure 4.14: Comparison of yawing moments

close this assumption is to being true. As can be seen, the assumption is quite good up until about $\beta = 30°$. Because the basic shape of both curves is similar, the motion may exhibit an oscillating η. The actual research and application of this possibility is left to be performed.

Another task left to do in the analysis of the Falling Leaf is to determine final energy level given arbitrary initial conditions. Being able to know how much energy was going to enter the system before reaching the steady oscillation and quantifying existing energy at the onset of the motion would solve this problem. The system is a nonconservative system until the quasi-steady oscillation is reached. Quantifying the energy that is to be added to the system as the oscillation grows would give the link between initial condition and the frequency and amplitude of the final oscillation.

Further consideration of how the change in density due to loss of altitude affects recovery of the Falling Leaf should be analyzed. Affect on the key parameter σ_{ref} is of importance and can lead to recovery guidelines based on the altitude that the Falling Leaf motion was entered.

The coordinate system proposed allowed the analysis of the Falling Leaf to reach a new level of understanding. The rotational coordinate system directly allowed for the key parameter σ_{ref} to be defined, as well as to allow the problem to be reduced to a point where energy methods could be introduced to help define final amplitudes and maximum rates. The

rotational coordinate system should be applied to other dynamic motions such as an aircraft spin. It may also be useful in the interpretation of rotary balance wind tunnel techniques that are being used today for the identification of 'dynamic' aerodynamics.

Appendix A

Global Aerodynamic Force and Moment Curves

The data presented is an effort to capture the general characteristics of how the force and moments behave at high angles of attack and sideslip. Data for the high angle of attack was somewhat accessible while the large sideslip data is quite lacking in todays wind tunnel testing schedules. The data presented is achieved from combining wind tunnel data from Ref [13] and the F-18C aerodynamic database. It is understood that a particular aircraft can vary quite drastically from what is to be presented yet the thrust of the work was to identify characteristics/parameters that one could vary to generally affect how the curve looks and behaves. Such as varying slopes and breakpoints of the curves. What is shown here is the first iteration of these curves. The identification of the parameters that have been mentioned is still left to be done for the next adventurous soul.

The only dependence of the force and moments is on angle of attack α and sideslip angle β, with those values in radians. Therefore it is bare airframe and no effort has been made to analyze how the dynamic rates affect the coefficients. In each section that follows, some key notes will be presented as to why some of the curves look the way they do, and the background as to the ideas involved in picking some of the extremum. A least squares curve fitting algorithm was performed on the data that was gathered. The functional form of the force and moment coefficients was based the shape of the data as well as intuitive thoughts as too what a particular force or moment coefficient should do at extreme values. For instance, body axis side force should not change as a function of α when $\beta = 90°$.

Lift Coefficient vs α and β: Figure A.1

$$C_L = \left(a + b\alpha + c\alpha^2 + d\alpha^3\right) \cos\left(\frac{2}{3}\beta\right)$$

$$a = -0.0204 \quad b = 5.6777$$
$$c = -5.4246 \quad d = 1.1645$$

No data was found that indicated a β dependence on the lift coefficient, yet intuitively it seems that there must be one. Conventionally wind tunnel testing has had small β sweeps where the lift force is not effected heavily. A cosine dependence on β was chosen and scaled such that zero lift was not generated at a 90° sideslip angle. The value of β where the lift coefficient is zero is outside the range of validity for this model, $\beta \pm 90°$.

Drag Coefficient vs α and β: Figure A.2

$$C_D = \left(a + b\alpha + c\alpha^2 + d\alpha^3 + e\alpha^4\right)\cos\beta + f$$

$$a = -1.4994 \quad b = -0.1995$$
$$c = \ 6.3971 \quad d = -5.7341$$
$$e = \ 1.4610 \quad f = \ 1.5036$$

The approach for this curve was stating that at 90°β the drag on the aircraft was the same regardless of angle of attack. The only choice in the matter is what should that value be. It is feasible to say maximum drag is at 90°α and zero β, imagine a flat plate at 90°α and while adding sideslip drag intuitively should go down. Minimum drag is at some low α and also no beta, yet when sideslip is increased drag goes up.

Body-axis Side Force Coefficient vs α and β: Figure A.3

$$C_Y = a\beta + b\sin(2\beta)\cos(2\alpha)$$

$$a = -0.9574 \quad b = 0.1286$$

It is important to remember that this is the *body-axis* side force. A linear relationship is a very good first approximation throughout the global domain. The small dependence on angle of attack that is observed is seen in wind tunnel data. Similarly to the drag coefficient, the side force at 90°β is the same regardless of angle of attack. Non-zero β must exist for non-zero side force.

Rolling Moment Coefficient vs α and β: Figure A.4

$$C_l = \left(a + b\alpha + c\alpha^3 + d\alpha\beta^2 + e\alpha^3\beta^2 + f\beta^2 + g\beta^4\right)\beta$$

$$\begin{aligned} a &= -0.0941 \quad & b &= -0.0513 \\ c &= \ \ 0.0055 \quad & d &= \ \ 0.0295 \\ e &= -0.0013 \quad & f &= \ \ 0.1276 \\ g &= -0.0338 \end{aligned}$$

The phenomenon that is seen has been observed in various aircraft. Rolling moment does peak at a given sideslip angle and even can change sign at large sideslip. This can be attributed to the combination of stalling of the vertical tail as well as issues like high-wing or low-wing aircraft. Disregarding the α dependence would be the first approximation, or possibly making it linear. A linear approximation in β is acceptable in the small β range, yet in the global sense it is quite poor. As can be seen, the curve is quite sine-like. As an afterthought, a very good representation of the global curve may be a sine-function in β and a linear α relationship in the amplitude and possibly frequency. The Taylor series expansion of the sine-function is,

$$a\sin(b\beta) = ab\beta - \frac{ab^3\beta^3}{3!} + \frac{ab^5\beta^5}{5!} - \cdots$$

Taking away the α dependence, it can be shown that the coefficients match up reasonably well. Using the coefficients of the β-term and the β^3-term and solving for a and b of the expansion above, the coefficient of the β^5-term can be checked and it is reasonably close. For the global characterization of this curve, a sine function may be simpler than the polynomial representation that is shown above. In the general case, the value of non-zero β where $C_l = 0$ is a function of α and is not easily extracted from the equation above.

Yawing Moment Coefficient vs α and β: Figure A.5

$$C_n = \left(a + b\alpha + c\alpha^2\right)\sin(2.5\beta) + \left(d + e\alpha + f\alpha^2\right)\sin(4.2\beta)$$

$$\begin{aligned} a &= -0.0125 \quad & b &= -0.1050 \\ c &= \ \ 0.0580 \quad & d &= \ \ 0.0406 \\ e &= -0.0038 \quad & f &= -0.0205 \end{aligned}$$

The global characteristics for this curve are quite interesting. Concentrating on zero sideslip angle, at low α $C_{n\beta}$ is positive as it should be for stability reasons. This weather-cock stability is lost as α is increased due to the vertical tail losing effectiveness. The sign of the yawing moment at high β can depend on whether the vertical tail is stalled and the location of the center of gravity in an axial sense.

Pitching Moment Coefficient vs α and β: Figure A.6

$$C_m = a\alpha + b\alpha\beta^2 + c\beta^2 + d$$

$$\begin{aligned} a &= -0.4174 \quad b = 0.1691 \\ c &= \ \ 0.0043 \quad d = 0.0893 \end{aligned}$$

The pitching moment is chosen to be linear in α which is not as detailed as much of the data for particular aircraft, yet the trend is what is to be captured. Intuitively, the presence of sideslip would decrease the pitching moment on the aircraft.

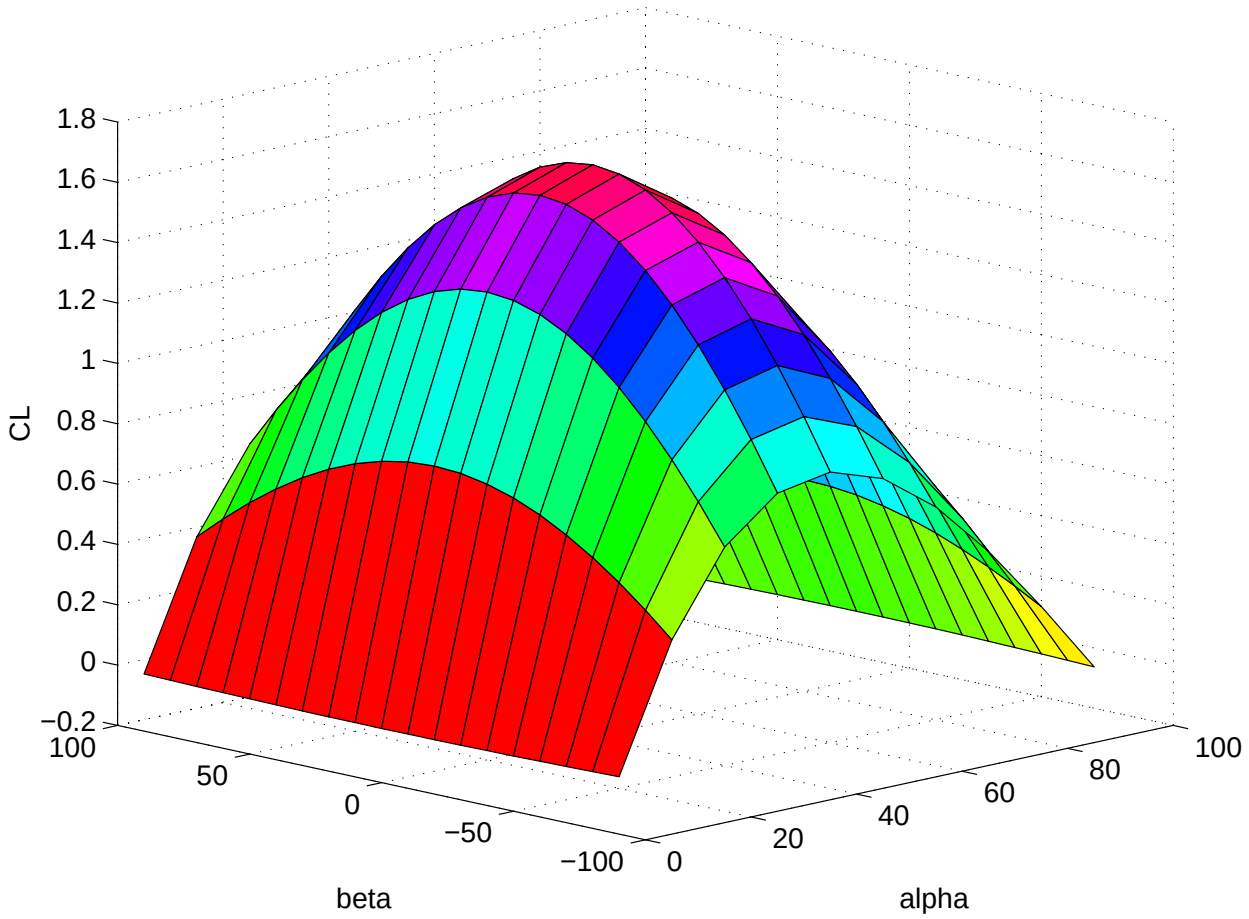

Figure A.1: Lift Coefficient

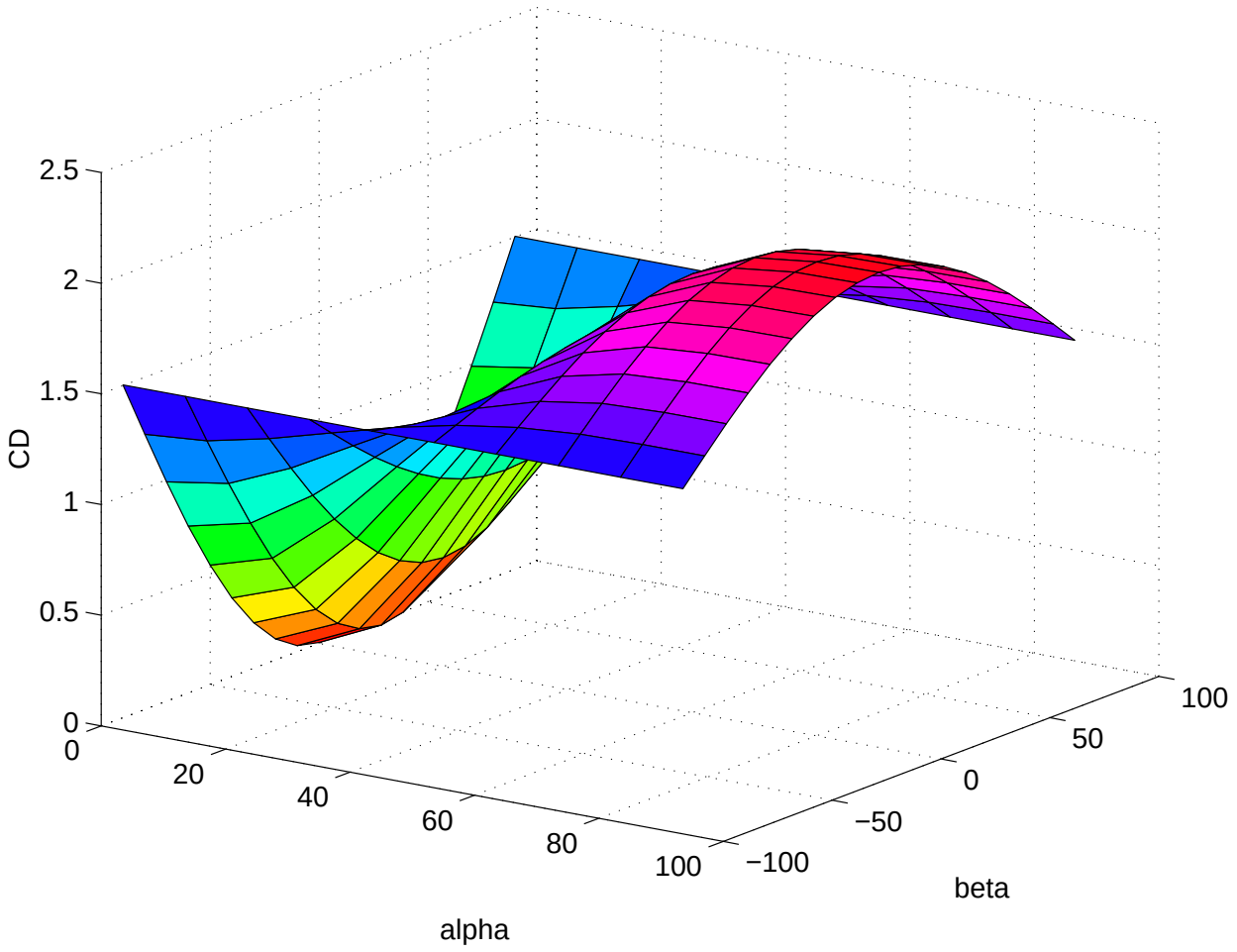

Figure A.2: Drag Coefficient

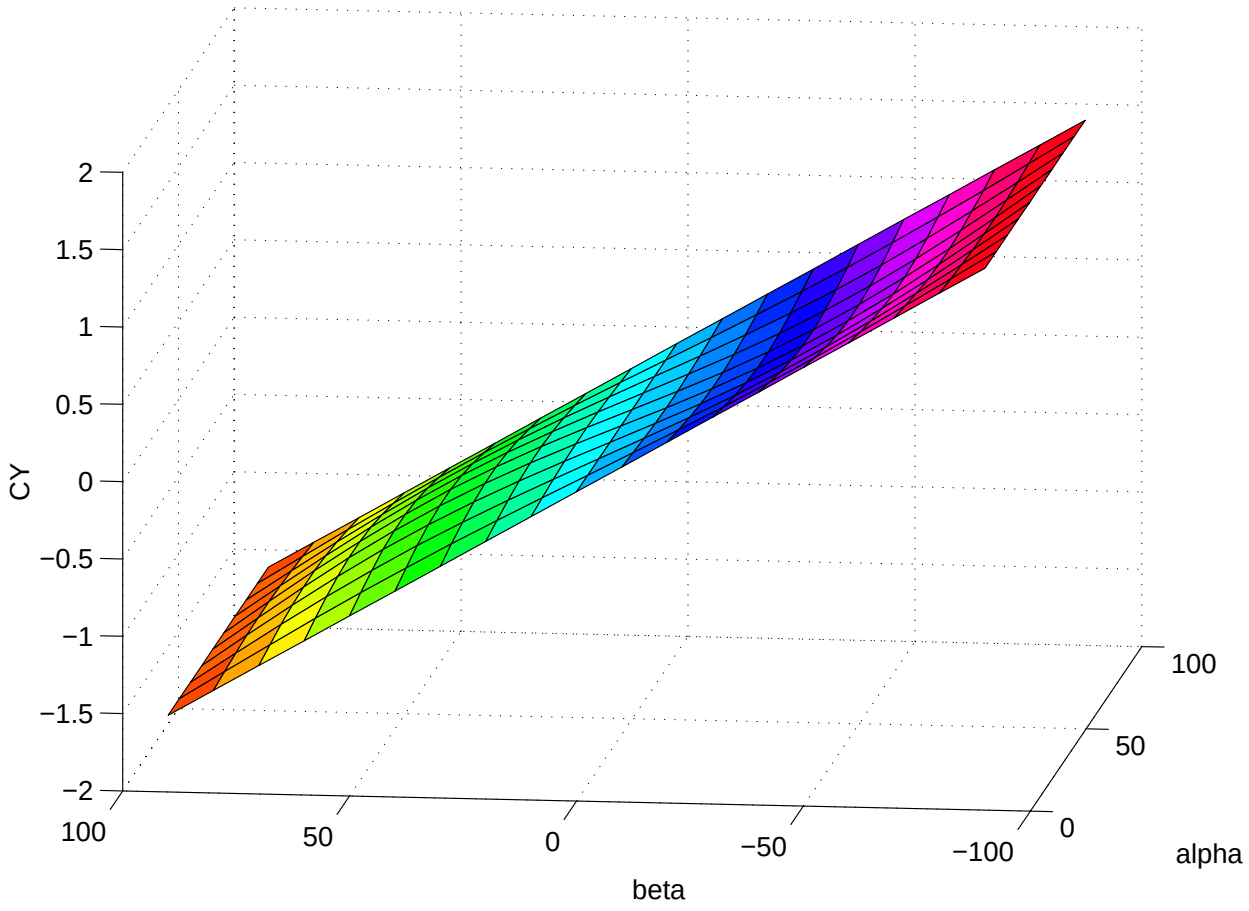

Figure A.3: Body-axis Side Force Coefficient

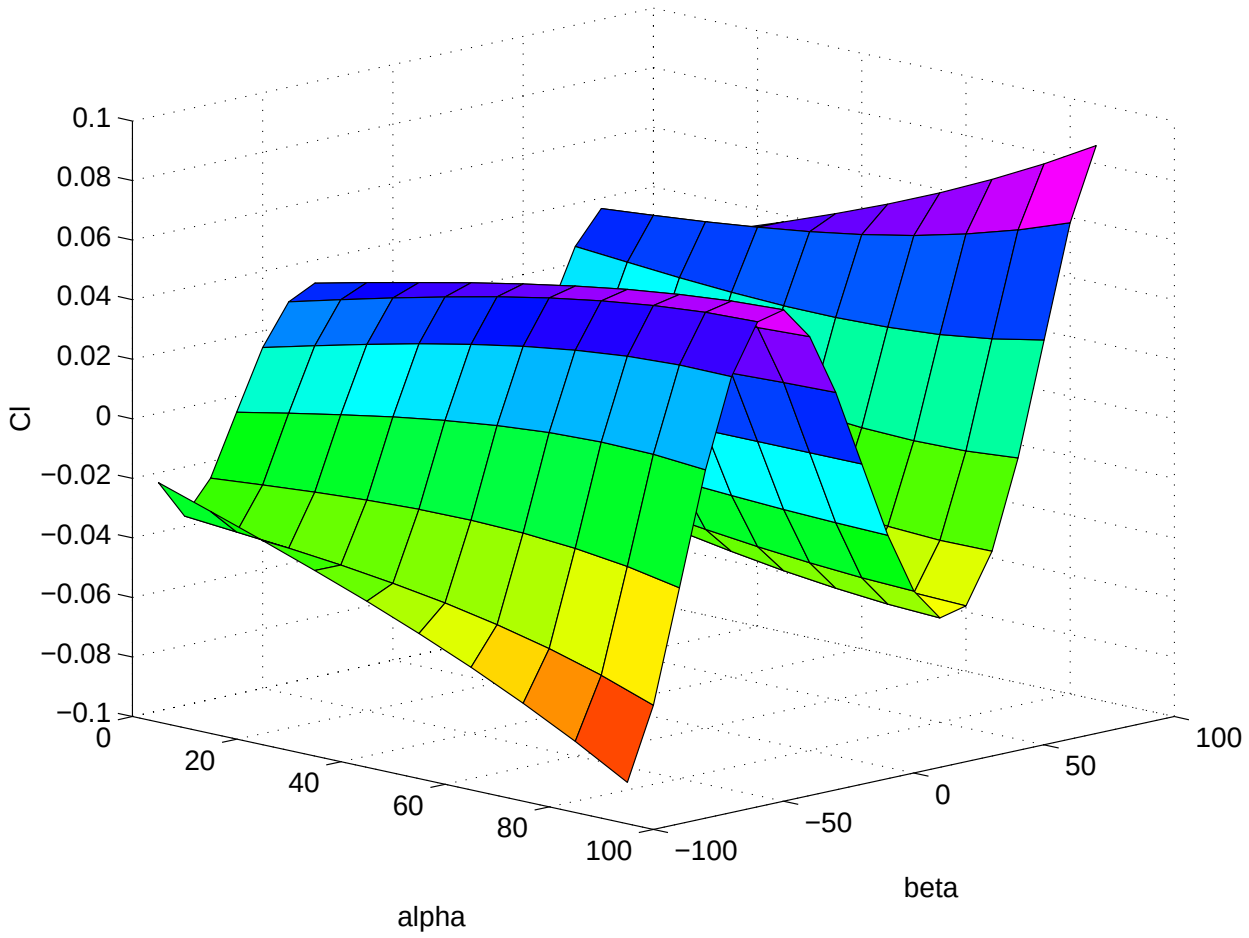

Figure A.4: Rolling Moment Coefficient

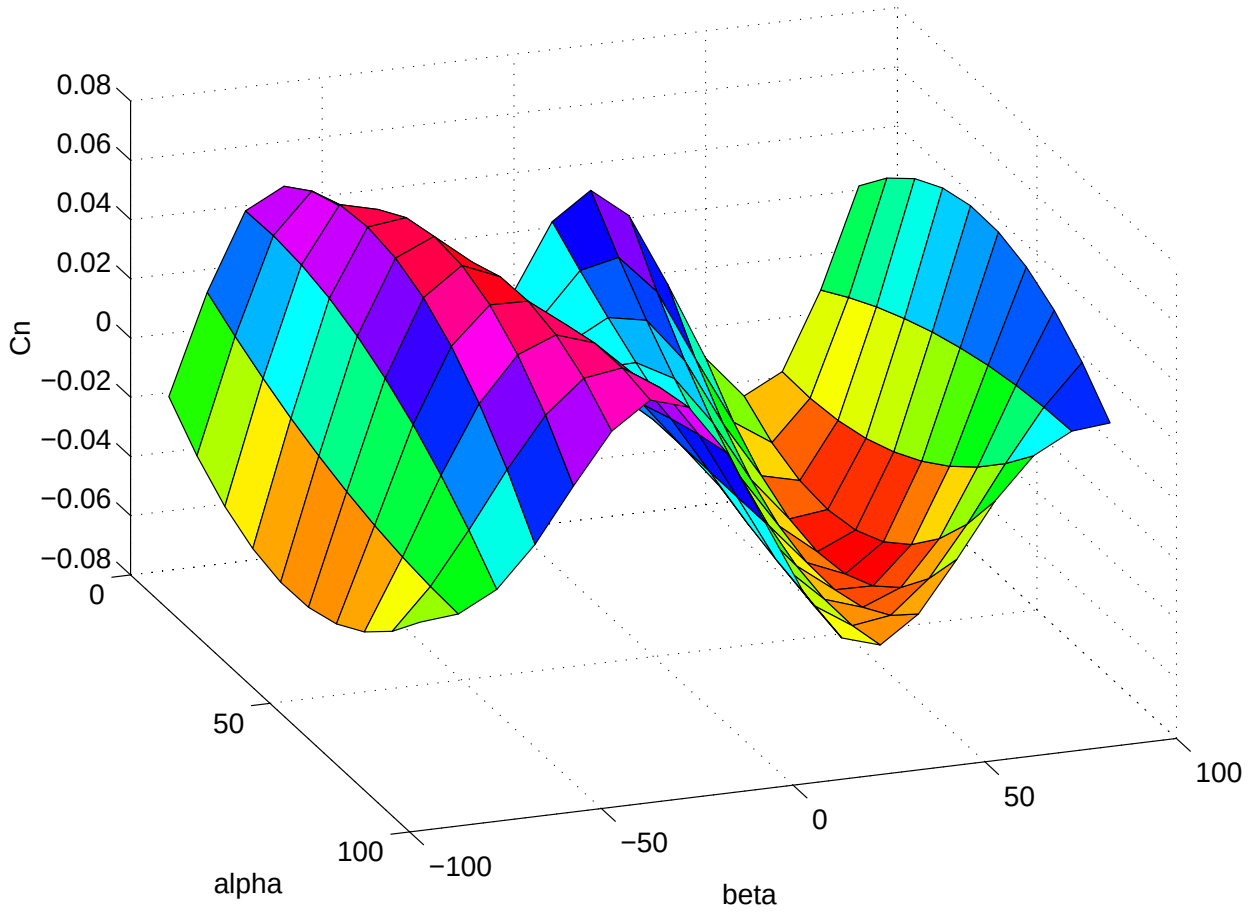

Figure A.5: Yawing Moment Coefficient

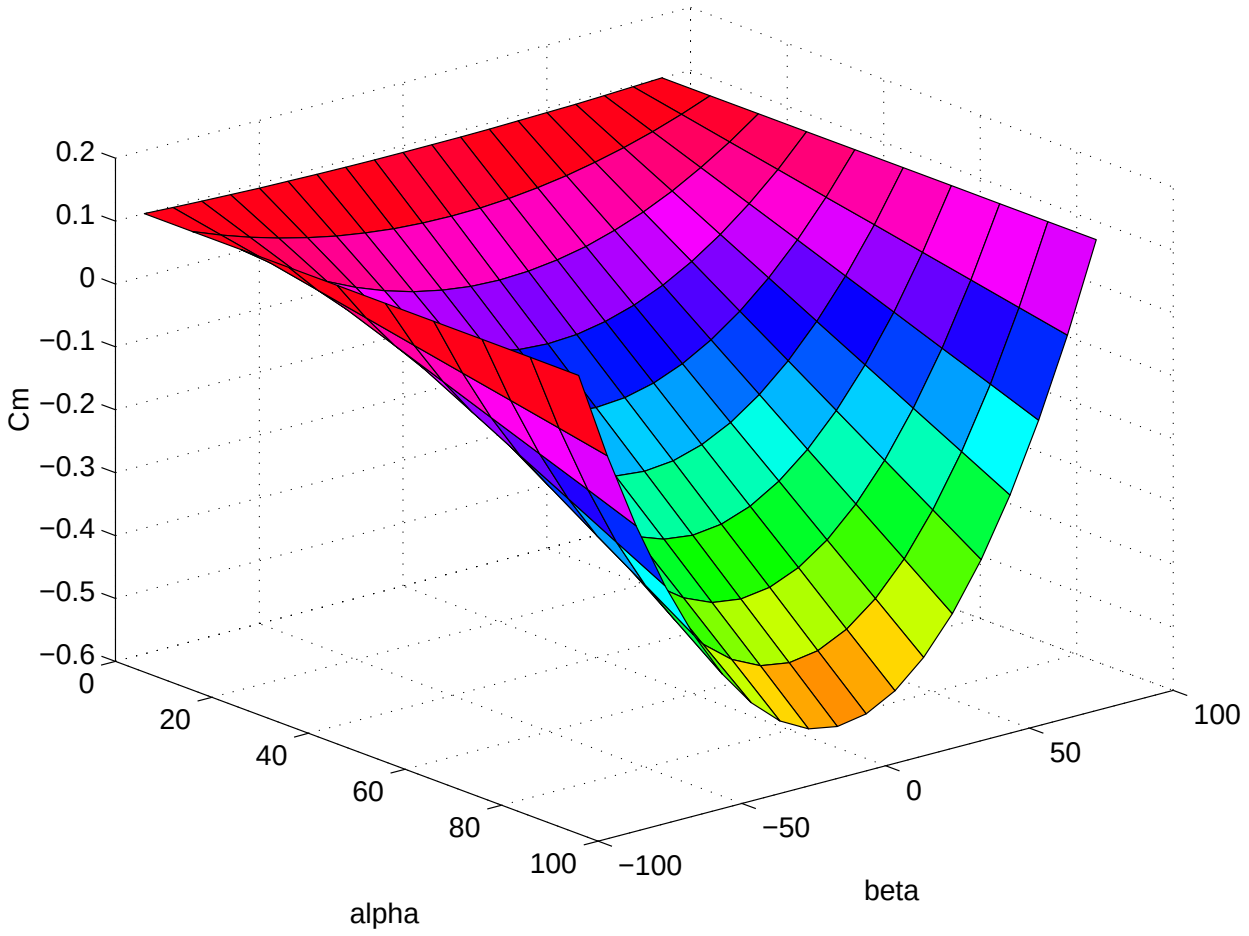

Figure A.6: Pitching Moment Coefficient

Bibliography

[1] Anne Chinnery and Christopher Hall. Motion of a rigid body with an attached spring-mass damper. *Journal of Guidance, Control, and Dynamics*, 18(6):1404–1409, 1995.

[2] Wayne C. Durham, Frederick H. Lutze, and William H. Mason. Kinematics and aerodynamics of the velocity vector roll. *Journal of Guidance, Control, and Dynamics*, 17(6):1228–1233, Nov-Dec 1994.

[3] John V. Foster. Investigation of the susceptibility of fighter airplanes to the out-of-control falling leaf mode. In NASA Langley Research Center, editor, *High-angle-of-attack Technology Conference*, Hampton, VA, 1996. ITAR.

[4] M.G. Goman and A.V. Khramtsovsky. Global stability analysis of nonlinear aircraft dynamics. Technical report, Central Aerohyrodynamic Institute (TsAGI), 1996.

[5] John W. Harris and Horst Stocker. *Handbook of Mathematics and Computational Science*, chapter 14, pages 539,542–543. Springer-Verlag, 1998.

[6] Juri Kalviste. Spherical mapping and analysis of aircraft angles for maneuvering flight. *Journal of Aircraft*, 24(8):523–530, 1997. Presented as Paper 86-2283, AIAA Atmospheric Flight Mechanics Conference, Aug 18-20, 1996.

[7] Frederick Lutze, Wayne Durham, and William Mason. Developement of lateral-directional departure criteria. Technical report, Virginia Polytechnic Institute and State University, June 1992. NASA/Larc Project NCC1-158.

[8] J.B. Planeaux and T.J. Barth. High angle of attach dynamic behavior of a model high performance aircraft. In *AIAA Atmospheric Flight Mechanics Conference*, number AIAA-88-4368, 1988.

[9] Richard F. Porter and James P. Loomis. Examination of an aerodynamic coupling phenomenon. *Journal of Aircraft*, 2(6):553–556, 1965.

[10] A. M. Skow and A. Titiriga. A survey of analytical and experimental techniques to predict aircraft dynamic characteristics at high angles of attack. *Dynamic stability parameters*, AGARD CP-235, 1978.

[11] Robert F. Stengel. Effect of combined roll rate and sidelip angle on aircraft flight stability. *Journal of Aircraft*, 12(8):683–685, August 1975.

[12] Brian L. Stevens and Frank L. Lewis. *Aircraft Control and Simulation*. John Wiley and Sons, Inc., New York, 1992.

[13] Jose Rafael Villeta. *Lateral-directional static and dynamic stability analysis at high angles of attack for the X-31 configuration*. Master of science thesis, George Washington University, Sept 1992.

Vita

Danny Lluch was born on August 6, 1972 to Constantino and Alicia in Arlington, Virginia. After finishing high school, Blacksburg was made his home for five years. During his stay, Dan received a B.S. in Aerospace Engineering from Virginia Tech along with the strong attraction to the field of aircraft dynamics. His interest in this field was initiated through undergraduate research consisting of spin analysis for a general aviation aircraft. He received a graduate student research position at NASA Langley were he formally initiated his research in the wonderful world of nonlinear aircraft dynamics. After seven months at NASA, Dan returned to Virginia Tech to complete his studies and receive his M.S. in Aerospace Engineering.